DOT/FAA/TC-26/11

Federal Aviation Administration
William J. Hughes Technical Center
Aviation Research Division
Atlantic City International Airport
New Jersey 08405

National Airport Pavement Test Facility Construction Cycle 9

Volume 1—Traffic Test Summary

February 2026

Final Report

This document is available to the U.S. public through the National Technical Information Services (NTIS), Springfield, Virginia 22161.

This document is also available from the Federal Aviation Administration William J. Hughes Technical Center at actlibrary.tc.faa.gov.

U.S. Department of Transportation
Federal Aviation Administration

NOTICE

This document is disseminated under the sponsorship of the U.S. Department of Transportation in the interest of information exchange. The United States Government assumes no liability for the contents or use thereof. The United States Government does not endorse products or manufacturers. Trade or manufacturer's names appear herein solely because they are considered essential to the objective of this report. The findings and conclusions in this report are those of the author(s) and do not necessarily represent the views of the funding agency. This document does not constitute FAA policy. Consult the FAA sponsoring organization listed on the Technical Documentation page as to its use.

This report is available at the Federal Aviation Administration William J. Hughes Technical Center’s Full-Text Technical Reports page: actlibrary.tc.faa.gov in Adobe Acrobat portable document format (PDF).

Technical Report Documentation Page

1. Report No.	2. Government Accession No.	3. Recipient's Catalog No.
DOT/FAA/TC-26/11		

4. Title and Subtitle	5. Report Date
NATIONAL AIRPORT PAVEMENT TEST FACILITY CONSTRUCTION CYCLE 9 VOLUME 1—TRAFFIC TEST SUMMARY	February 2026
	6. Performing Organization Code ANG-E262

7. Author(s)	8. Performing Organization Report No.
Hasan Kazmee*, Scott Murrell*, Lia Ricalde*, Timothy Parsons*, Ebenezer Duah*, and Dr. David R. Brill	

9. Performing Organization Name and Address	10. Work Unit No. (TRAIS)
U.S. Department of Transportation Federal Aviation Administration Airport Pavement R&D Section William J. Hughes Technical Center for Advanced Aerospace Atlantic City International Airport, NJ 08405 *ARA, Inc. 2628 Fire Road Suite 300 Egg Harbor Twp, NJ 08234	11. Contract or Grant No. 692M15-20-D-00004

12. Sponsoring Agency Name and Address	13. Type of Report and Period Covered
U.S. Department of Transportation Federal Aviation Administration Airport Engineering Division 800 Independence Ave., SW Washington, D.C. 20591	Final Report
	14. Sponsoring Agency Code AAS-100

15. Supplementary Notes

The Federal Aviation Administration Aviation Research Division COR was Murphy Flynn.

16. Abstract

Construction Cycle 9 (CC9) was the ninth in a series of full-scale airport pavement tests performed at the Federal Aviation Administration (FAA) National Airport Pavement Test Facility (NAPTF), and the fifth involving flexible pavements. It consisted of ten flexible pavement test items assigned to four test areas: (1) Fatigue Model and Base Course Thickness, (2) Geosynthetics, (3) Cement-Treated Permeable Base, and (4) Overload. Test items were constructed in 2019, and traffic testing took place between November 6, 2020, and April 2, 2024. This report contains a general description and summary of CC9 planning, construction, and test execution. Detailed results and analyses of the individual tests are contained in separate volumes.

17. Key Words	18. Distribution Statement
National Airport Pavement Test Facility (NAPTF), Construction Cycle 9 (CC9), Flexible pavement, FAARFIELD, Asphalt fatigue, Geosynthetics, Cement-treated permeable base (CTPB), Overload	This document is available to the U.S. public through the National Technical Information Service (NTIS), Springfield, Virginia 22161. This document is also available from the Federal Aviation Administration William J. Hughes Technical Center for Advanced Aerospace at actlibrary.tc.faa.gov.

19. Security Classif. (of this report)	20. Security Classif. (of this page)	21. No. of Pages	22. Price
Unclassified	Unclassified	89	

TABLE OF CONTENTS

LIST OF FIGURES

LIST OF TABLES

LIST OF ACRONYMS

2D	2 Duals in tandem (four-wheel)
3D	3 Duals in tandem (six-wheel)
3-D	Three dimensional
AC	Advisory Circular
ACN	Aircraft classification number
ACR	Aircraft classification rating
ASTM	American Society for Testing Materials
ASG	Asphalt strain gauge
BDF	Bridge deck finisher
CBR	California Bearing Ratio
CC	Construction cycle
CC7	Construction cycle 7
CC8	Construction cycle 8
CC9	Construction cycle 9
CD	Crack density
CS	Coil sensor
CTPB	Cement-treated permeable base
D	Dual (two-wheel)
ERDC	U.S. Army Engineer Research and Development Center
FAA	Federal Aviation Administration
FAARFIELD	FAA Rigid and Flexible Iterative Elastic Layered Design
HMA	Hot mix asphalt
HWD	Heavy weight deflectometer
ICAO	International Civil Aviation Organization
ID	Identifier
ksi	kips per square inch
LOESS	Locally estimated scatterplot smoothing
LSG	Longitudinal asphalt strain gauge
LWD	Lightweight deflectometer
MS	Moisture sensor
NAPTF	National Airport Pavement Test Facility
NAPTV	National Airport Pavement Test Vehicle
NDG	Nuclear density gauge
NDT	Nondestructive testing
PC	Pressure cell
PCI	Pavement condition index
PCN	Pavement classification number
PCR	Pavement classification rating
pcf	Pounds per cubic feet
PV	Plateau value
PSPA	Portable seismic pavement analyzer
RDEC	Ratio of dissipated energy change
S	Single (one-wheel)
SPU	Signal processing unit
SSR	Subgrade stress ratio

T	Thermocouple
TSG	Transverse strain gauge
USCS	Unified Soil Classification System

EXECUTIVE SUMMARY

From 2020 to 2024, the Federal Aviation Administration (FAA) executed a series of full-scale traffic tests on flexible airport pavements at the National Airport Pavement Test Facility (NAPTF), designated Construction Cycle 9 (CC9). Within CC9, there were four distinct tests: fatigue model and base course thickness, geosynthetics, cement-treated permeable base (CTPB), and overload. These four tests were intended to generate full-scale test data for the evaluation of flexible airport pavement design models, investigate the performance of alternative paving materials for airport flexible pavements, and support the development of allowable overload criteria. CC9 construction was completed in December 2019, and traffic testing took place between November 6, 2020, and April 2, 2024.

The total test area was 300 ft long by 60 ft wide, organized into ten test items of varying cross-sections. All test items were constructed on a clay subgrade processed to California Bearing Ratio (CBR) 5. Test items included extensive instrumentation that provided data on pavement performance and response to loads throughout the test. This report documents overall CC9 planning and design, construction, material characterization, and traffic test execution through the end of the traffic test period. It does not cover post-traffic investigation of the pavement layers pending physical removal of the CC9 test items, which is planned for a later date. Detailed results and analysis of the individual tests are covered in separate companion reports as follows:

Volume 2—Test Results and Analysis, Part 1: Fatigue Model and Base Course Thickness Test
Volume 3—Test Results and Analysis, Part 2: Geosynthetics Test
Volume 4—Test Results and Analysis, Part 3: Cement-Treated Permeable Base Test
Volume 5—Test Results and Analysis, Part 4: Overload Test

1. INTRODUCTION

Construction Cycle 9 (CC9) is the ninth in a series of full-scale tests on airport pavements conducted at the Federal Aviation Administration (FAA) National Airport Pavement Test Facility (NAPTF), and the fifth involving flexible airport pavements. CC9 construction was completed in December 2019, and traffic testing took place between November 6, 2020, and April 2, 2024. Some of the tests provided follow-on data to the previous flexible pavement construction cycle (CC7), which was completed in December 2016. Test data and additional information on the NAPTF testing program may be found at https://www.airporttech.tc.faa.gov/NAPTF .

The NAPTF, located at the FAA William J. Hughes Technical Center for Advanced Aerospace, Atlantic City International Airport, New Jersey, was commissioned on April 12, 1999. It is a unique test facility that produces full-scale pavement performance data to support the development and verification of airport pavement thickness design procedures and other FAA airport pavement guidance. The NAPTF provides a controlled enclosed test environment where full-scale experimental test pavements are constructed and subjected to simulated aircraft traffic loads using the National Airport Pavement Test Vehicle (NAPTV). Using visual observations, embedded instrumentation, and nondestructive testing (NDT), researchers study the effects of aircraft traffic loading on pavement materials and thickness designs through accelerated life cycle tests.

1.1 OBJECTIVES

CC9 consisted of ten test items organized into four test areas: fatigue model and base course thickness, geosynthetics, cement-treated permeable base (CTPB), and overload. Briefly, the objectives for each CC9 test were as follows:

- Fatigue model and base course thickness: Verify the FAA Rigid and Flexible Iterative Elastic Layered Design (FAARFIELD) fatigue model based on the ratio of dissipated energy change (RDEC) and compare FAARFIELD model predictions of pavement life sensitivity (to base course thickness) to full-scale test results.

- Geosynthetics: Investigate the effect of geosynthetics on flexible airport pavement performance.

- CTPB: Evaluate the performance of P-307 CTPB as a stabilized base under flexible airport pavements.

- Overload: Generate data to support the development of strain criteria for allowable overload in flexible airport pavements.

The following sections show how the design of each test area addressed the above objectives.

1.1.1 Fatigue Model and Base Course Thickness Test Area

The fatigue model and base course thickness test area was designed to support refinements to the FAARFIELD pavement design program. Within FAARFIELD, the asphalt fatigue model is based on the RDEC model (Carpenter et al., 2003), which uses a property derived from an asphalt beam fatigue test (the plateau value [PV]), to predict the number of cycles to fatigue failure (Carpenter et al., 2003; Carpenter & Shen, 2006; and Shen & Carpenter, 2007). While this parameter was based on laboratory testing data, full-scale test data are required to validate, adjust, and modify the fatigue model. The NAPTF CC9 fatigue model test, in combination with earlier data from CC7, provides the necessary data.

The test items in the fatigue model and base course thickness test area were designed with varying base thicknesses. This was done to compare the effect of base course thickness on pavement life in controlled full-scale tests, with life predictions made using the FAARFIELD design model. There is good reason to believe that FAARFIELD's relatively high sensitivity to base course thickness (compared to the sensitivity to asphalt layer thickness) does not adequately reflect the real behavior of pavements. The CC9 test items are designed to test this hypothesis.

1.1.2 Geosynthetics Test Area

The current FAARFIELD design model does not account for the effect of pavement reinforcement. Zornberg (2012) discussed the potential of geosynthetic reinforcement to extend the life of flexible pavements, identifying the lateral restraint mechanisms that lead to increased shear stiffness at the soil/geosynthetic interface. An analytical study supported by the U.S. Army Engineer Research and Development Center (ERDC) found that using geogrids for reinforcement of flexible airfield pavements may extend pavement life up to 26% (Tirado et al., 2014). However, there is a need for full-scale test data showing the effects of geosynthetics on the performance of flexible airfield pavements. Three test items in CC9 were designated as part of the geosynthetics test. Two test items included a geosynthetic separation fabric above the subgrade, and one test item included a geogrid at the base/subbase interface. A third did not include geosynthetics and was the experimental control.

1.1.3 Cement-Treated Permeable Base Test Area

CTPB layers have been used successfully for removing water rapidly from within the pavement structure (Hall et al., 2005) while providing additional load distribution capacity for flexible pavements. CTPB uses the cement paste to stabilize open-graded base course material and reduce or eliminate rutting susceptibility (Liang, 2007). Currently, the FAA does not recommend CTPB as a stabilized base under flexible pavements due to its susceptibility to reflective cracking (FAA, 2018). Furthermore, it is unknown if CTPB construction specifications and design properties developed for rigid pavements are suitable for use with flexible pavement structures. There is a need for full-scale testing performance data to assess the applicability of CTPB for use with flexible airfield pavements and to identify adequate design and construction parameters. In CC9, one test item included a CTPB base layer, while the companion test item had a standard base layer and served as the experimental control.

1.1.4 Overload Test Area

The overload traffic tests conducted by the FAA during CC7 evaluated the overload criteria in International Civil Aviation Organization (ICAO) Annex 14 (ICAO, 2022), which allows occasional aircraft overloads on flexible airport pavements. At the time of the CC7 test, the effective guidance was based on the Aircraft Classification Number-Pavement Classification Number (ACN-PCN) system, which has since been superseded by the Aircraft Classification Rating–Pavement Classification Rating (ACR–PCR) system. The CC7 tests identified potential criteria for limiting overload magnitude, but follow-on testing was warranted. The CC9 Overload test was designed to identify thresholds for vertical top-of-subgrade strain or alternative criteria through accelerated pavement testing. Two CC9 test items were designed as replicates of the CC7 overload test items; one test item received overloads 75% above the PCR while the other served as the control.

1.2 NATIONAL AIRPORT PAVEMENT TEST FACILITY TERMINOLOGY

1.2.1 National Airport Pavement Test Facility Test Terminology

The following sections define terms and phrases commonly used at the NAPTF.

Construction Cycle (CC). CC refers to the overall test project including design, construction, traffic testing, post-traffic testing, data collection, data analysis, and final demolition. Each CC is developed with specific test objectives in mind. Typically, a CC is dedicated to either rigid or flexible pavement testing.

Test Area. Each CC is divided into multiple test areas as required by the test objectives. Dividing the test pavement into test areas allows the FAA to conduct multiple experiments simultaneously. A test area can be made up of one or more test items.

Transition Area. Transition areas separate the test items in the longitudinal direction, avoiding abrupt changes in layer thickness at test item boundaries. Transition areas are of sufficient length to allow vehicle startup and shutdown while maintaining a constant speed and load over the test items themselves, and to allow room for load changes and stabilization between test items.

Test Item. A test item is a unit of pavement within the test area characterized by a unique combination of pavement structure and test traffic. For CC9, each test area was divided into two test items, designated north and south, on the corresponding sides of the facility centerline. Each test item is designated by an identifier consisting of three letters, followed by a dash and two additional characters.

- The first letter corresponds to the strength of the subgrade (L = low strength, M = medium strength, H = high strength).
- The second letter corresponds to the type of pavement structure (F = flexible, R = rigid).
- The third letter corresponds to the type of base (S = stabilized, C = conventional/unstabilized, G = slab-on-grade/no base).
- The last two characters give the sequential numbering of the test item, and whether it is on the north (N) or south (S) side of the centerline.

As an example, in this report the designation LFC-5N refers to the north test item of Test Area 5 that is built on a low strength subgrade (L), using a flexible (F) pavement, with an aggregate (i.e., conventional, C) base course. Test items are numbered from west to east.

Wander Pattern. The NAPTV executes a wander pattern with a repeated sequence of 66 passes arranged in 9 longitudinal tracks. The lateral spacing between adjacent tracks is 10.25 in. The NAPTV wander pattern is designed to approximate a normal lateral distribution of aircraft traffic with a standard deviation from centerline equal to 30.54 in.

1.2.2 Federal Aviation Administration Work Item Modifiers

In general, NAPTF test items follow the material and construction standards in FAA Advisory Circular (AC) 150/5370-10H, *Standard Specifications for Construction of Airports* (FAA, 2018). However, research objectives may require deviation from some aspects of the standard. To indicate that the construction specification is altered, work items are modified with the following designations: M = Modified, R = Research, MR = Modified Research. Material items listed below are modified from the standard FAA specifications.

- P-152MR Subgrade: Work Item P-152MR is a prepared subgrade composed of soil that provides the specified design California Bearing Ratio (CBR) values for test items constructed on low strength subgrades. The subgrade material is prepared in the excavated bed of the NAPTF or the FAA Subgrade Processing building in accordance with the project specifications.

- P-209MR Crushed Aggregate Base Course: Work Item P-209MR is a base course composed of crushed aggregate.

- P-401MR Asphalt Mix Pavement Surface Course: Work Item P-401MR is a hot mix asphalt (HMA) pavement course composed of mineral aggregate and asphalt binder mixed in a central mixing plant, placed on a prepared base or stabilized course, and compacted. It can be used for multiple pavement courses but is typically used as a surface course.

2. DESIGN AND CONSTRUCTION OF TEST AREAS

2.1 DESCRIPTION OF TEST AREAS

CC9 was built on the western end of the NAPTF building as shown in Figure 1. All test areas were built on clay subgrade with a nominal California Bearing Ratio (CBR) of 5 (hence “low-strength,” L).

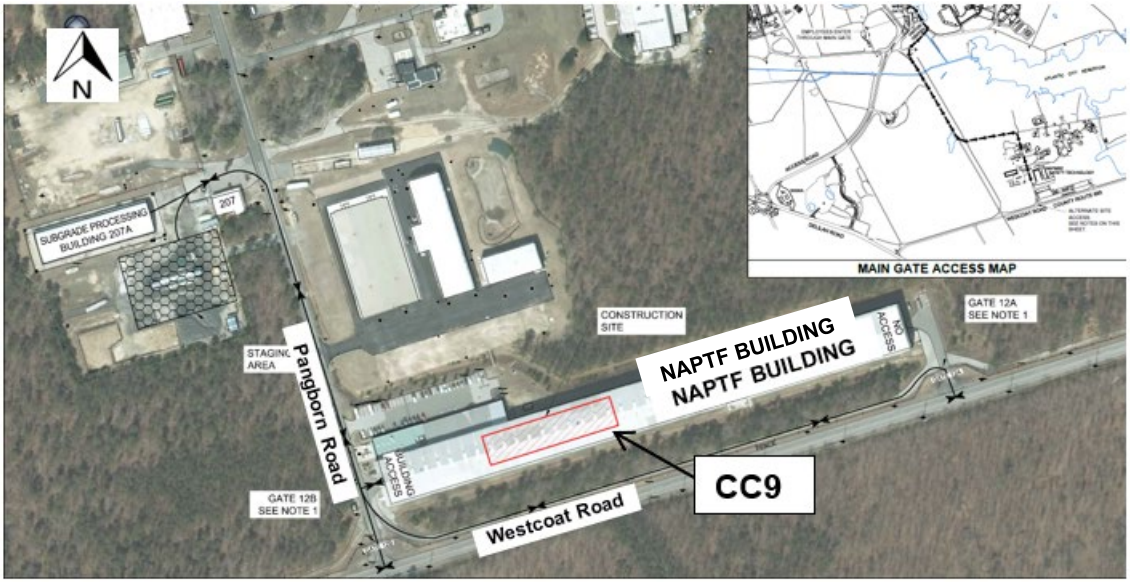

Figure 1. Location of CC9 within NAPTF

CC9 consisted of ten test items, each 45 ft long by 30 ft wide (five north and five south of the centerline), as shown in Figure 2. Test items were separated by 15-foot transition areas. Figure 2 shows how the 10 test items were organized into four test areas. Table 1 summarizes the test items included in each test and the materials for each layer. All test items had a clay subgrade processed to CBR 5. Test item LFC-4S served as the shared control for two tests, geosynthetics and CTPB. Test items LFC-3N and LFC-3S had geosynthetic inclusions, which are discussed in Section 2.1.2.

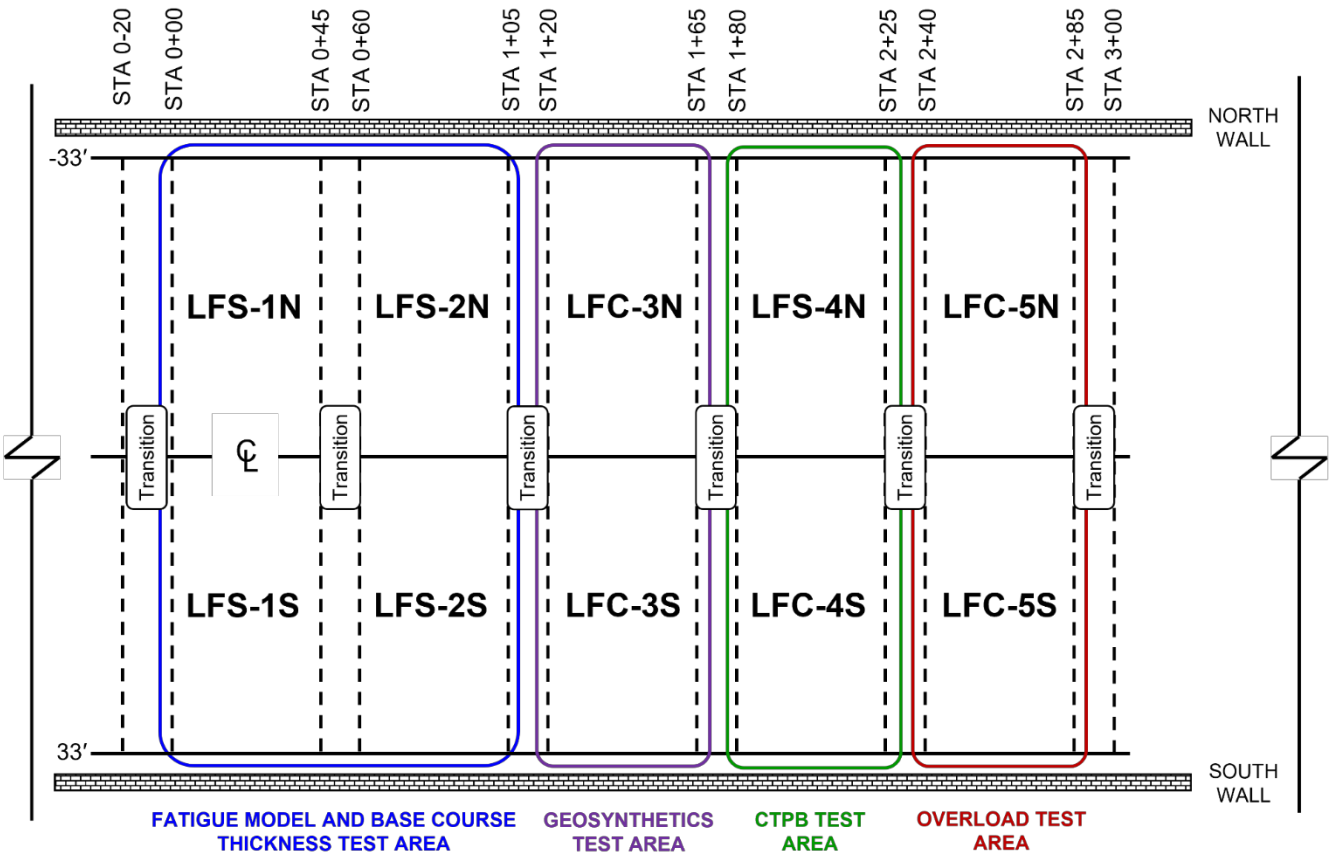

Figure 2. General Layout of the CC9 Test Items

Table 1. Construction Cycle 9 Test Areas

Test Area	Included Test Items	Surface	Base No. 1	Base No. 2/ Subbase
Fatigue Model and Base Course Thickness	LFS-1N LFS-1S LFS-2N LFS-2S	HMA (PG 76-22)	HMA (PG 76-22)	Crushed Aggregate P-209MR
Geosynthetics	LFC-3N LFC-3S LFC-4S	HMA (PG 76-22)	Crushed Aggregate P-209MR	Subbase P-154MR
CTPB	LFS-4N LFC-4S	HMA (PG 76-22)	CTPB P-307MR, or Crushed Aggregate P-209MR	Subbase P-154MR
Overload	LFC-5N LFC-5S	HMA (PG 64-22)	Crushed Aggregate P-209MR	Subbase P-154MR

2.1.1 Fatigue Model and Base Course Thickness Test Items

The four test items included in the fatigue model and base course thickness test area were LFS-1N, LFS-1S, LFS-2N, and LFS-2S. Test items were designed with stabilized (i.e., bound) bases and improved subbases in conformance with FAA standards for flexible pavements serving heavy aircraft, except that the relative thicknesses of asphalt and crushed stone layers were varied, such that the relative contributions of the layers to pavement life could be isolated. Table 2 shows the design thicknesses of the various layers and the preliminary estimates of passes to failure by FAARFIELD, assuming traffic from the 6-wheel NAPTF gear with 58,000 pounds per wheel. As shown, FAARFIELD (v. 2.0) predicts the following sensitivities:

- For 26-in. P-209 base: 22% (2 in.) increase in HMA thickness increases life by 160%.
- For 30-in. P-209 base: 22% (2 in.) increase in HMA thickness increases life by 200%.
- For 11-in. HMA: 15% (4 in.) increase in P-209 thickness increases life by 562%.
- For 9-in. HMA: 15% (4 in.) increase in P-209 thickness increases life by 472%.

Figure 3 shows the as-built cross-sections. While the as-built thicknesses of the asphalt surface and asphalt base layers deviated somewhat from the design, the relative thicknesses of total asphalt and crushed stone base material were close to the design.

Table 2. Design Thicknesses of Fatigue Model and Base Course Thickness Test Items

Test Item	Design Thickness, in.			FAARFIELD 2.0 Passes to Failure
	HMA Surface	HMA Base	P-209MR Cr. Agg.	
LFS-1N	4	7	26	5,870
LFS-1S	4	5	26	2,250
LFS-2N	4	7	30	38,860
LFS-2S	4	5	30	13,010

2.1.2 Geosynthetics Test Items

The geosynthetics test area included test items LFC-3N, LFC-3S, and LFC-4S. These test items had nominally identical layer thicknesses and received identical traffic. The only difference was that LFC-3N and LFC-3S included a Class 2 P-154MR separation fabric installed on top of the clay subgrade. In addition, LFC-3N was reinforced with a Class B geogrid at the base/subbase interface (top of the P-154MR subbase layer). LFC-3S had no geosynthetic inclusions and served as a control. The nominal pavement structure in all three sections was 29-in. subbase, 8-in. crushed aggregate base, and 5-in. HMA surface. The as-built cross-sections of these test items are shown in Figure 3 and Figure 4. As shown, the final dimensions deviated slightly from the design but were sufficiently close for comparison.

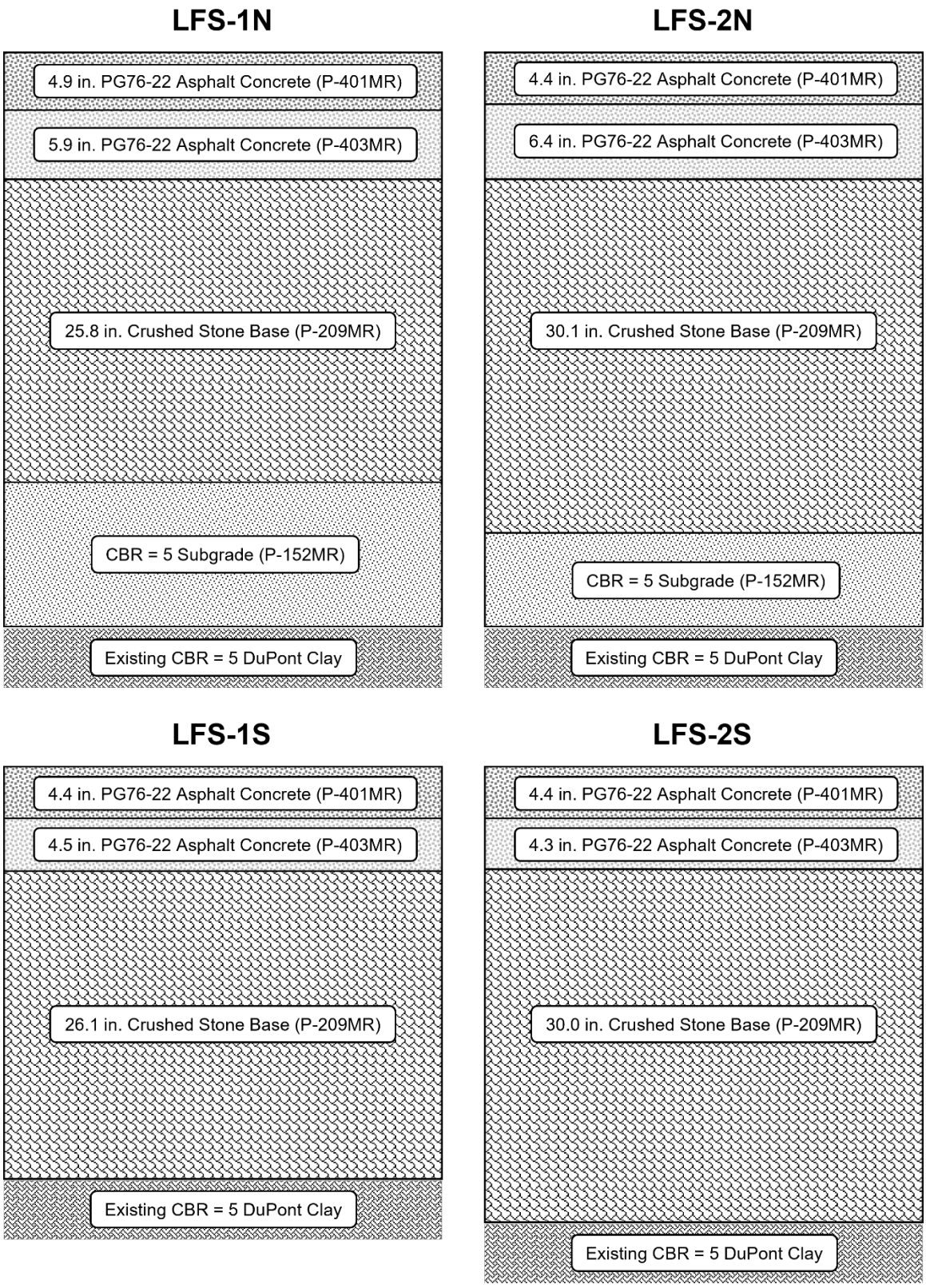

Figure 3. As-Built Cross-Sections of Fatigue Model and Base Course Thickness Test Items

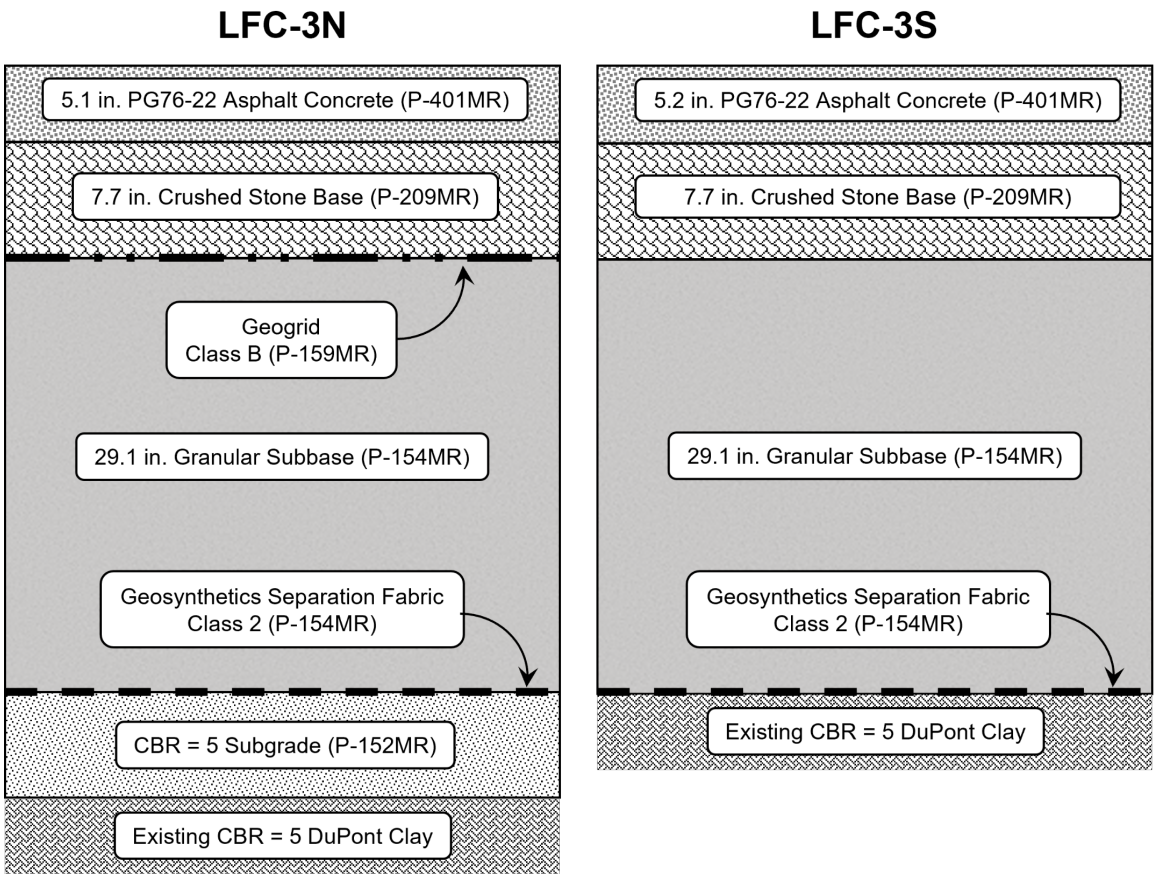

Figure 4. As-Built Cross-Sections of Test Items in Geosynthetics Test Area

2.1.3 Cement-Treated Permeable Base Test Items

The two test items in the CTPB test area were LFS-4N and LFC-4S. The only difference in the designed cross-section was that LFC-4S incorporated standard materials (5-in. HMA surface, 8-in. P-209MR crushed aggregate base, 29-in. P-154MR subbase), while LFS-4N substituted a P-307MR CTPB of equal thickness for the P-209 layer. This arrangement allowed the FAA to evaluate the structural performance of CTPB versus a standard base, with LFC-4S acting as the experimental control. As shown in Figure 5, the as-built cross-sections were close enough to the design to enable a one-to-one comparison.

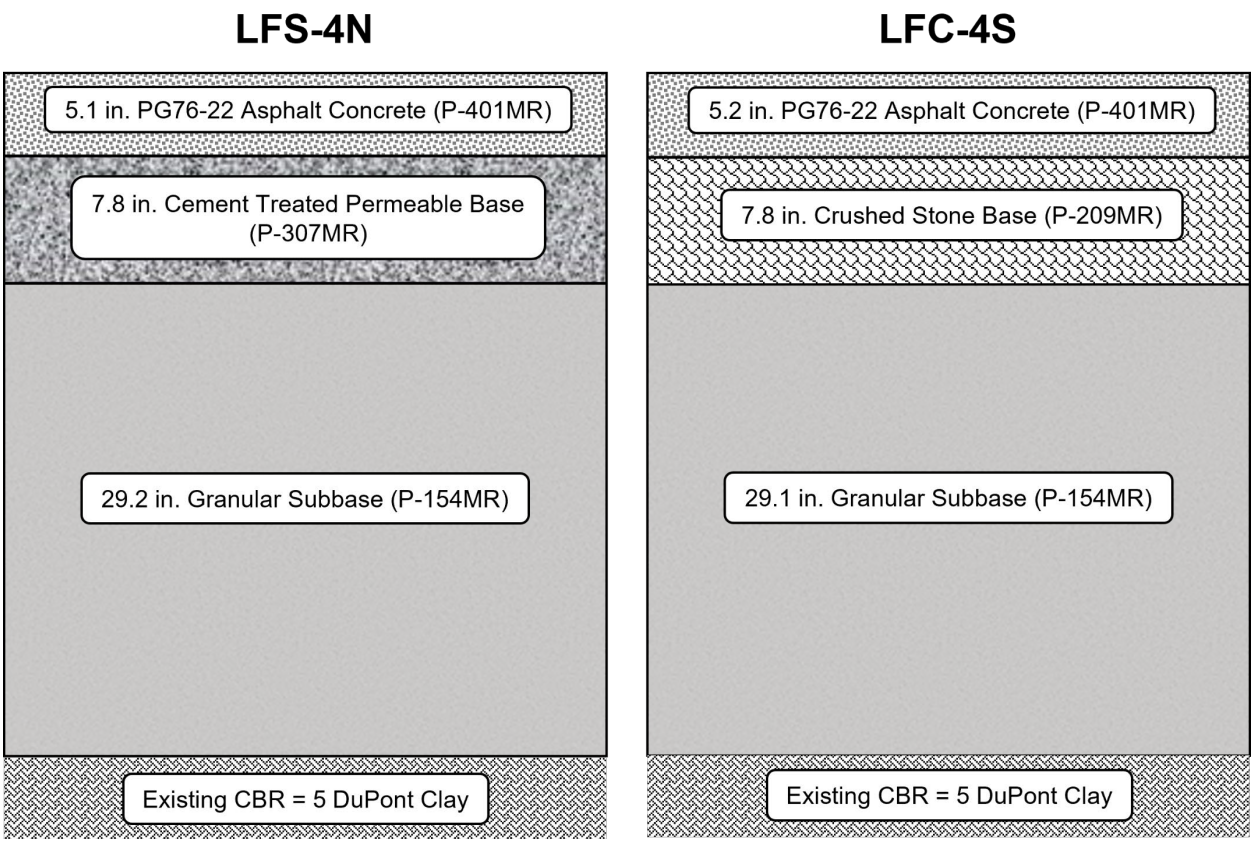

Figure 5. As-Built Cross-Sections of Test Items in CTPB Test Area

2.1.4 Overload Test Items

The dimensions of the two overload test items, LFC-5N and LFC-5S, were chosen to match the previous CC7 overload test items. In both CCs, the design was meant to represent a light load or general aviation airport pavement that may receive occasional overloads from heavy aircraft. Therefore, the vertical dimensions were small relative to the other eight test items: 3-in. HMA surface, 6-in. P-209MR crushed aggregate base, 20-in. P-154MR subbase. Furthermore, while the HMA surface layer conformed to FAA Item P-401, it used an unmodified PG 64-22 binder. Figure 6 shows areas where clay subgrade material was replaced and reprocessed. This was necessary because, while test item LFC-5S replaced an older CC7 test item of the same dimensions, LFC-5N replaced a CC7 test item with a deeper total structure. Therefore, it was necessary to build up the subgrade on the LFC-5N side to match the top-of-subgrade elevations.

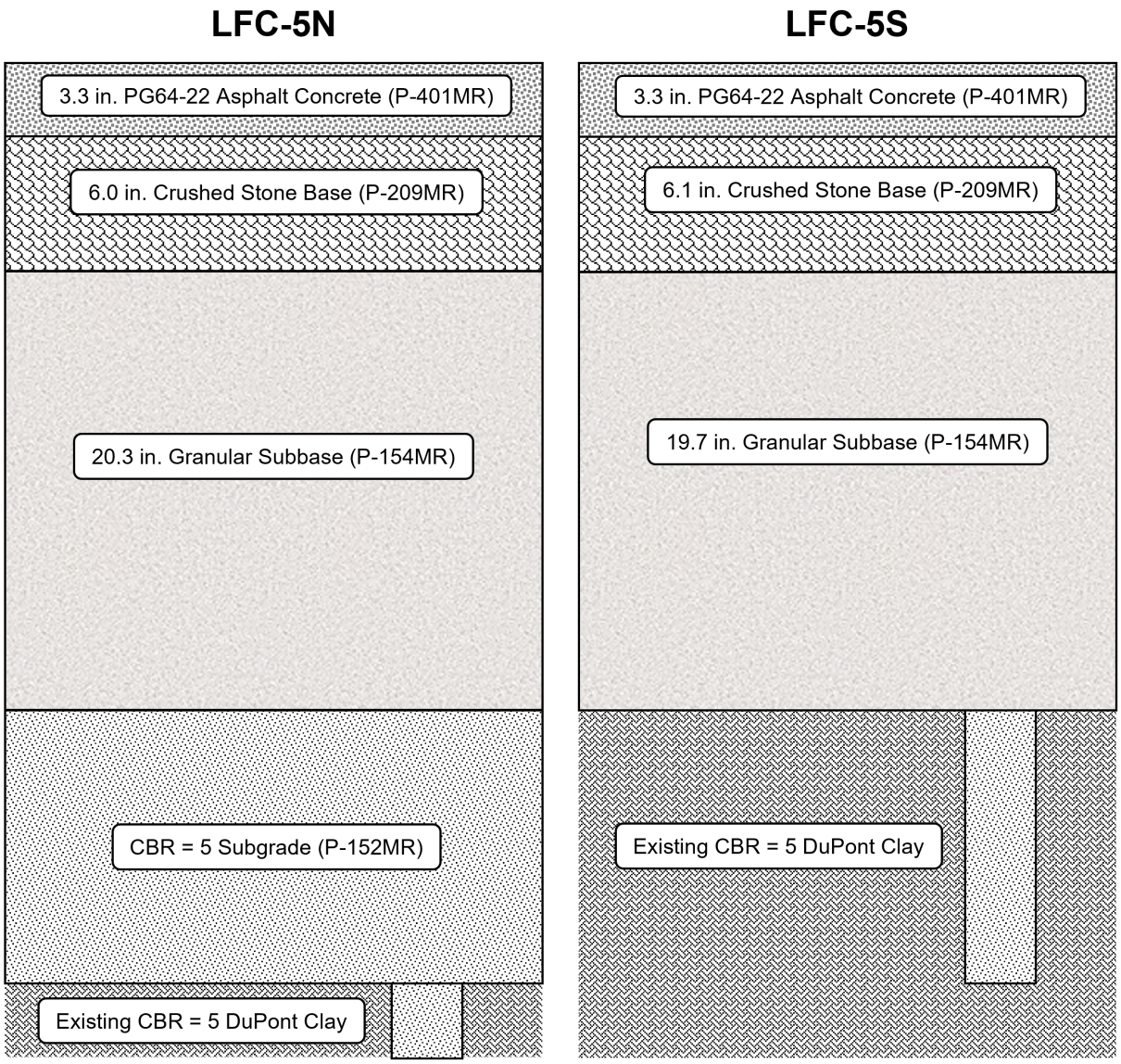

Figure 6. As-Built Cross-Sections of Test Items in the Overload Area

2.2 CONSTRUCTION

Construction of CC9 started on February 4, 2019, with off-site processing of the clay subgrade material, and ended on December 23, 2019, after the completion of pavement marking. This report contains only a general overview of CC9 construction activities. Full construction documentation is provided in Tomlinson et al. (2022). Additional discussions of test area-specific construction highlights, quality control and assurance, and in-place testing may be found in the companion CC9 reports, Volumes 2 through 5.

2.2.1 Subgrade (P-152MR)

Subgrade construction work was done for all test items (station 0+00 to 2+85). Due to the profile left over from CC7 (where test items on the south were shallow compared to those on the north), north of centerline was infill, while south of centerline was incut. Clay cuts from the south were used as fill material for the north side. As needed, additional clay fill was hauled from the NAPTF Subgrade Processing Facility (located on site approximately 800 ft northwest of the NAPTF). For the stockpiled clay from the processing facility, engineers identified a target moisture content of approximately 23.5% to 24.0% to achieve CBR 5.

The subgrade was accepted based on CBR (±0.5 of target), smoothness, and grade. Following CBR acceptance, the surface was trimmed using an excavator with a grading bucket to attain the final grade. Once the finished surface passed grade and smoothness, engineers conducted material characterization testing, followed by sensor installation.

2.2.2 Granular Subbase (P-154MR)

Subbase construction following the P-154 modified specification was performed in the geosynthetics, CTPB, and overload test areas (stations 1+20 to 2+85). As in previous CCs, the subbase material consisted of carbonate-based manufactured quarry screenings (USCS SP-SM). Subbase material was compacted to a target dry density of 138.3 pounds per cubic feet (pcf) (or higher) and moisture content between 2% and 6%. The target density corresponded to the maximum achievable density at 6% moisture content per the modified proctor curve. The maximum of 6% moisture content was intended to limit the potential for drain-down of water into the subgrade. The final P-154MR surface lift was slightly overbuilt. Following acceptance testing, the surface was trimmed to achieve the design elevation using a grader. Once the finished surface passed grade and smoothness, engineers conducted material characterization testing, followed by sensor installation.

2.2.3 Geosynthetics and Geogrid (P-159MR)

As shown in Figure 4, a Class 2 separation fabric (Mirafi nonwoven 160N) was installed at the surface of the subgrade (between the clay subgrade and P-154MR subbase) in two test items in the Geosynthetics test area. As reported by the manufacturer, the nonwoven geotextile had a CBR puncture strength of 434 lb; grab tensile strengths in the machine and cross directions of 201 and 172 lb, respectively; and trapezoid tear strength for both machine and cross directions of 77 lb (Tomlinson et al., 2022, Appendix F). The 12.5-foot-wide fabric was placed transversely across the width of the test item with an overlap of 18 in. for each transverse placement. Also, as shown in Figure 4, a Class B geogrid (Tensar® Biaxial BXSQ2020) was installed at the interface between the base and subbase in test item LFC-3N. The biaxial geogrid had a 1.5-in. square aperture with minimum rib thicknesses of 0.04 and 0.03 in. along the machine and cross-machine directions. The manufacturer reported the tensile strengths at 2% and 5% strains, and ultimate strength, as 450, 890, and 1,370 lb/ft respectively. The biaxial geogrid was cut into three widths (13.1 ft, 8.3 ft, and 13.1 ft) and placed longitudinally from station 1+13 to station 1+73. with a 1.5-ft overlap between cuts.

2.2.4 Crushed Aggregate Base Course (P-209MR)

Crushed aggregate material meeting the P-209MR modified specification was used as a component in all test items except LFS-4N. In test items LFC-3N/S, LFC-3S, and LFC-5N/S, the crushed aggregate material was placed as a base course on top of the granular subbase (P-154MR). In the fatigue model and base course thickness test area (test items LFS-1N/S and LFS-2N/S), the crushed aggregate base material was used as an improved subbase and placed directly on the clay subgrade. Crushed aggregate base material was compacted to a target dry density of 151.3 pcf (or higher) and moisture content between 1.5% and 5.5%. The target density corresponds to the maximum modified proctor density. The maximum 5.5% moisture content was intended to limit the potential for drain-down of water into the subgrade. For moisture control during placement, water was added to the material as needed by means of a spray bar attachment on a bridge deck finisher (BDF) equipped to travel on the rails at the NAPTF.

Crushed aggregate base was accepted based on density, smoothness, and grade. A nuclear density gauge (NDG) was used to measure density and moisture content in situ at depths not exceeding the lift thickness. Once the target moisture content was achieved, the P-209MR was compacted for NDG acceptance testing. The thickness of compacted lifts was between 4 and 8 in. The final P-209MR surface lift was slightly overbuilt. Following NDG acceptance testing, the surface was trimmed to achieve the design elevation using a grader. Once the finished surface passed grade and smoothness testing, engineers conducted material characterization tests, followed by sensor installation.

2.2.5 Cement-Treated Permeable Base

For test item LFS-4N, engineers developed a CTPB mix design meeting specification Item P-307MR (3). In addition to the items in Table 3, a water-reducing admixture was incorporated into the mix at a rate of 6 fl. oz/yd. The mix design produced a 7-day average compressive strength (ASTM, 2015) of 640 psi, meeting the FAA's mix design requirement (400–800 psi). Using the developed mix, engineers placed a test strip (ASTM, 2020a) and measured the permeability at 2019 ft/day. The measure permeability exceeds the upper limit on coefficient of permeability per AC 150/5370-10H, Item P-307 (500–1500 ft/day).

Table 3. Cement-Treated Permeable Base Mix Design

Material	Type	Quantity per Unit Volume
Portland Cement	Type I	130 lb/yd^3
Slag Cement	Ground granulated blast furnace slag - grade 120	70 lb/yd^3
Coarse Aggregate	Stone size 57 per ASTM C33	2,300 lb/yd^3
Fine Aggregate	Sand	327 lb/yd^3
Water	Potable (water-cement ratio = 0.36)	72 lb/yd^3
Air Content		35%
Total		2,899 lb/yd^3

CTPB construction on LFS-4N was completed in two placements using a form-riding, triple-roller tube paver. The placements took place one week apart during October 2019. The surface of

the P-154MR subbase course was dampened shortly before each placement to prevent moisture loss of the CTPB mix from absorption by the underlying aggregate. After initial consolidation with the first pass of the form-riding paver, the 5-in. target thickness was achieved with four and six additional passes for the first and second placement, respectively. Base material (P-209MR) was used to complete the base course construction over a 3-ft width for the north shoulder of LFS-4N. After the finished surface passed grade and smoothness, engineers conducted material characterization tests. No instrumentation was installed within the CTPB.

2.2.6 Asphalt Concrete Surface Course and Stabilized Base (P-401MR/P-403MR)

Two asphalt mixes were used for CC9. The overload test area used a P-401MR mix with PG 64-22 (unmodified) binder, while the other test areas used a PG 76-22 polymer-modified binder. The same aggregate gradation and asphalt content were used for both mixes. The mix was designed with an asphalt content of 5% to produce air voids of 3.5% in the laboratory.

Asphalt paving was completed in three days from December 10–13, 2019. Neat binder (PG 64-22) was used as tack coat on lower lifts. After acceptance for density (NDG test), surface grade, and smoothness, contractors extracted cores for laboratory acceptance testing. Finally, engineers performed a variety of field characterization tests on the accepted product. Appendix A summarizes the asphalt acceptance and material characterization test results for all test areas.

2.3 INSTRUMENTATION

The CC9 test pavement included the following sensor types: asphalt strain gauges (ASGs), pressure cells (PCs), thermocouples (Ts), moisture sensors (MSs), and coil sensors (CSs). Appendix B lists locations of all embedded sensors, referenced by longitudinal station (along the NAPTF centerline), offset (negative values left/north, positive values right/south of centerline), and depth from finished surface. The convention used to name the sensors consists of three components, separated by dashes: sensor type, test item, and sequential number. For example, TSG-LFS2S-4 stands for transverse (asphalt) strain gauge (TSG) in test item LFS-2S (LFS2S), number four (4).

In addition to the sensors in Appendix B, the FAA placed a small number of experimental sensors in the geosynthetics test area under cooperative research agreements between the FAA and universities. The Pennsylvania State University researchers installed a limited number of "smart rocks," sensors equipped with accelerometers and intended to mimic the behavior of aggregate particles in base layers. The smart rocks have a limited battery life, and, unfortunately, due to delays caused by the 2020 Covid-19 pandemic, they could not acquire data during traffic. The University of Illinois at Urbana-Champaign provided bender element sensors to measure changes in aggregate layer modulus in the geosynthetic-reinforced test items. Bender elements are addressed in a separate report (Tutumluer et al., 2024).

Each test item included longitudinal ASGs (LSG) and TSGs at the bottom of the asphalt layer to measure horizontal strains. Eight ASGs were installed in each of the 10 test items (4 LSGs and 4 TSGs) for a total of 80. PCs were installed in all the test items at various depths. ASGs were positioned such that a pass on the center track of the wander pattern (Track 0) caused the maximum response (wheel passing directly over the sensors). PCs were placed at the center of

the trafficked lane (offsets ±15 ft), so that an offset wander position (Pass +3 or -3) caused the maximum PC response from a pass of dual tires.
Thermocouple trees were installed in all north test items except LFS-2N. Only one thermocouple tree was installed in the south test items (LFS-1S). MSs were installed at depths within the subgrade to monitor changes in moisture content.

CC9 was the first NAPTF CC to use induction coils for monitoring the behavior of unbound layers. The induction-coil-based strain measurement system (known as ε-mu, an acronym for strain (ε) measuring unit) has been used extensively to monitor permanent deformation and strain in pavement subsurface layers. The system was originally developed by Selig and Grangaard (1970). The data acquisition process was later automated by Dawson (1994). In CC9, the CS pairs located at the top of unbound layers were intended to operate in dynamic mode to record transient strain responses to aircraft loads. CS stacks installed throughout the entire thickness of the P-209MR base course in specific test items were intended to operate in static mode to capture and monitor permanent deformation.

3. TEST EQUIPMENT AND METHODS

3.1 TEST EQUIPMENT

The NAPTV can be programmed for controlled aircraft wander simulation and can operate in manual or fully automatic modes. The NAPTV can simulate typical aircraft wander by varying the lateral position of the carriages to approximate a normal distribution. The test vehicle is composed of two carriages that can accommodate up to five load modules spaced 57 in. apart in tandem. Each load module used in CC9 has two wheels with a typical dual spacing of 54 in. This allows for configurations of up to 20 wheels, with loads up to 75,000 lb per wheel. Figure 7 shows the photograph of the NAPTV.

Figure 7. National Airport Pavement Test Vehicle

For the following CC9 test areas, both north and south carriages of the NAPTV were configured as a six-wheel (3D) gear: Fatigue Model, Geosynthetics, and CTPB (Figure 8). For the overload test area, both north and south carriages were configured as a two-wheel (2D) gear. The basic wander pattern consisted of 66 vehicle passes, arranged in 9 discrete tracks (or lateral offset positions). The vehicle speed was 2.5 mph. Nominal tire pressure was 255 psi for all test areas except overload, for which the nominal tire pressure was 200 psi.

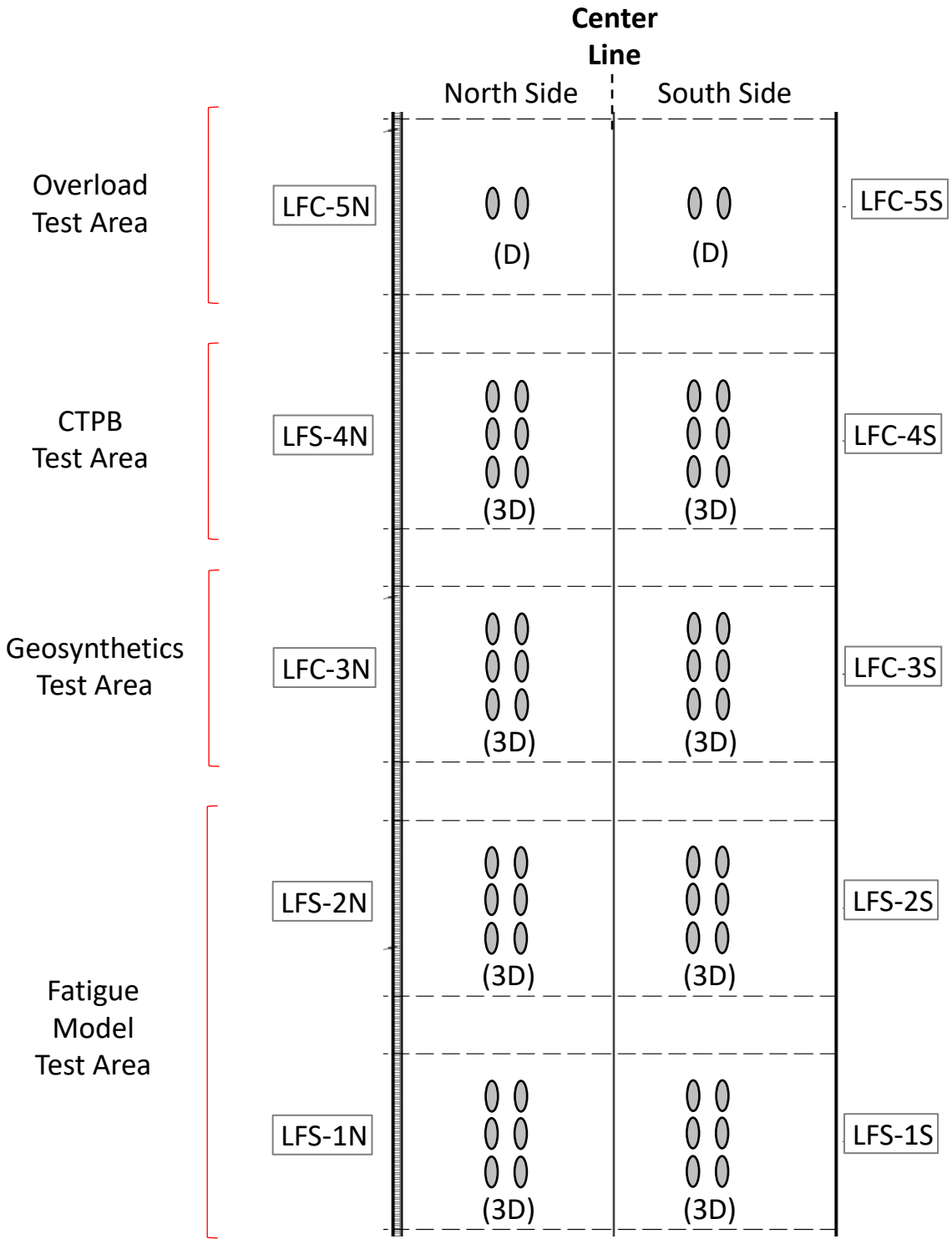

Figure 8. Gear Configurations Used in CC9 Traffic Test

3.2 TEST DESCRIPTION

3.2.1 Pre-Traffic Tests

Prior to the start of full-load traffic tests on CC9, the FAA completed several preliminary operations using the NAPTV at reduced loads. The preliminary (pre-traffic) tests were slow-roll response test, proof-roll test, and ramp-up response test (the last on the overload test area only). In addition, the FAA performed a suite of NDT tests after construction acceptance and before the start of traffic testing for the purpose of establishing the baseline conditions. The schedule of pre-traffic operations is shown in Table 4. A complete description of the NDT testing, including the baseline tests, may be found in Mazzotta et al. (2024).

Table 4. Schedule of Pre-Traffic Tests

Test	Dates	Test Items
Baseline NDT (Set 1)	September 10, 2020	All
Slow-roll response test	November 6–20, 2020	All
Baseline NDT (Set 2)	Jan. 28/Feb. 4, 2021	All
Proof-roll test	February 23, 2021	All
Post-proof-roll baseline NDT (Set 3)	February 25, 2021	All
Slow-roll response test (Redo)	March 1–2, 2021	LFS-1N/S, LFS-2N/S
Ramp-up response test	March 8, 2021	LFC-5N
Pre-traffic baseline NDT (Set 4)	March 18–April 2, 2021	LFS-1N/S, LFS-2N/S, LFC-3N/S, LFS-4N, LFC-3S
Pre-traffic baseline NDT (Set 4)	June 24–30, 2021	LFC-5N/S

3.2.1.1 Slow-Roll Response Test

The purpose of the slow-roll response test was to verify the functionality of in-pavement sensors for a range of loads and vehicle speeds. The slow-roll response test was executed November 6–20, 2020, on all test items. During the initial test, a malfunction was observed in one of the NAPTF signal processing units (SPU-1) that affected responses from test items LFS-1 and LFS-2. The test was redone (March 1–2, 2021) on only those test items after repairs to SPU-1.

Pavement responses (stresses, strains, deflections) were recorded for the following gear configurations: single (one-wheel) (S), dual (two-wheel) (D), 2D, 3D. For all test items except those in the overload test area, the response test variable matrix was as follows:

- Vehicle speed (mph): 0.5, 1.6, 2.5
- Gear offset from centerline (ft): ±8.25, ±10.50, ±12.75, ±15.00, ±17.25, ±19.50
- Wheel Loads (lb): 12,000, 24,000, 36,000
- Tire Pressure: 255 psi.
- Passes: two passes for each wheel load at each offset (one forward, one return).

For the overload test area only (LFC-5N, LFC-5S) the response test variable matrix was the same as above, except that the wheel loads were 8,000 lb, 12,000 lb, and 16,000 lb.

Sensor responses from the slow-roll response tests were mostly correct, i.e., the signal shapes were generally as expected, and peak response values from ASGs increased with increasing load and slower vehicle speed. However, the slow-roll response tests revealed two problems with respect to PCs and CS pairs:

1. Some PCs, specifically those in the upper structural layers of test items LFC-3N, LFC-3S, and LFC-4S, were undersized compared to the peak loads received. Installed PCs had a standard rating of 58.0 psi but could read up to 1.5 times their rated pressure (87 psi) per the manufacturer's specification. Slow-roll response test data at 0.5 mph showed that PCs at the bottom of the base layer were subject to maximum pressures exceeding 90 psi, and, as a result, the response peaks were cut off at high loads.

2. The output from CS pairs in dynamic mode was very sensitive to the vehicle movements, resulting in an unusual "hump"-shaped response curve that tended to overwhelm the actual load-induced deflection response. In Figure 9, the large magnitude rise and fall of the curve is simply noise induced by the passage of the NAPTV (and its electric motors). The actual response to the wheel load is indicated by the highlighted area. To extract the peak response of interest, it was necessary to remove the unwanted part of the signal by applying a postprocessing script consisting of a series of two locally estimated scatterplot smoothing (LOESS) filters (coarse and fine) to the original data.

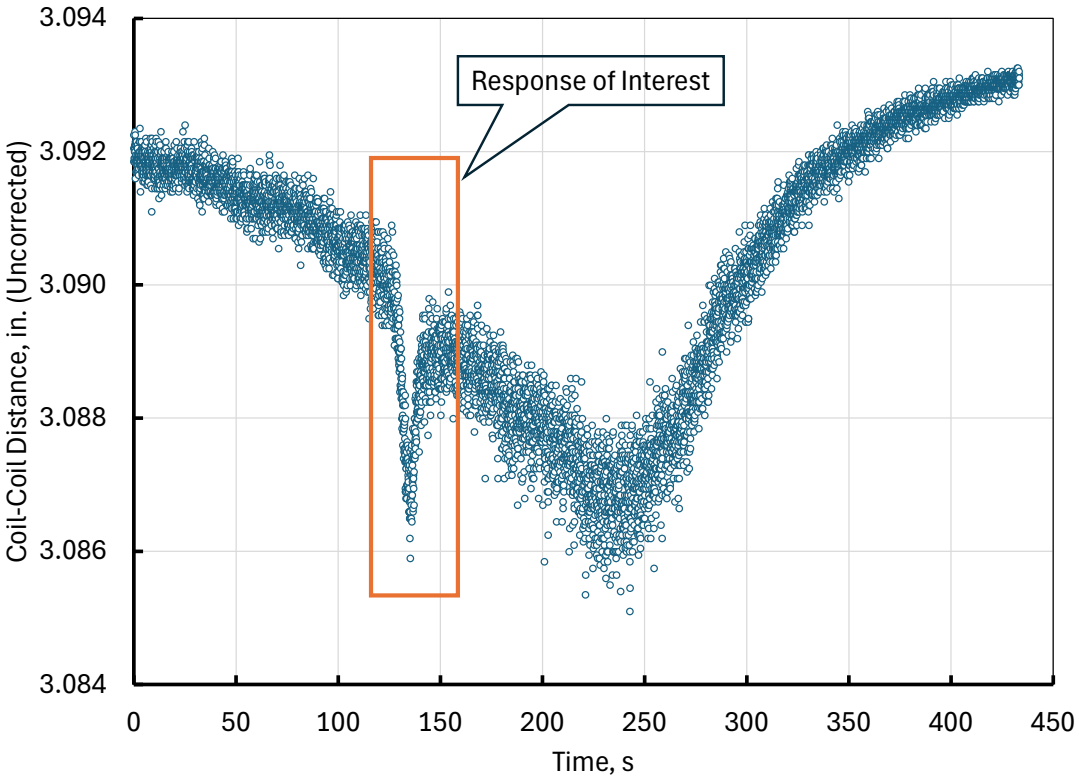

Figure 9. Example of an Uncorrected CS Response to Slow-Rolling Response Test Data—Response of CS Pair CS-LFS-2N-3/4 (Pass 41, November 13, 2020)

3.2.1.2 Proof-Roll Test

The proof-roll test was performed on February 23, 2021, by executing the special wander pattern in Table 5 and Figure 10. The purpose of the proof-roll test was to cover the trafficked surface completely and expose any weak areas. Loads were kept low to avoid damage. All test areas, except the overload test area, received proof-roll traffic from a two-wheel (D) gear at 20,000 lb per wheel. The overload test area (LFC-5N, LFC-5S) received traffic from a two-wheel (D) gear at 15,000 lb per wheel.

Table 5. Carriage Positions for Each Pass of Proof-Roll Wander

Pass Sequence	Direction (W = West E = East)	Carriage Centerline Location (ft)	
		North	South
1	W–E	-19.34	2.68
2	E–W	-19.34	2.68
3	W–E	-18.507	3.513
4	E–W	-18.507	3.513
5	W–E	-17.674	4.346
6	E–W	-17.674	4.346
7	W–E	-16.841	5.179
8	E–W	-16.841	5.179
9	W–E	-16.008	6.012
10	E–W	-16.008	6.012
11	W–E	-15.175	6.845
12	E–W	-15.175	6.845
13	W–E	-14.342	7.678
14	E–W	-14.342	7.678
15	W–E	-13.509	8.511
16	E–W	-13.509	8.511
17	W–E	-12.676	9.344
18	E–W	-12.676	9.344
19	W–E	-11.843	10.177
20	E–W	-11.843	10.177
21	W–E	-11.01	11.01

Pass Sequence	Direction	Carriage Centerline Location (ft)	
		North	South
22	E–W	-11.01	11.01
23	W–E	-10.177	11.843
24	E–W	-10.177	11.843
25	W–E	-9.344	12.676
26	E–W	-9.344	12.676
27	W–E	-8.511	13.509
28	E–W	-8.511	13.509
29	W–E	-7.678	14.342
30	E–W	-7.678	14.342
31	W–E	-6.845	15.175
32	E–W	-6.845	15.175
33	W–E	-6.012	16.008
34	E–W	-6.012	16.008
35	W–E	-5.179	16.841
36	E–W	-5.179	16.841
37	W–E	-4.346	17.674
38	E–W	-4.346	17.674
39	W–E	-3.513	18.507
40	E–W	-3.513	18.507
41	W–E	-2.68	19.34
42	E–W	-2.68	19.34

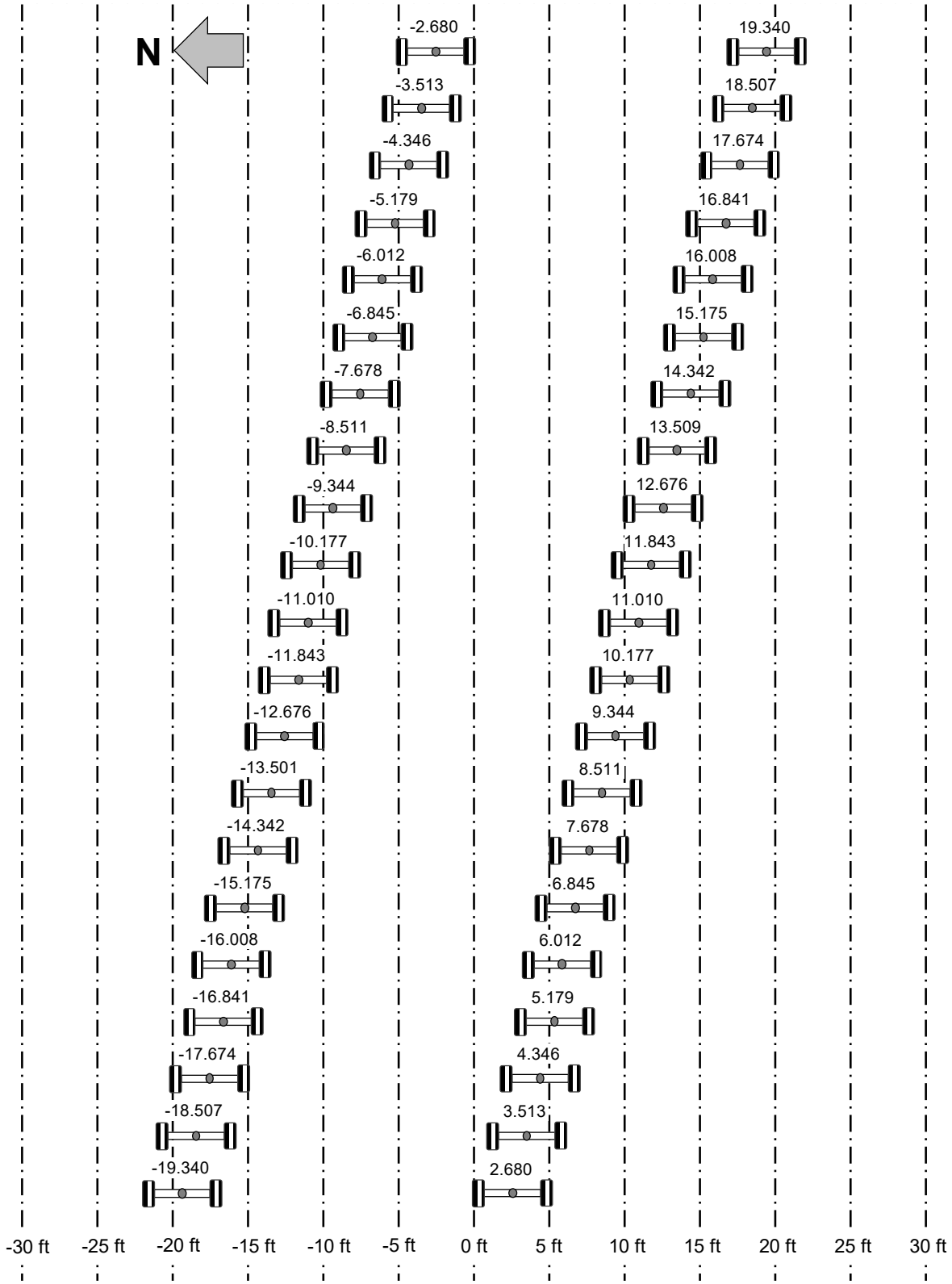

Figure 10. Carriage Positions for Each Pass of Proof-Roll Wander

3.2.1.3 Ramp-up Response Test

The ramp-up response test was executed on March 8, 2021, on test item LFC-5N only. The purpose of the ramp-up response test data was twofold:

- Confirm that that planned wheel loads would be sufficient to fail the overload test items within a reasonable time.
- Adjust the planned wheel loads if the test revealed significant discrepancies between measured and predicted responses.

The test was conducted on test item LFC-5N using a "D" gear configuration. The vehicle speed was 2.5 mph, and the nominal tire pressure was 255 psi throughout the test. The test was conducted using the following test procedure:

1. Traffic the entire length of the LFC-5N on Track 0 (test item center line at offset -15 ft) using the above parameters. Traffic in both directions (west-to-east and east-to-west) at an initial wheel load of 16,000 lb.
2. After trafficking in both directions, check the test item for damage. Had any significant damage (e.g., surface rut and cracks) been observed at this stage, the ramp-up response test would have been terminated. However, no damage was observed.
3. Monitor the total vertical strain from CS pair CS-LFC5N-3/4 for any indication of disproportionate damage to the subgrade. In addition, monitor unrecoverable strains (i.e., the difference between left and right offset on the response curve) between load increments.
4. Increase the wheel load in 5,000-lb increments. Repeat steps 2 through 4 until either (a) damage is observed in the CS pair response, or (b) the wheel load reaches 56,000 lb. In execution, the load reached the target of 56,000 lb with no damage observed.

3.2.1.4 Baseline Nondestructive Testing

Pre-traffic NDT and characterization consisted of four elements:

1. Heavy weight deflectometer (HWD) to obtain back-calculated layer moduli and verify construction uniformity,
2. Portable seismic pavement analyzer (PSPA) measurements to obtain in situ HMA layer modulus,
3. Initial transverse profile measurements using a straightedge following ASTM E1703, to identify pre-existing surface ruts, and
4. Laser scanning of the entire pavement surface using a Leica Model P20 360° laser scanner.

Four sets of HWD and PSPA tests were conducted on the untrafficked pavement surface, as follows:

- The initial set of baseline testing was conducted before any other pre-traffic activities. In addition to uniformity tests, HWD drops were conducted at selected sensor locations (PCs and CSs) to verify instrumentation response.
- Set no. 2 was performed in conjunction with the slow-roll response test.
- Set no. 3 was conducted post-proof-roll.
- Set no. 4 was conducted just before the start of the traffic test.

HWD and PSPA tests were conducted at six locations in each test item. Figure 11 shows the location of tests for test items LFS-1 and LFS-2. Other test items had a similar layout. Test locations were marked on two transverse lines located at the third points of the test item (gray lines in Figure 11), so that the tests covered the instrumented area. The offsets 15 ft left and right of the facility centerline align with the center of traffic for the north and south test items respectively. The ±5 and ±25-foot transverse offsets align with the untrafficked areas of the test items.

For test items LFC-5N and LFC-5S, HWD testing was conducted with a four-drop loading sequence beginning with an approximate 24,000-lb seating load. Subsequent loads were approximately 6,000 lb, 12,000 lb, and 24,000 lb. For all other test items, HWD testing was conducted with a four-drop loading sequence beginning with an approximate 36,000-lb seating load. Subsequent loads were approximately 12,000 lb, 24,000 lb, and 36,000 lb.

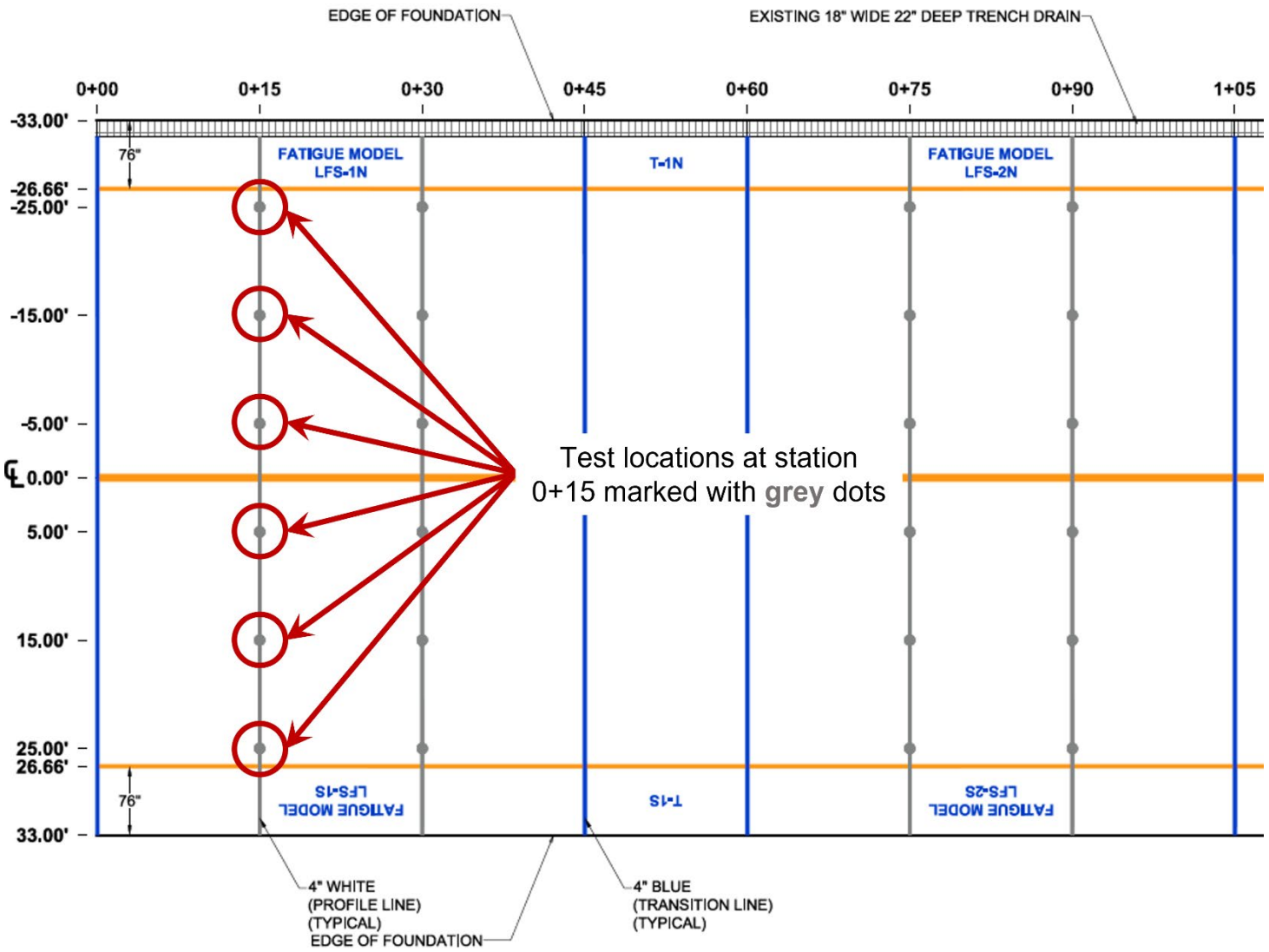

Figure 11. Sample HWD and PSPA Testing Locations in Fatigue Test Items

3.2.2 Traffic Test

Table 6 summarizes the full traffic test history on CC9. As shown in Table 6, not all test items were trafficked simultaneously. Reasons for different trafficking schedules for different test items were:

1. The start of traffic on the overload test (LFC-5N and LFC-5S) was delayed until the results of the preliminary ramp-up response test (Section 3.2.1.3) could be fully analyzed and the overload magnitude finalized.

2. Following the first overload (July 1, 2021), "catch-up" traffic was applied to the overload test area only, to match the number of passes on all test items.

3. After the failure of test items LFC-3N, LFC-3S, LFS-4N, and LFC-4S, traffic was continued on test items LFC-5N and LFC-5S only. By trafficking only LFC-5 and delaying traffic on LFS-1 and LFS-2 until colder weather arrived, NAPTF operators could (a) avoid unnecessary and time-wasting vehicle "flyovers" over the failed test items and (b) finish the overload test sooner (i.e., before the colder temperatures).

4. One of the key goals of the fatigue model and base course thickness test was to observe the development of asphalt fatigue in those test items. In contrast to the other test items where warm temperatures were preferred, cooler temperatures were better for testing LFS-1 and LFS-2. In the last phase of testing in 2023 and 2024, the FAA decided to place test items LFS-1 and LFS-2 under traffic only during the cold winter months. From March 30, 2023, to January 24, 2024, no traffic took place on CC9; during that period the vehicle was used to traffic CC8 in a different part of the NAPTF.

Table 6. Construction Cycle 9 Traffic Summary

	Passes on Test Items			
Dates	LFS-1/2	LFC-3/4	LFC-5	Load Description
4/5/2021–6/3/2021	5,544	5, 544	0	Traffic test items 1–4
7/6/2021	0	0	66	First overload LFC-5N
7/6/2021–7/28/2021	0	0	5,478	Traffic LFC-5 only
8/2/2021–10/14/2021	7,066	7,066	7,066	Traffic all test items
10/15/2021–2/21/2022	0	0	0	Vehicle down for maintenance
2/22/2022–3/28/2022	3,956	3,956	3,956	Resume traffic all test items
3/29/2022	0	0	66	Second overload LFC-5N
3/29/2022–10/5/2022	24,354	24,354	24,288	Traffic all test items
10/12/2022	0	0	396	Third overload LFC-5N
10/13/2022–12/21/2022	0	0	15,312	Traffic LFC-5 only
1/3/2023–3/29/2023	13,662	0	0	Traffic test items LFS-1/2
1/25/2024–4/2/2024	20,460	0	0	Traffic test items LFS-1/2
Total	75,042	40,920	56,628	

Between October 15, 2021, and February 21, 2022, the NAPTV was out of service for maintenance and repair. This resulted in an unexpected interruption of traffic. While the traffic

pause was not planned, it nevertheless allowed engineers to analyze the results of traffic stoppage followed by resumption. These effects are discussed in detail in the volumes covering results and analysis for individual tests. Appendix C contains a detailed log of traffic applied to all test items.

3.2.2.1 Failure Criteria

Ahlvin et al. (1971) defined failure criteria as when:

(i) Surface upheaval of the pavement adjacent to the traffic wander exceeds 1 in., or
(ii) Surface cracking becomes so severe that the pavement no longer remains waterproof.

These failure criteria were adopted in all preceding flexible pavement construction cycles. CC9 test items were considered failed when either or both conditions were met. For the fatigue model and base course thickness test, based on the performance of similar test items in previous NAPTF CCs, it was not expected that test items LFS-1 and LFS-2 would necessarily fail according to criterion (ii) (i.e., subgrade shear failure), although significant cracking of the asphalt surface was expected. The geosynthetics and CTPB test items were tested past the point of technical failure, for the sake of collecting as much post-failure data as possible.

3.2.2.2 Wander Pattern

The wander pattern consisted of 66 passes (sequences) arranged in 9 wheel tracks, as shown in Table 7 and Figure 12. Passes are in both directions, west-to-east (odd) and east-to-west (even). The even-numbered (return) pass is always along the same track as the preceding odd-numbered pass, but in the opposite direction. The complete wander pattern is detailed in Table 8.

Table 7. Construction Cycle 9 Wander Tracks

	Carriage Centerline Location, ft	
Track No.	North	South
-4	-18.412	11.588
-3	-17.559	12.441
-2	-16.706	13.294
-1	-15.853	14.147
0	-15.000	15.000
1	-14.147	15.853
2	-13.294	16.706
3	-12.441	17.559
4	-11.588	18.412

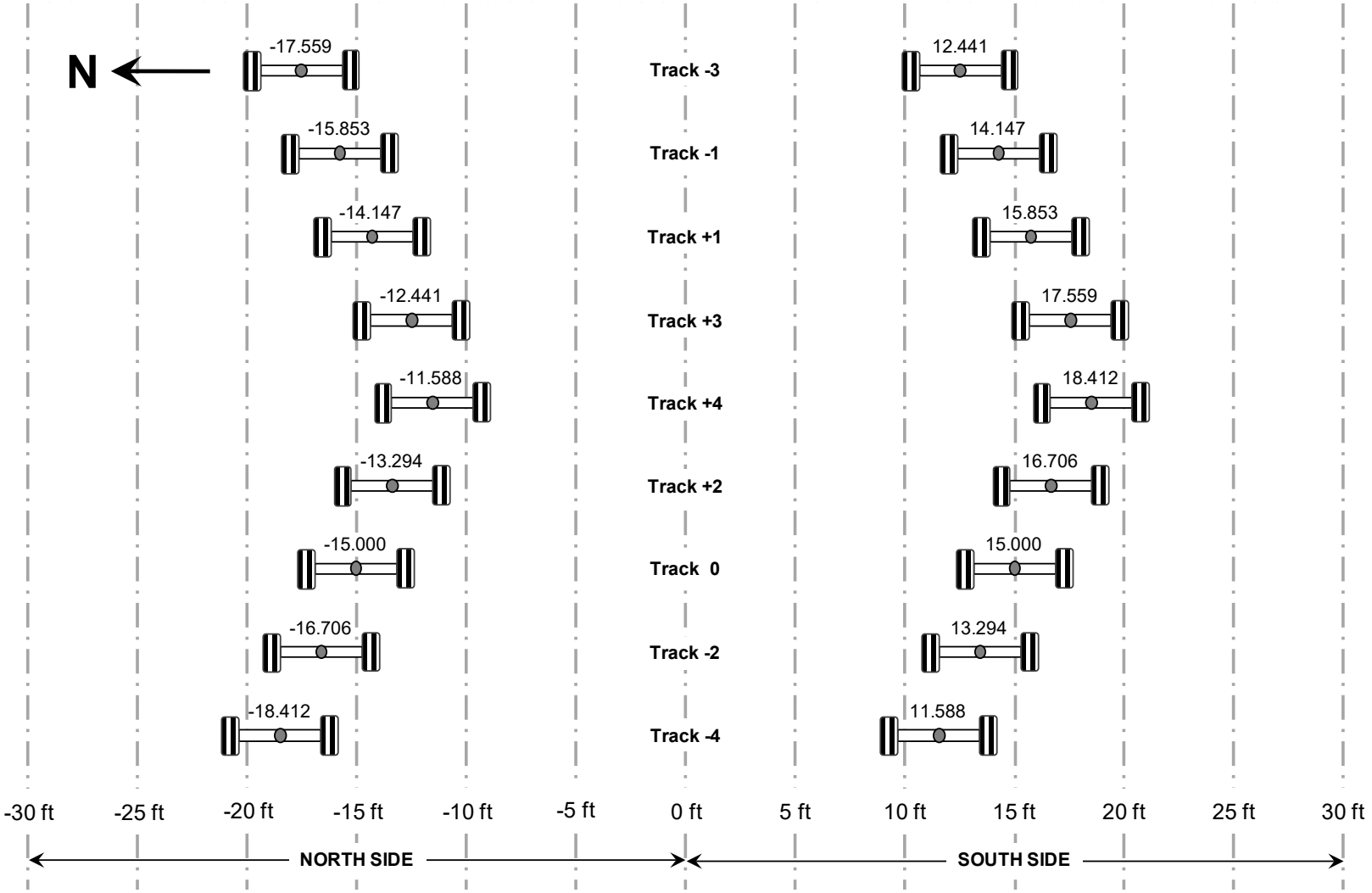

Figure 12. Construction Cycle 9 Wander Tracks

Table 8. Construction Cycle 9 Wander Pattern

Seq. No.	Direction W = West E = East	Track No.	Carriage Centerline Location (ft)	
			North	South
1	W–E	-4	-18.412	11.588
2	E–W	-4	-18.412	11.588
3	W–E	-2	-16.706	13.294
4	E–W	-2	-16.706	13.294
5	W–E	0	-15.000	15.000
6	E–W	0	-15.000	15.000
7	W–E	2	-13.294	16.706
8	E–W	2	-13.294	16.706
9	W–E	4	-11.588	18.412
10	E–W	4	-11.588	18.412
11	W–E	3	-12.441	17.559
12	E–W	3	-12.441	17.559
13	W–E	1	-14.147	15.853
14	E–W	1	-14.147	15.853
15	W–E	-1	-15.853	14.147
16	E–W	-1	-15.853	14.147
17	W–E	-3	-17.559	12.441
18	E–W	-3	-17.559	12.441
19	W–E	-4	-18.412	11.588
20	E–W	-4	-18.412	11.588
21	W–E	-2	-16.706	13.294
22	E–W	-2	-16.706	13.294
23	W–E	0	-15.000	15.000
24	E–W	0	-15.000	15.000
25	W–E	2	-13.294	16.706
26	E–W	2	-13.294	16.706
27	W–E	4	-11.588	18.412
28	E–W	4	-11.588	18.412
29	W–E	3	-12.441	17.559
30	E–W	3	-12.441	17.559
31	W–E	1	-14.147	15.853
32	E–W	1	-14.147	15.853
33	W–E	-1	-15.853	14.147

Seq. No.	Direction	Track No.	Carriage Centerline Location (ft)	
			North	South
34	E–W	-1	-15.853	14.147
35	W–E	-3	-17.559	12.441
36	E–W	-3	-17.559	12.441
37	W–E	3	-12.441	17.559
38	E–W	3	-12.441	17.559
39	W–E	1	-14.147	15.853
40	E–W	1	-14.147	15.853
41	W–E	-1	-15.853	14.147
42	E–W	-1	-15.853	14.147
43	W–E	-3	-17.559	12.441
44	E–W	-3	-17.559	12.441
45	W–E	-2	-16.706	13.294
46	E–W	-2	-16.706	13.294
47	W–E	0	-15.000	15.000
48	E–W	0	-15.000	15.000
49	W–E	2	-13.294	16.706
50	E–W	2	-13.294	16.706
51	W–E	-2	-16.706	13.294
52	E–W	-2	-16.706	13.294
53	W–E	0	-15.000	15.000
54	E–W	0	-15.000	15.000
55	W–E	2	-13.294	16.706
56	E–W	2	-13.294	16.706
57	W–E	1	-14.147	15.853
58	E–W	1	-14.147	15.853
59	W–E	-1	-15.853	14.147
60	E–W	-1	-15.853	14.147
61	W–E	1	-14.147	15.853
62	E–W	1	-14.147	15.853
63	W–E	-1	-15.853	14.147
64	E–W	-1	-15.853	14.147
65	W–E	0	-15.000	15.000
66	E–W	0	-15.000	15.000

3.2.2.3 Test Procedures

The fatigue model and base thickness course, geosynthetics, and CTPB test areas all received traffic from the NAPTV configured as a 3D gear with a wheel load of 58,000 lb and tire pressure of 255 psi. This gear load and configuration was maintained throughout the test, except that starting on March 7, 2023 (pass number 48313) and through the end of the test, the wheel loads on LFS-1 and LFS-2 were increased to 65,000 lb. The vehicle speed was 2.5 mph in both the west-to-east and east-to-west directions.

For the overload test, the basic gear configuration was a D gear with a wheel load of 36,000 lb and tire pressure of 200 psi, the same load used for normal traffic on the CC7 overload test. Overload passes used the same gear configuration as normal traffic, but with the wheel loads increased to 57,000 lb, and tire pressure increased to 255 psi, resulting in an overload of approximately 75% based on the ACR-PCR ratio. Information on how the overload magnitude was determined, the sequencing of overload passes, and other details of the overload test procedure are found in *Volume 5—Test Results and Analysis, Part 4: Overload Test*.

Because the overload test used a different set tire pressure than the other tests (200 versus 255 psi), it was not possible to use the same set of tires when trafficking all test items on the same pass of the NAPTV. Instead, the NAPTV was configured so that three of the four D modules on each carriage were used for LFC-1 through LFC-4, and the fourth D module was used only for LFC-5. This arrangement is shown in Figure 13, where carriage 1, module 1 and carriage 2, module 2 (red) were used for LFC-5. Modules 2, 3, and 4 on carriage 1, and 3, 4, and 5 on carriage 2 (black) were used for the 3D gear in all other tests. The fifth (S) module on each carriage was not used.

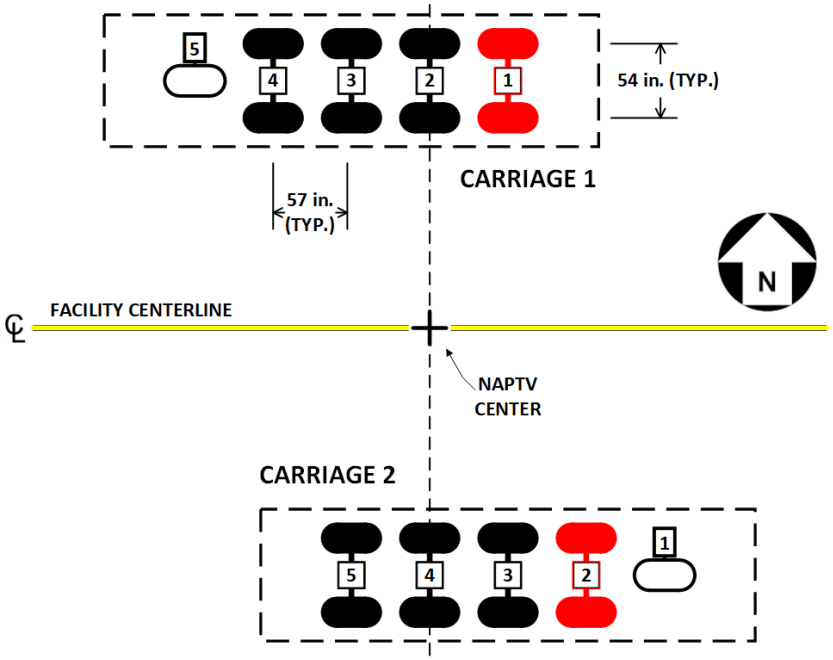

Figure 13. National Airport Pavement Test Vehicle Module Layout for CC9

3.2.2.4 Performance Monitoring

Daily monitoring and testing involved the following items.

1. Dynamic responses—Engineers monitored the horizontal strains in the asphalt layer (ASG), vertical strains in multiple layers (CS), vertical stresses in multiple layers (PC), and bender elements within the geogrid-reinforced test items.

2. Static data—Engineers monitored static (hourly) temperature and moisture data.

3. Manual distress survey—Engineers performed visual distress surveys periodically per ASTM D5340 (ASTM, 2020b). Visual inspections took place on the non-traffic days. Engineers also prepared and regularly updated cumulative distress maps, in which the distresses were color-coded to keep track of exactly when new distresses were observed.

4. Physical straightedge—Engineers performed physical straightedge measurements of rut depth following ASTM E1703. Measurements were taken at two locations within each test item. Physical straightedge measurements were used as a reference for point cloud-based, three-dimensional (3-D) surface mapping using a Leica Model P20 3D laser scanner.

5. NDT—Following the same testing pattern discussed in Section 3.2.1.4 , engineers regularly conducted HWD and PSPA tests at three transverse offsets along two longitudinal stations in each test item. Tests were conducted during the non-traffic days throughout traffic testing. Details of the NDT testing program are discussed in Mazzotta et al. (2024).

In addition, engineers monitored pavement conditions via the following indexes:

1. Pavement Condition Index (PCI)—Engineers monitored the pavement condition for each test item following ASTM D5340. PCI data were stored in databases created in the FAA pavement management system, FAA PAVEAIR. Because there was some minor rutting due to the proof roll and pre-traffic tests, any ruts measured at the start of trafficking were "zeroed out" for the purpose of subsequent damage tracking. Thus, the PCI value for each test item on day one of trafficking was set to 100.

2. Crack density (CD)—CD is a metric for damage quantification and is defined as the portion of pavement surface that is occupied by distresses. A grid of uniform elements or units was established for each test item. If any portion of a unit is distressed, the entire unit area is considered distressed. The CD area is determined by counting for the number of units exhibiting distresses. Therefore, the accuracy of CD increases with the number of discrete units within the area of interest. Crack measurements with an adequately small unit size can ensure a true representation of the distressed surface. Following CC7 practices (Garg et al., 2020), the CDs of CC9 test items were computed using 1- by 1-foot unit size in the traffic area only.

4. SUMMARY OF PRELIMINARY FINDINGS

Traffic on CC9 ended on April 2, 2024. This section documents key outcomes and some broad preliminary findings, which may be subject to revision based on the results of future post-traffic investigations. Detailed analysis and results from the individual test areas may be found in subsequent volumes of this report.

4.1 FATIGUE MODEL AND BASE COURSE THICKNESS TEST

The overall performance of the fatigue model and base course thickness test items was characterized by surface rut depth and surface cracking. Figure 14 shows maximum rut depth versus passes (average of two measurements) for each test item. Rut depths were measured at two stations per test item (see Figure 11) using a 16-foot magnesium straightedge, with the center of the straightedge aligned with the center of the traffic lane. The technician visually located the point of maximum rut depth and recorded it along with the corresponding transverse offset. Figure 14 provides a quick comparison of the relative effects of increasing asphalt thickness versus base thickness. As shown, a 2-in. increase in P-401MR HMA thickness had a much more significant effect on rut performance than a 4-in. increase in P-209MR base thickness, all else being equal. Figure 15 shows the same increase in rut depth but plots it versus time rather than passes, showing periods of traffic and no traffic. As discussed in Section 3.2.2.4 , the physical straightedge measurements were used to check the surface profiles obtained from 3-D laser scans of the entire test area surface (which were time-consuming and, therefore, performed less frequently). Appendix D contains a color fringe plot of the deformed surface following the cessation of traffic. Figure 16 shows examples of transverse profiles obtained from the final laser scan. It is clear from these profiles that surface upheaval was minimal for test items LFS-1 and LFS-2. Surface rutting was consistently higher on the south test items (thinner HMA) than on the north test items.

Measurable surface cracks did not develop until late in the test and, when they did, they affected the south test items (thinner HMA) much more than the north test items. Indeed, no signs of fatigue cracking were observed in LFS-1N or LFS-2N after more than 75,000 passes, even after the load was increased (at 48,313 passes) to 65,000 lb per wheel. Figure 17 shows the final crack patterns as mapped by visual inspectors.

Beyond the surface deformation, CS pairs provided insight into the distribution of permanent deformation in the base layer. Figures 18 and 19 show the contributions of the P-209MR base course sublayers to total deformation of the base course, based on the output of individual CS pairs that make up the stack. The following observations can be drawn:

- Figures 18 and 19 show that the location of maximum deformation within the base layer is 0.5–0.75 in. from the top of the layer.

- CS stack data suggest that most of the permanent deformation takes place in the P-209MR base layer. The maximum straight-edge rut depth is greater than the total deformation within the base layer as measured by the CS stack. The difference is the contribution from all other layers including the subgrade.

- The summed deformations from individual CS pairs exhibit a trend similar to the surface rut accumulation.

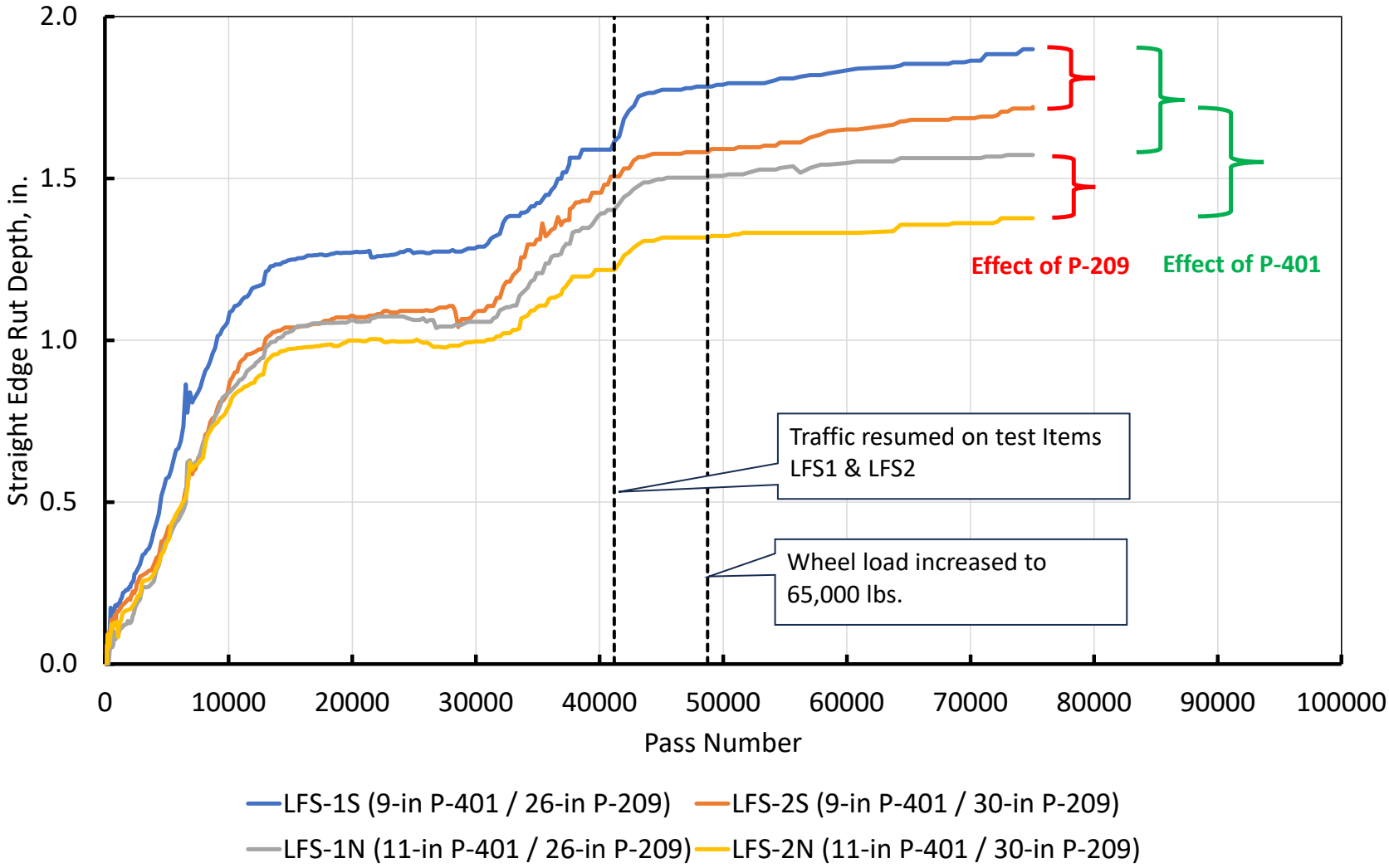

Figure 14. Maximum Rut Accumulation with Passes, Test Items LFS-1 and LFS-2

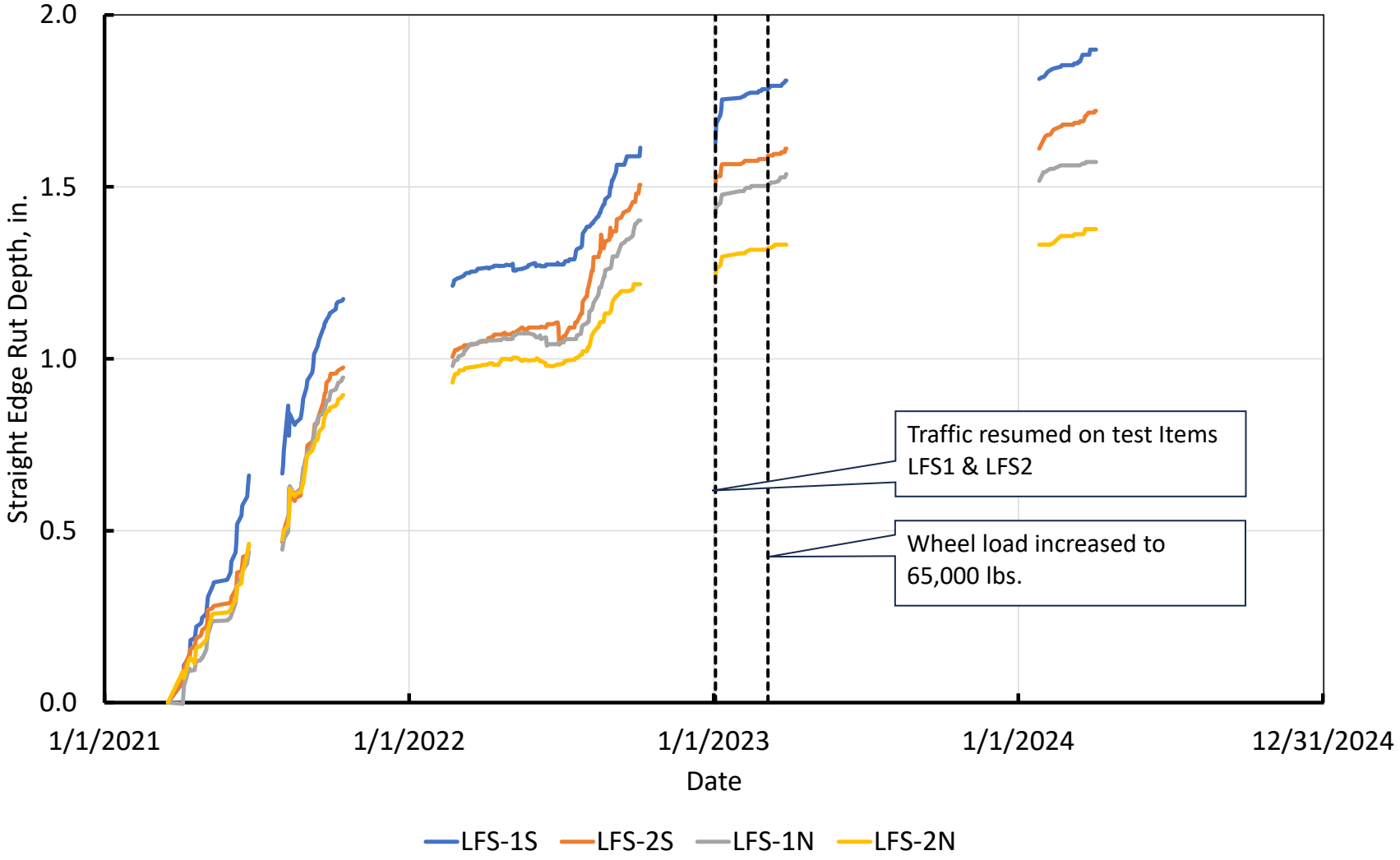

Figure 15. Maximum Rut Accumulation with Time, Test Items LFS-1 and LFS-2

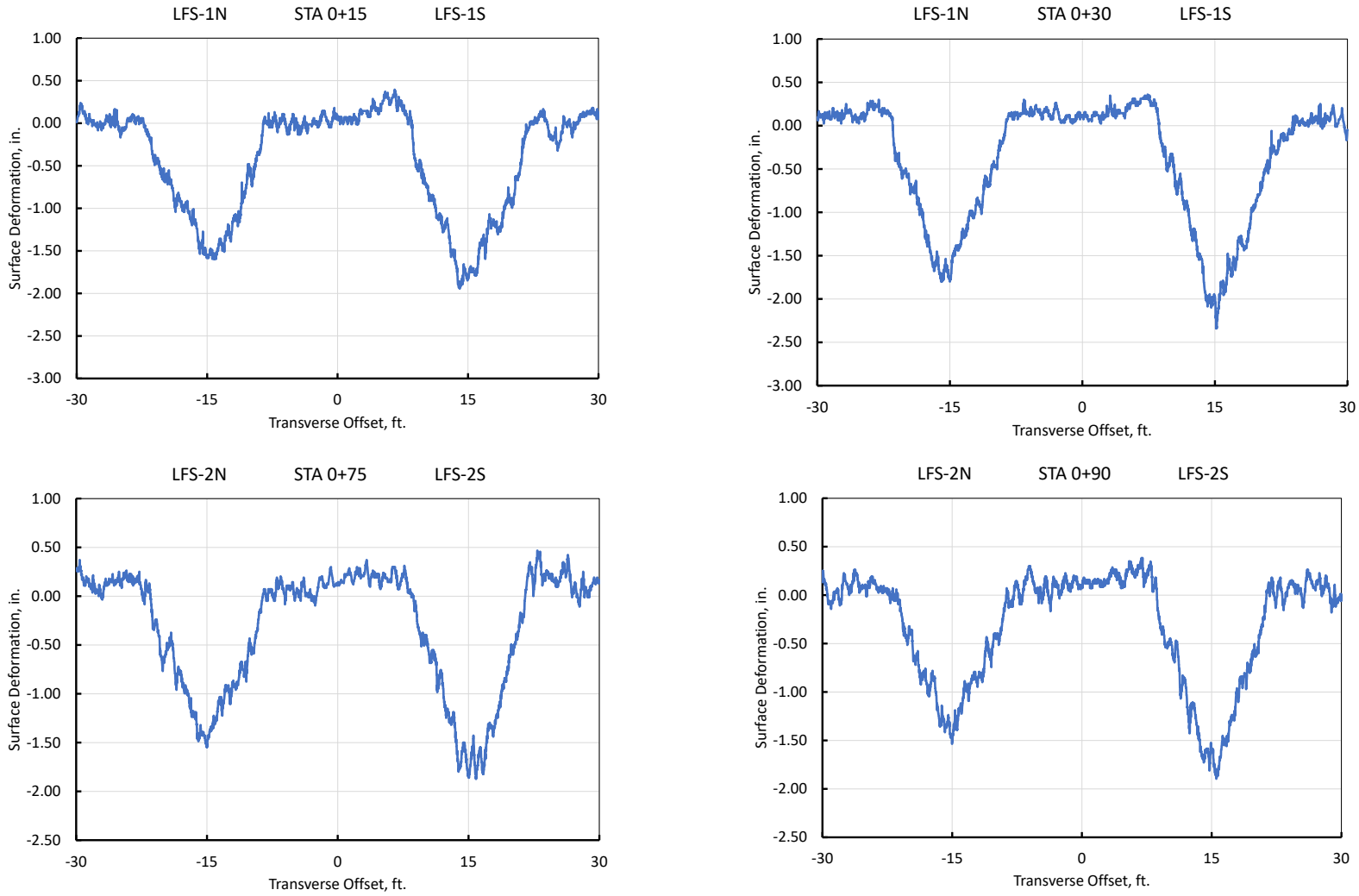

Figure 16. Transverse Surface Profiles Extracted from 3D Laser Scans, Test Items LFS-1 and LFS-2 (April 4, 2024, end of test)

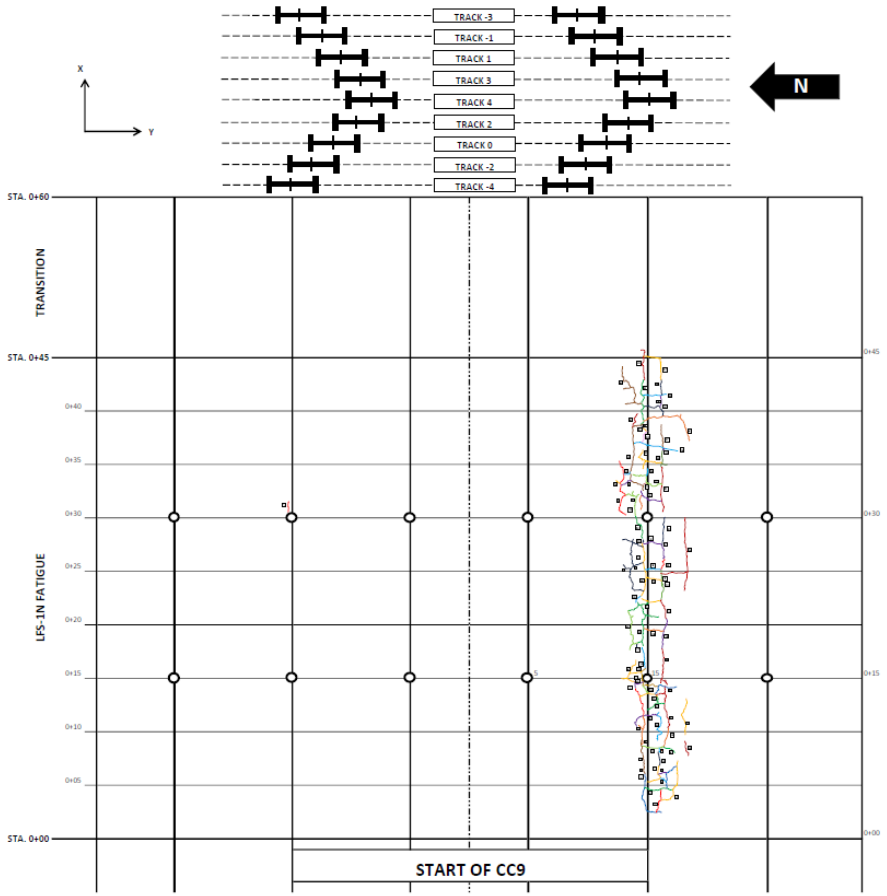

(a) Test items LFS-1N and LFS-1S

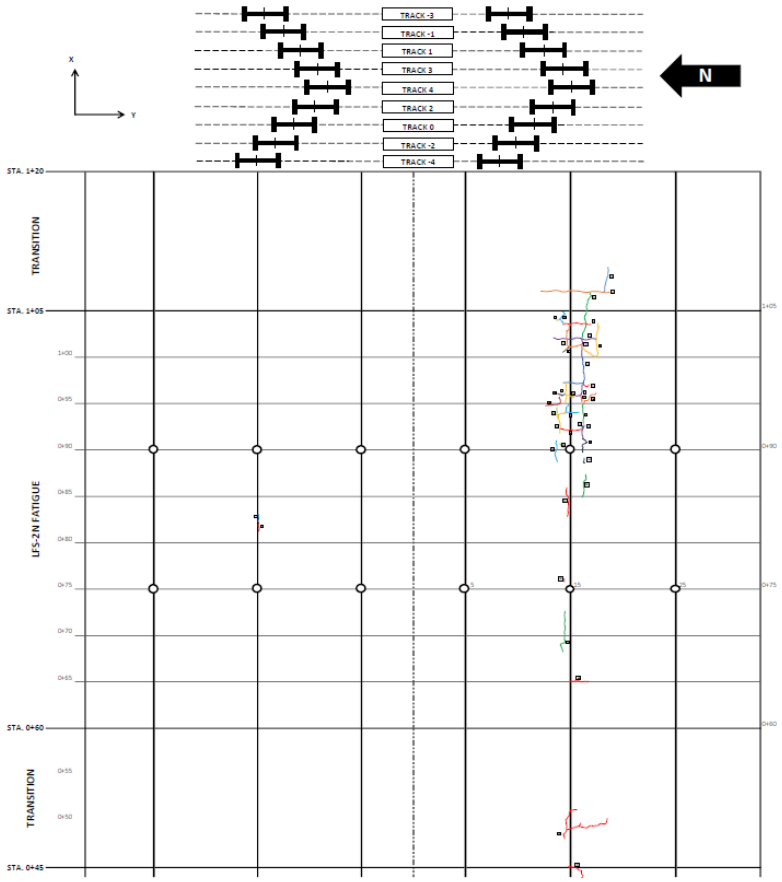

(b) Test items LFS-2N and LFS-2S

Figure 17. Final Surface Crack Map, Test Items LFS-1 and LFS-2 (April 18, 2024)

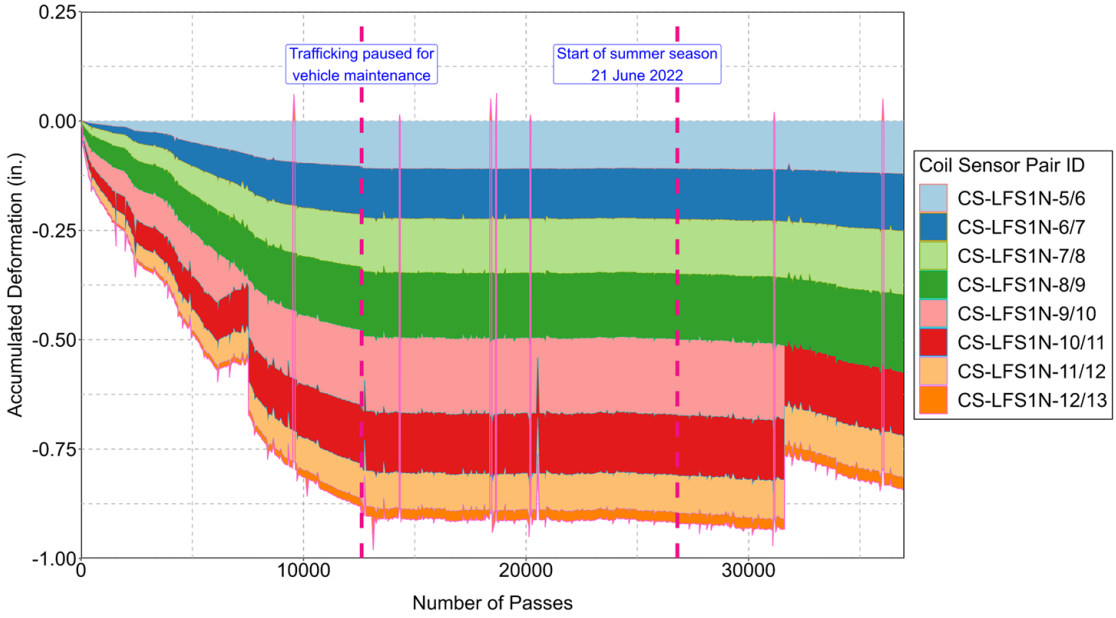

Figure 18. Contribution of Sublayers to Total Base Course Deformation, Test Item LFS-1N

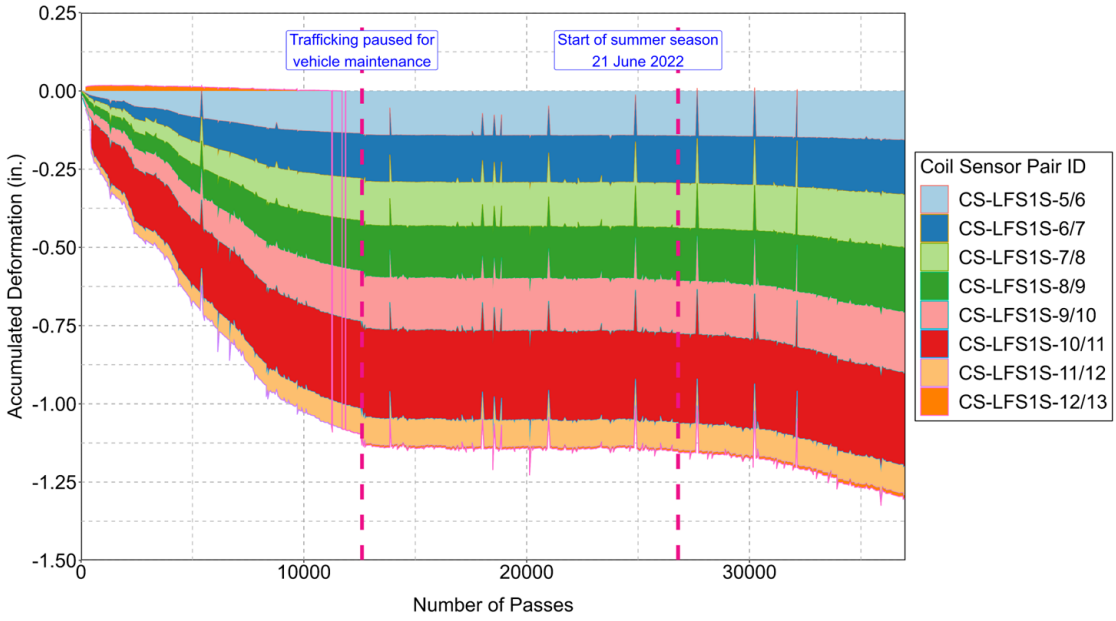

Figure 19. Contribution of Sublayers to Total Base Course Deformation, Test Item LFS-1S

4.2 GEOSYNTHETICS TEST

In contrast to the fatigue model and base course thickness test (Section 4.1), all test items in the geosynthetics test exhibited what might be termed a “classic” structural failure, characterized by deep rutting in the wheel path and upheaval exceeding 1 in. outside the wheel path. Significant

rutting was noted early in the traffic test, with all three test items (LFC-3N, LFC-3S, and LFC-4S) reaching a rut depth of 1.5 in. by 10,000 passes. The presence of geomaterials in tests items LFC-3N and LFC-3S did not serve to delay the onset of rutting. At the point where traffic was stopped on test items LFC-3 and LFC-4 (40,920 passes), there was concern that further traffic on those test items could damage the tires or load modules, due to the abrupt vertical drop-off at the transition between LFS-2 (with relatively little rutting) and LFC-3. Figure 20 shows the significant upheaval (exceeding 3 in. by the end of the test) on test item LFC-3S.

Figure 20. Straightedge Showing Extent of Surface Upheaval on Test Item LFC-3S (photo November 3, 2022)
(The trafficked area is on the left. The shoulder was initially level with the curb on the right).

The overall performance of the geosynthetics test items was characterized by surface rut depth and upheaval, and surface cracking. Figure 21shows the progression of surface rutting as measured by straightedge (see Section 4.1). Some of the initial high rutting was attributed to inadequate compaction of base or subbase layers, which may have delayed mobilization of the geogrid. In addition, a localized area of soft subbase in LFC-3 may have contributed to relatively higher deformations and upheaval in that test item. The effect of underlying construction issues is discussed in *Volume 3—Test Results and Analysis, Part 2: Geosynthetics Test*.

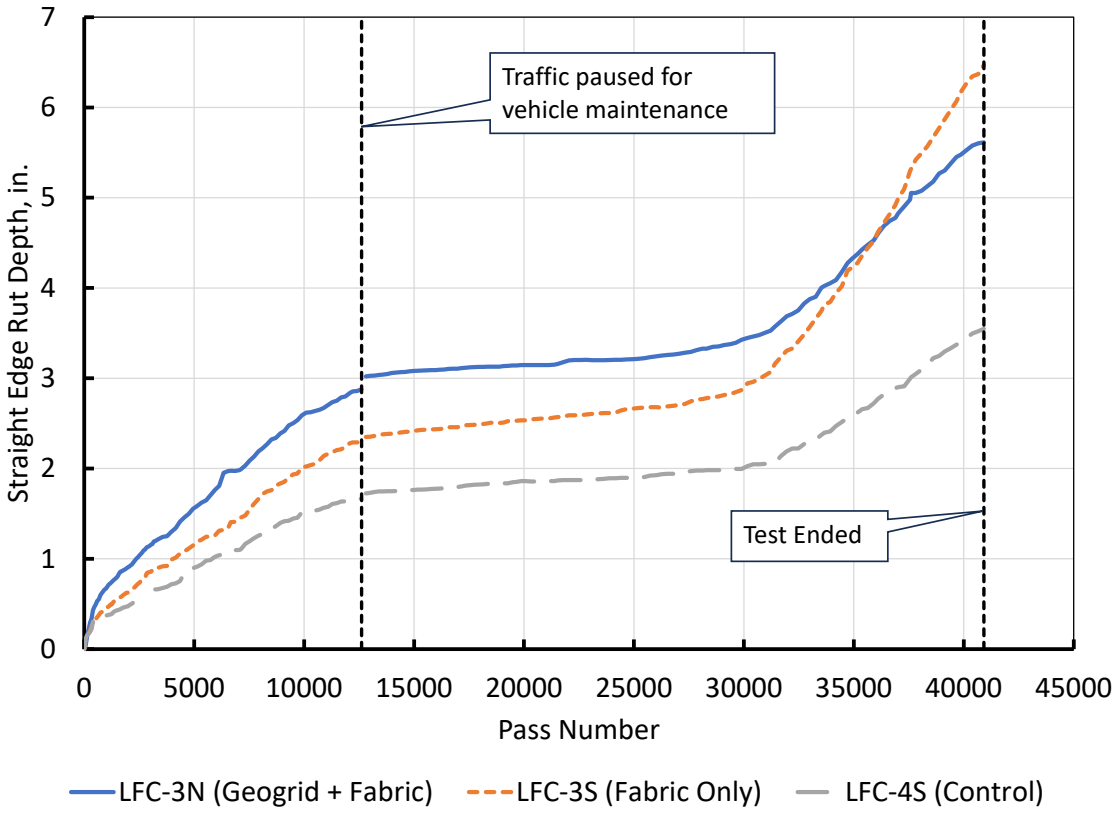

Figure 21. Maximum Rut Accumulation with Passes, Geosynthetics Test Items

Figure 22 shows transverse profiles for the geosynthetics test items as extracted from a 3-D laser surface scan. The scan was conducted on October 20, 2022, at the conclusion of traffic on the Geosynthetics test area. The color fringe plot may be found in Appendix D. Transverse profile deformations are computed with reference to the baseline scan conducted on April 2, 2021, hence positive values of deformation represent upheaval. In comparing Figures 21 and 22, bear in mind that the straight edge rut depth is the vertical distance measured between the trough and a point on the straight line joining the two peaks. When there is significant upheaval (as in Figure 21), the straight edge rut depth must be greater than the surface deformation at the trough (as an absolute value) relative to the baseline.

The strategic placement of bender elements within the geosynthetics test area allowed researchers to analyze the effect of the geosynthetic inclusions on base layer stiffness. A detailed analysis of sensor data, including bender elements and CS pairs in combination with PCs, concluded that geogrid stabilization provided some improvement to in situ subbase modulus compared to the unstabilized test item (Tutumluer et al., 2024).

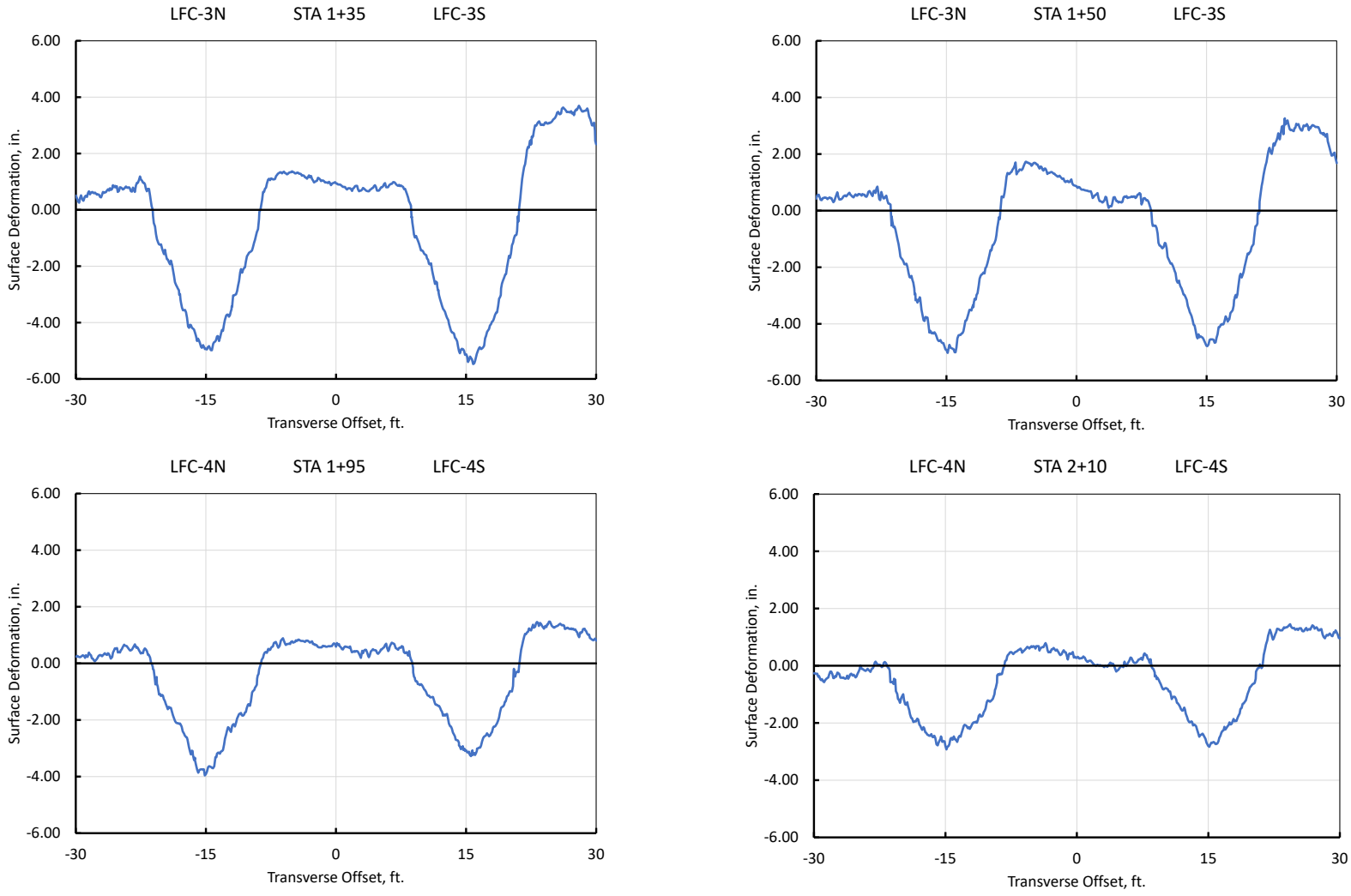

Figure 22. Transverse Surface Profiles Extracted from 3-D Laser Scans, Test Items LFC-3 and LFC-4 (October 20, 2022, end of test)

4.3 CEMENT-TREATED PERMEABLE BASE TEST

The CTPB test compared performance of test item LFC-4N to control test item LFC-4S. The two items were identical in design except that LFC-4N had a P-307MR permeable base (Section 2.2.5) in lieu of a standard base, and they received identical traffic. Figure 23 shows the progression of surface rutting as measured by straightedge (see Section 4.1). Figure 23 plots the rut accumulation curves as measured at individual stations rather than the average for each test item to better show the nonuniformity of rutting observed in the CTPB test item. In LFC-4N, the rutting at Sta. 1+95 was consistently higher than at Sta. 2+10, which may indicate a local weak spot. Except for the observed nonuniformity, the rutting performance of the two test items was similar.

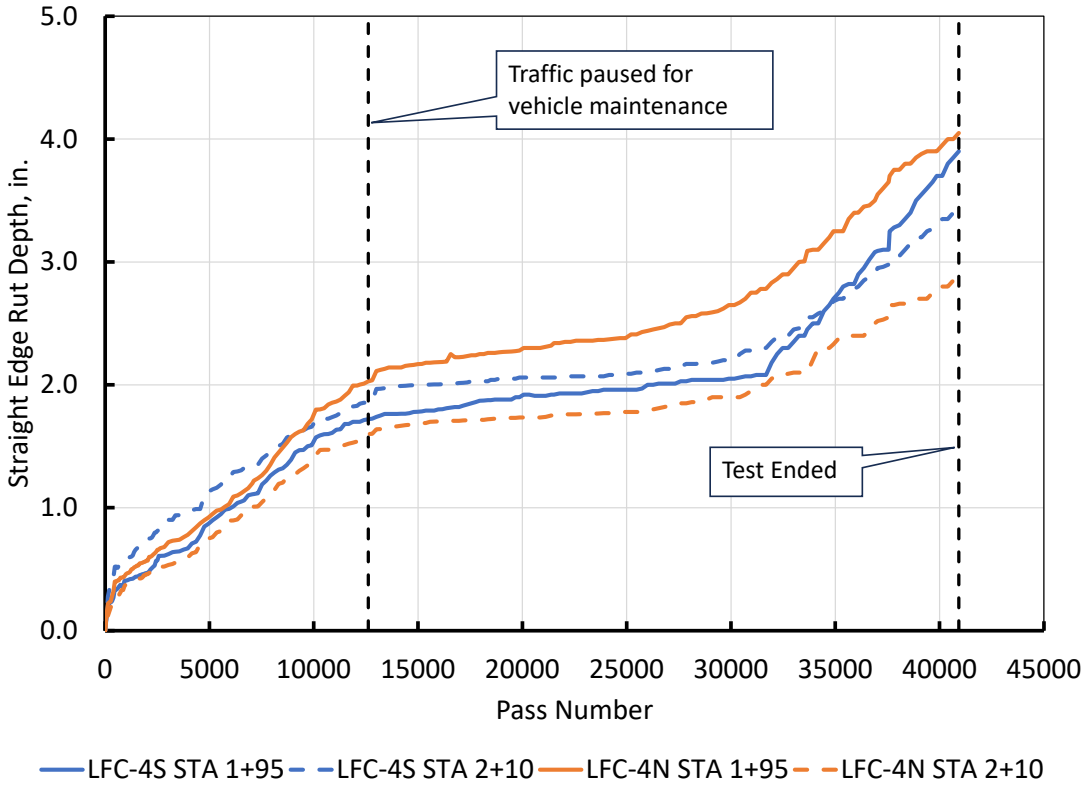

Figure 23. Maximum Rut Accumulation with Passes, CTPB Test Items

Figure 24 shows the comparison of transverse profiles for test item LFC-4 at the end of the test. As shown, both test items developed significant upheaval outside of the traffic lane, with maximum upheaval for LFC-4S exceeding the 1-in. threshold just before pass 37,554. The specific profiles in Figure 24 show a final maximum upheaval of approximately 1.4 in.; however, an analysis of the full deformed 3-D surface using a computer program called SurfaceD found a maximum upheaval for LFC-4S of 1.7 in. The maximum upheaval for LFC-3N did not exceed the 1-in. threshold after more than 40,000 passes, so cannot be considered technically failed according to the adopted failure criterion. Nevertheless, it came close to that threshold, with an estimated maximum upheaval of 0.8 in. from analysis of the final 3-D laser surface scan.

In addition to rutting and upheaval, engineers closely monitored the surface cracking. Figure 25 shows the final cracking condition of the test pavement surface. Figure 25 shows significantly more low-severity longitudinal and transverse cracks in the control test items versus the CTPB test item (183 versus 29 linear ft).

A key goal of the CTPB test was to develop data to support the inclusion of P-307 CTPB as a standard material for structural pavement design in FAARFIELD. This comparative test confirmed that the behavior in a full-scale traffic test of CTPB meeting P-307 is intermediate between a standard high-quality aggregate base (P-209) and a fully bound material (P-403). Rutting and cracking performance was superior to the companion P-209 test item. However, the failure was characteristic of flexible pavements with conventional bases, i.e., it exhibited significant upheaval. (It is assumed that the CTPB test item would have exceeded the 1-in. upheaval criteria had it continued to receive traffic.) Hence, it is reasonable to set the modulus of P-307 intermediate between aggregate materials and asphalt-stabilized base for design.

The CC9 NDT final report (Mazzotta et al., 2024) gives backcalculated values of in situ modulus for the P-307MR base layer from HWD data. As shown in Figure 25, the initial (pre-traffic) backcalculated modulus was approximately 600,000 psi, but degraded rapidly under traffic to between 75,000 and 200,000 psi. Engineers also performed lightweight deflectometer (LWD) tests directly on the CTPB at the time of construction, which determined that the 28-day average LWD modulus was 309,300 psi (with a range of 250,000–400,000 psi). The FAA NextGen Pavement Materials Laboratory performed resilient modulus (M_R) tests on CTPB cores (discussed in *Volume 4, Test Results and Analysis, Part 3: CTPB Test*). The laboratory data were somewhat questionable due to the difficulty of attaching linear variable displacement transducers (LVDTs) to the permeable material samples, but they gave repeatable results (General Dynamics Information Technology, 2019). Depending on the state of confinement, the average M_R was in the range of 180,000–600,000 psi. Considering the variability of field measurements and laboratory data, an appropriate default design modulus for this material is 300,000 psi, with an allowable range of 200,000–400,000 psi.

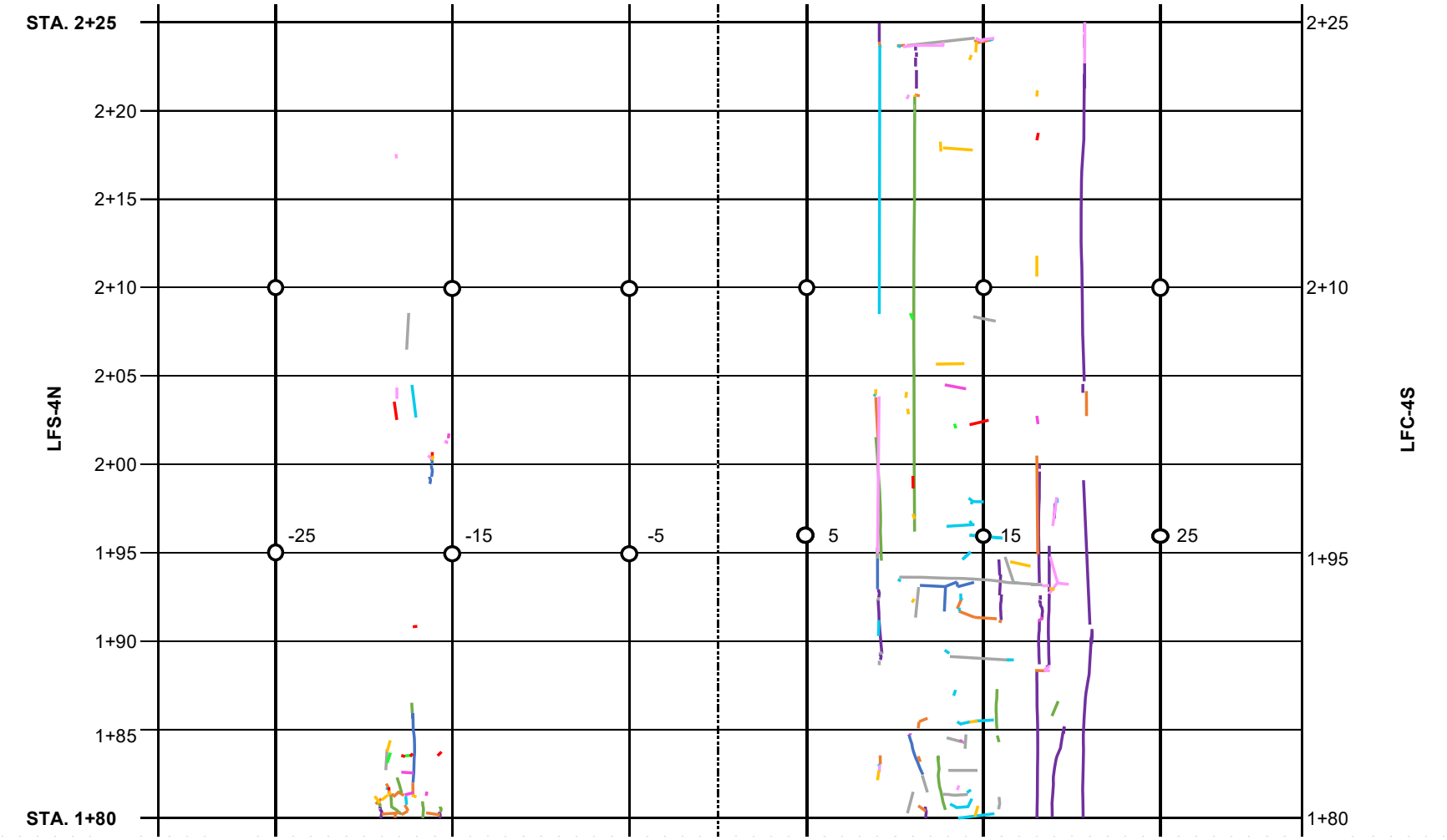

Figure 24. Final Surface Crack Map, Test Items LFC-4N and LFC-4S, October 2022

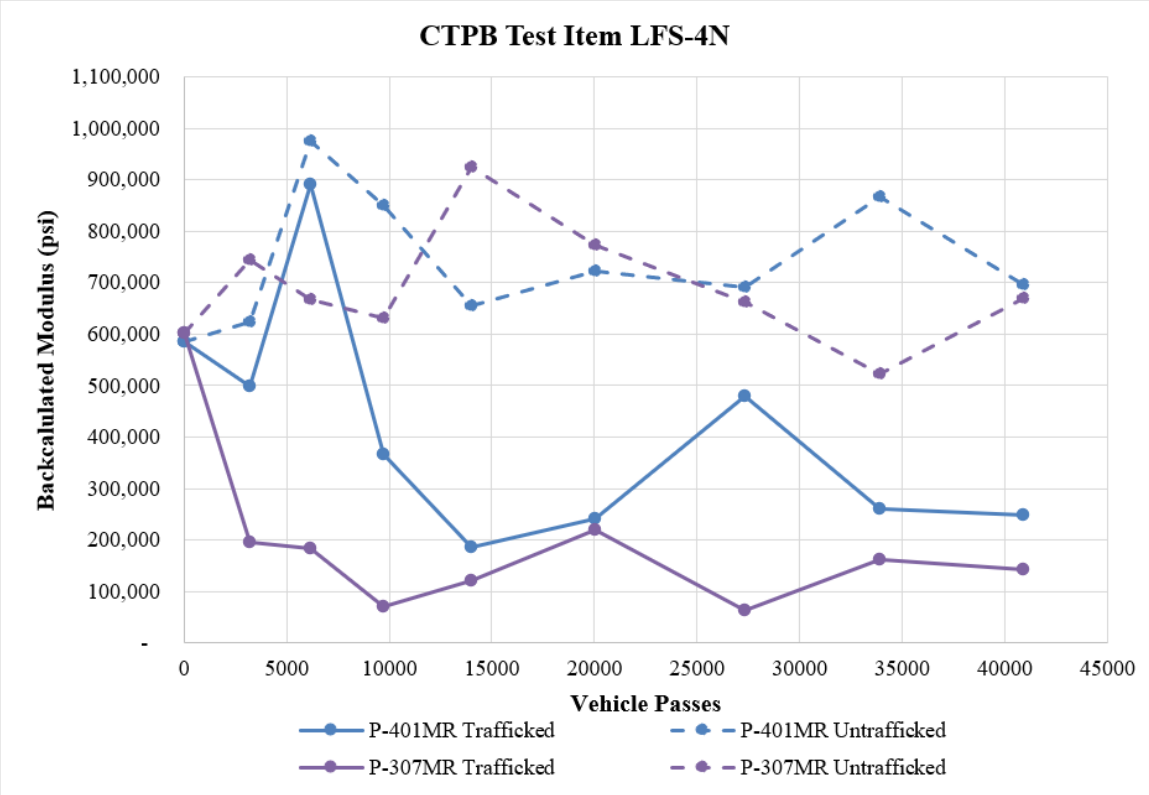

Figure 25. Backcalculated Moduli for LFS-4N (Mazzotta et al., 2024)

4.4 OVERLOAD TEST

The overload test compared the performance of test item LFC-5N to control test item LFC-5S. The two items were identical in design and load history, except that LFC-4N received three series of overloads in addition to the regular design traffic. Figure 26 shows the progress of surface rutting. Test item LFC-5N responded to the third overload with a one-time increase of rut depth, but upon resumption of the normal load, the rate of rut accumulation was unchanged compared to the control. Neither LFC-5N (overload) nor LFC-5S (control) exhibited upheavals exceeding the 1-in. threshold for shear failure, although upheaval in parts of LFC-5N approached 0.75 in. by the end of the test (Figures 27 and 28). Due to extensive surface cracking covering the entire trafficked area (Figure 29), both test items could be considered failed according to criterion (ii) in Section 3.2.2.1 . This test demonstrated that, under some conditions, flexible airport pavements may experience repeated overloads up to 75% higher than the design strength (when evaluated by the ACR-PCR method) without measurably reduced performance.

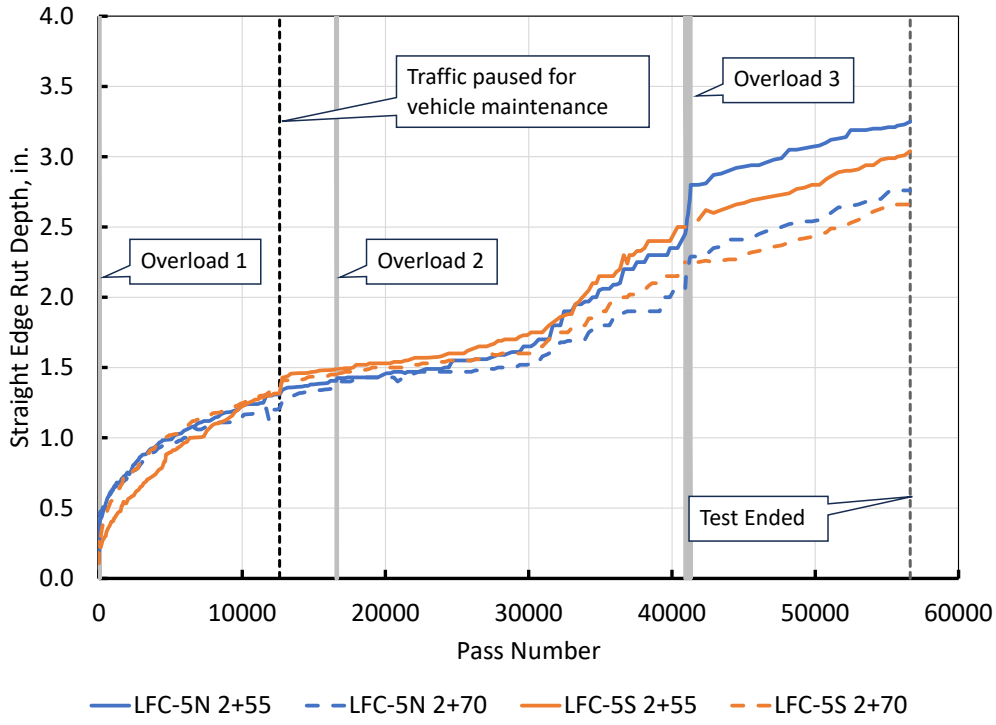

Figure 26. Surface Rut Accumulation in Overload Test Items Measured with Straightedge

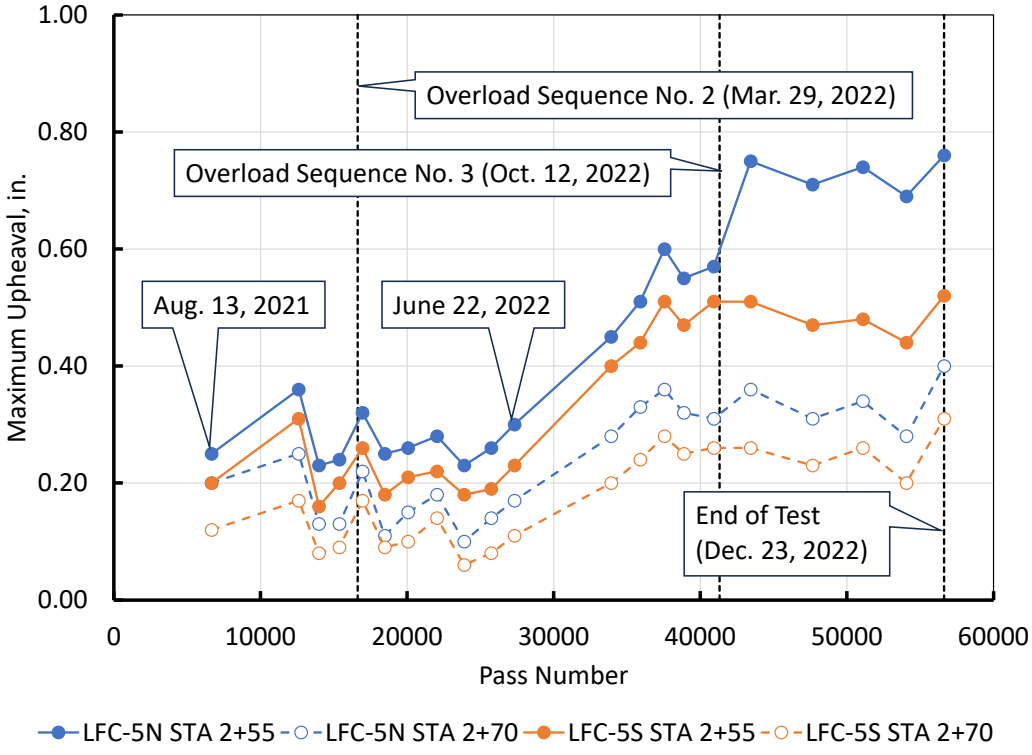

Figure 27. Surface Upheaval in Overload Test Items from 3-D Laser Scans

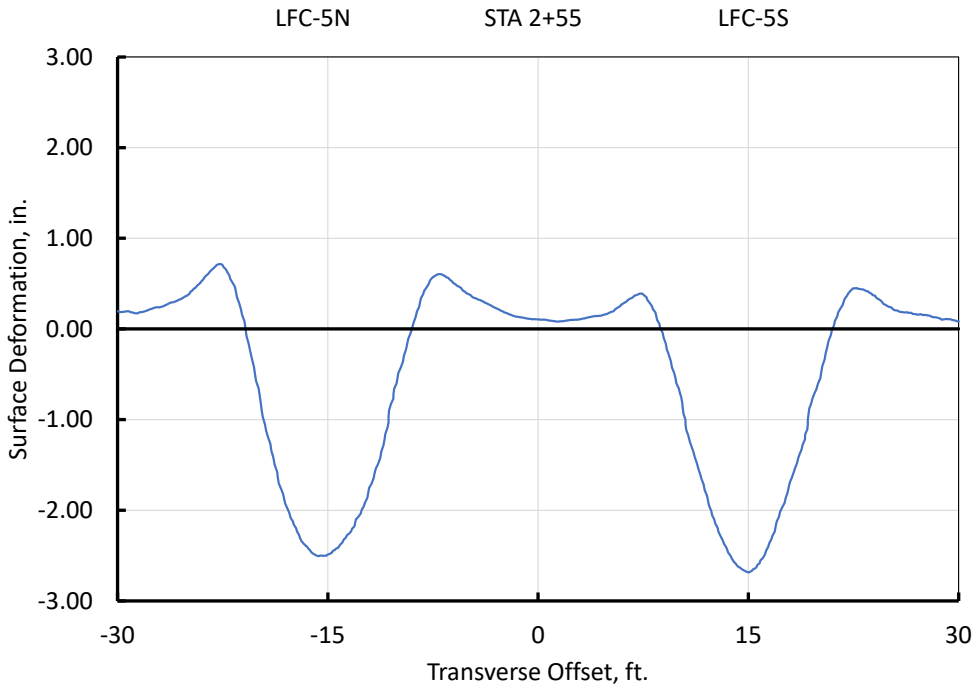

(a) STA 2+55

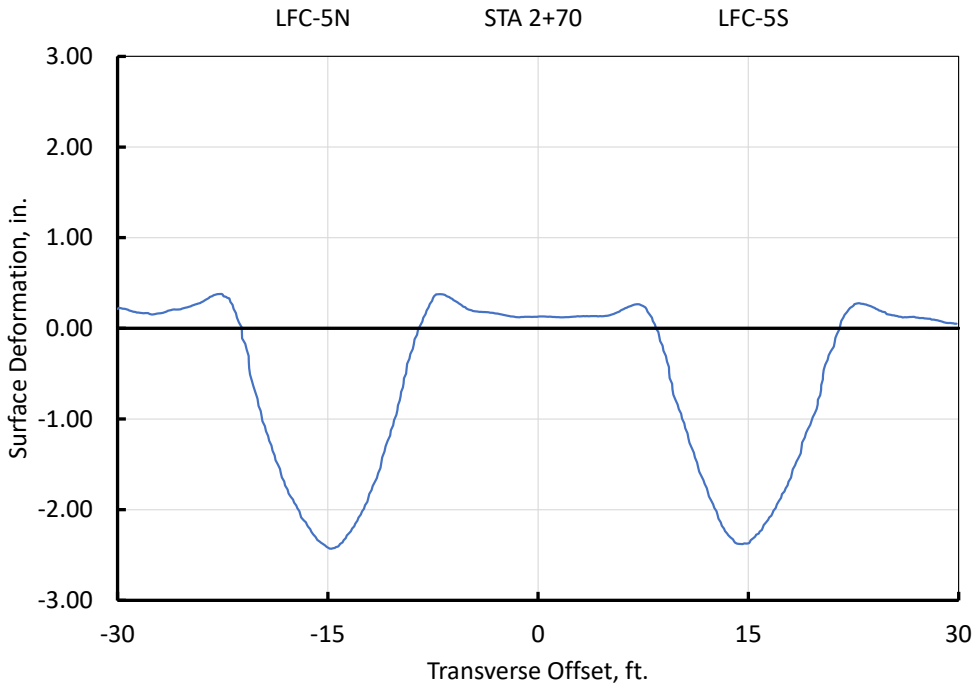

(b) STA 2+70

Figure 28. Transverse Surface Profiles Extracted from 3-D Laser Scans, Test Items LFC-5N and LFC-5S (December 23, 2022, end of test)

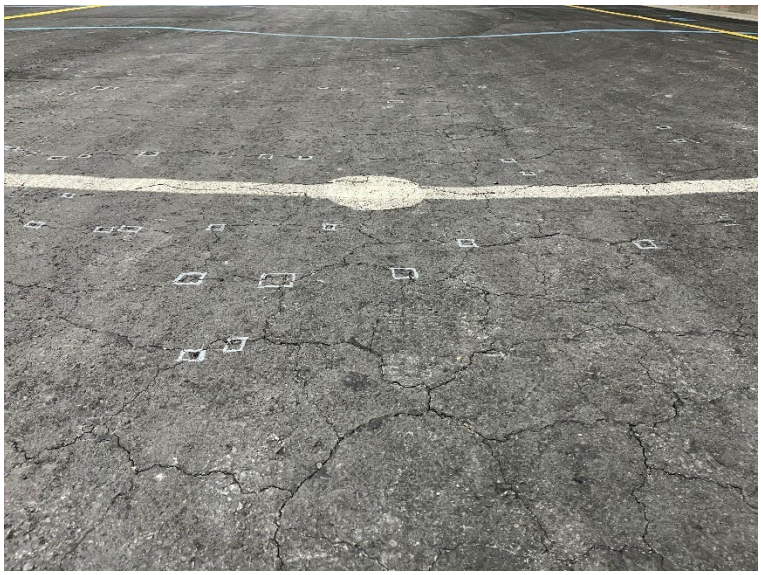

Figure 29. Extensive Interconnected Cracks on the Surface of Test Item LFC-5S (end of test)

Placement of CS pairs and PCs at the top of the subgrade allowed direct measurement of vertical compressive strains and stresses under traffic. Figure 30 shows plots of peak vertical compressive strain (a) and peak vertical stress (b) at the top of the clay subgrade for test item LFC-5. As shown, the compressive strain (ratio of measured deflection to the distance between coils) varied considerably throughout the test, while the peak vertical stress remained relatively stable. Initially, the research team intended to use the overload test results to identify a threshold level of subgrade strain that separates allowable from non-allowable overloads for a given pavement structure. However, the evolving nature of in situ vertical strain over the pavement life, and its strong dependence on various non-load-related factors (e.g., moisture, traffic history), made it challenging to use vertical strain as a practical indicator for overload assessment. Therefore, the research team proposed an alternative criterion for detailed analysis of overloads in accordance with Annex 14 requirements, based on the concept of subgrade stress ratio (SSR), defined as the ratio of applied shear stress to the estimated soil shear strength (Bejarano & Thompson, 1999). Development of the SSR-based overload criterion, which requires a laboratory estimate of soil shear strength, is discussed in detail in *Volume 5, Test Results and Analysis, Part 4: Overload Test*.

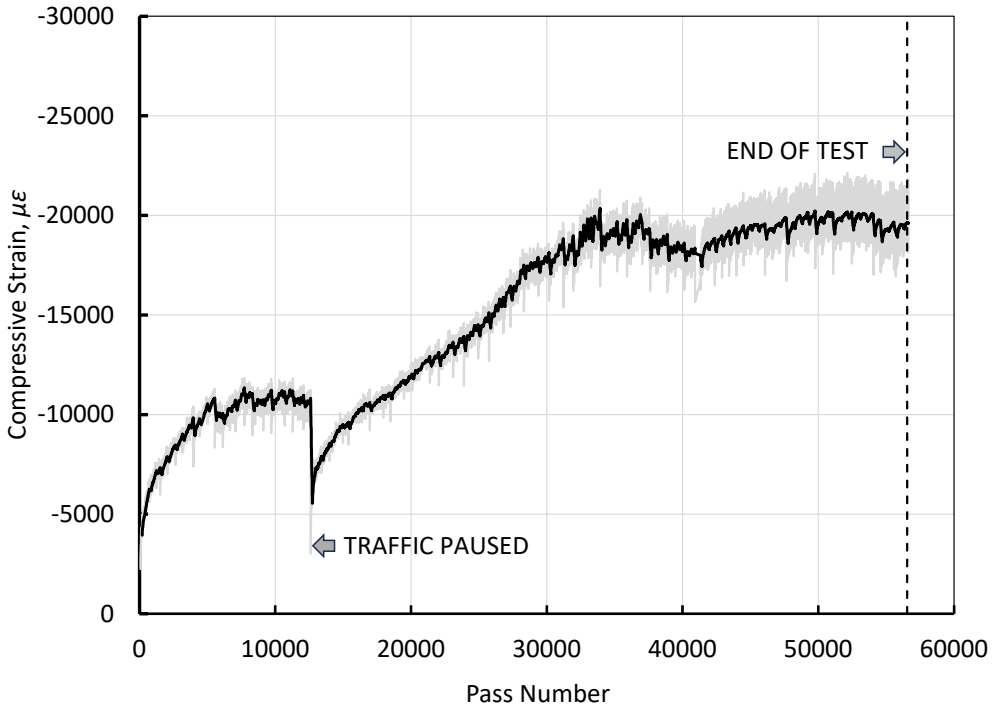

(a)

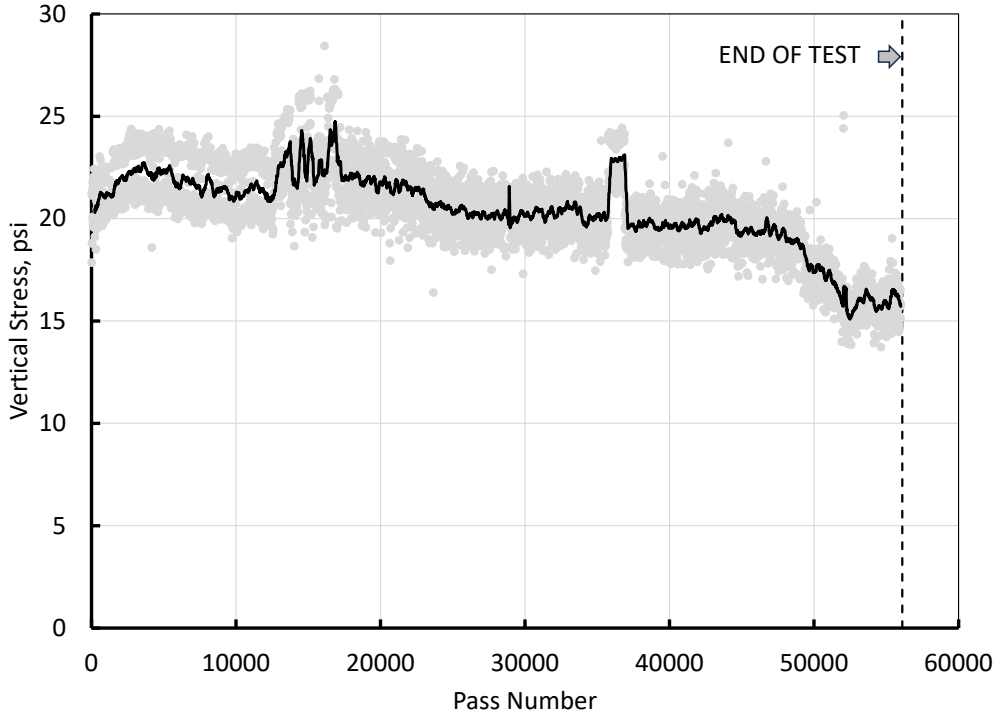

(b)

Figure 30. Subgrade Peak Responses with Traffic for Test Item LFC-5 (Control, no overloads applied): (a) Vertical Strain from CS Pair CS-LFC5-1/2; (b) Vertical Strain from PC-LFC5S-2 (Solid line represents 20-point moving average.)

5. CONCLUSIONS

This report covers the construction cycle (CC)9 traffic test from test item design and construction through the end of full-scale traffic on April 4, 2024. The CC9 test included four distinct, full-scale tests distributed on ten flexible pavement test items. Separate volumes of this report present detailed analyses of each of the four tests based on data to date. It is expected that additional data will be obtained from removal and further post-traffic testing of failed test items and materials, and future planned activities. Key results from the traffic testing phase are as follows.

- Fatigue Model and Base Course Thickness Test
  - All four test items (LFS-1N, LFS-2N, LFS-1S, and LFS-2S) were non-failures after more than 75,000 passes, following the established failure criteria.
  - A 2-in. increase in asphalt thickness had a much more significant effect on rut performance than a 4-in. increase in crushed aggregate base thickness, all else being equal.
  - Likewise, the asphalt layer was more effective in controlling fatigue cracking. No evidence of fatigue cracking was observed in LFS-1N or LFS-2N (relatively thicker asphalt) by the end of the test. Limited surface cracking was observed in both LFS-1S and LFS-2S (thinner asphalt).
  - Coil sensor (CS) measurements showed that most of the permanent deformation is concentrated in the crushed aggregate base, with the maximum deformation located approximately 0.5–0.75 in. from the top of the layer.
- Geosynthetics Test
  - All three test items (LFC-3N, LFC-3S, and LFC-4S) experienced significant upheaval outside the traffic lane, characteristic of structural shear failure.
  - Presence of geomaterials in tests items LFC-3N (geogrid plus separation fabric) and LFC-3S (separation fabric only) did not serve to delay the onset of rutting.
  - Initial rutting in reinforced test items was attributed to inadequate compaction of base or subbase layers, which may have delayed mobilization of the geogrid in LFC-3N.
- Cement-Treated Permeable Base (CTPB) Test
  - Rutting performance of the two test items (LFC-4N and LFC-4S) was similar.
  - Test item LFC-4S (control) failed according to the 1-in. upheaval criterion at 37,554 passes. Test item LFC-4N (CTPB) reached a maximum upheaval of approximately 0.8 in. by the end of the test.

- The test confirmed that the structural performance of CTPB meeting P-307 under full-scale traffic is intermediate between a standard high-quality aggregate base (P-209) and a fully bound material (P-403).

- An appropriate default design modulus for item P-307 (CTPB) is 300,000 psi, with an allowable range of 200,000–400,000 psi.

- Overload Test

  - Overloads up to 75% above pavement classification rating (PCR) did not noticeably affect flexible pavement life.

  - Neither LFC-5N (overload) nor LFC-5S (no overload) experienced 1-in. surface upheaval by the end of the test. Both test items developed extensive interconnected surface cracking.

  - Researchers monitored vertical strain at the top of the subgrade using inductive CS pairs. It was shown that the maximum in situ compressive strain under load varied throughout the period of test due to non-load-related factors, making this response unsuitable as an indicator of allowable overload. The research team proposed a criterion based on the subgrade stress ration (SSR) concept.

6. REFERENCES

Ahlvin, R. G., Turnbull,W. J., Sale, J. P., & Maxwell, A. A. (1971). *Multiple-wheel heavy gear load pavement tests. Volume 1* (Technical Report No. AFWL-TR-70-113*)*. Air Force Weapons Laboratory: Kirkland, New Mexico. https://apps.dtic.mil/sti/pdfs/AD0889705.pdf

Carpenter, S. H., Ghuzlan, K. A., & Shen, S. (2003). Fatigue endurance limit for highway and airport pavements. *Transportation Research Record: Journal of the Transportation Research Board*, *1832*(1), 131–138. https://doi.org/10.3141/1832-16

Carpenter, S. H., & Shen, S. (2006). Dissipated energy approach to study hot-mix asphalt healing in fatigue. *Transportation Research Record: Journal of the Transportation Research Board*, *1970*(1), 178–185. https://doi.org/10.1177/0361198106197000119

Dawson, A. (1994). *The ε-mu system, user's manual* (2nd ed.). Nottingham, UK: University of Nottingham.

FAA. (2018). *Standard specifications for construction of airports* (Advisory Circular [AC] 150/5370-10H). U.S. Department of Transportation, Federal Aviation Administration. https://www.faa.gov/airports/resources/advisory_circulars/index.cfm/go/document.current/documentnumber/150_5370-10

Hall, J. W., Mallela, J., & Smith, K. L. (2005). *Stabilized and drainable base for rigid pavement* (Research Report No. IPRF-01-G-002-021(G)). Innovative Pavement Research Foundation, Skokie, IL. http://www.iprf.org/products/FinalGuide(10.27.05).pdf

International Civil Aviation Organization (ICAO). (2022). *Annex 14 to the Convention on—Aerodromes. Volume I, Aerodrome Design and Operations*. (9th ed.). ICAO. https://caa.gov.kz/storage/app/media/updated%20apps%20for%20ICAO%20Convention/AN14_v1_Aerodrome%20Design%20and%20Operations%202022%20ed.pdf

Liang, R. Y. (2007). *Evaluation of drainable bases under asphalt pavements* (Research Report No. FHWA/OH-2007/10). U.S. Department of Transportation, Federal Highway Administration, Washington, DC. https://rosap.ntl.bts.gov/view/dot/39577

Mazzotta, C., Murrell, S., Evans, D., & Breder, E. (2024). *Exploring construction cycle 9 with nondestructive testing: Innovations and insights in full-scale airport pavement testing* [Report in preparation].

Selig, E. T., & Grangaard, O. H. (1970). A new technique for soil strain measurement. *Materials Research and Standards*, *10*(11), 19–21.

Shen, S., & Carpenter, S. H. (2007). Development of an asphalt fatigue model based on energy principles. *Asphalt Paving Technology: Association of Asphalt Paving Technologists-Proceedings of the Technical Sessions*, *76*, 525–574.

Tirado, C., Carrasco, C., Nazarian S., Norwood, G. J., & Tingle, J. S. (2014, August 5–7). *Benefits of inclusion of geosynthetic products in reinforcement of flexible airfield pavements using three-dimensional finite element modeling*. In Proceedings of the 2014 FAA Worldwide Airport Technology Transfer Conference, Galloway, New Jersey. https://www.airporttech.tc.faa.gov/Collaboration/Past-Conferences-Events/Airport-Technology-Transfer-Conference-2014/ArtMID/4468/ArticleID/289/Evaluation-of-Benefits-of-Inclusion-of-Geosynthetic-Products-in-Reinforcement-of-Flexible-Airfield-Pavement

Tomlinson, C, D. Traverso, C. Cary, and M. Brynick. (2020). *Construction cycle 9 (CC9) construction report* (DOT/FAA/TC-22/1). U.S. Dept. of Transportation, Federal Aviation Administration. https://www.airporttech.tc.faa.gov/Products/Airport-Pavement-Papers-Publications/Airport-Pavement-Detail/construction-cycle-9-cc9-construction-report

Tutumluer, E., Kang, M., & Qamhia, I.I.A. (2024). *Analysis of granular base/subbase in airport pavements using embedded sensors*. (DOT/FAA/TC-24/31). U.S. Dept. of Transportation, Federal Aviation Administration. https://www.airporttech.tc.faa.gov/Products/Airport-Pavement-Papers-Publications/Airport-Pavement-Detail/analysis-of-granular-basesubbase-in-airport-pavements-using-embedded-sensors

Zornberg, J.G. (2012). Ingenuity in geotechnical design using geosynthetics. In *Geotechnical Engineering State of the Art and Practice: Keynote Lectures from GeoCongress 2012, Geotechnical Special Publication No. 226*, 398-419. https://doi.org/10.1061/9780784412138.0016

APPENDIX A—ASPHALT ACCEPTANCE AND CHARACTERIZATION DATA

Table A-1. Material Acceptance and Characterization Results for the Fatigue Model Test Area

Test Item	Material[1]	Parameter	Average	Standard Deviation	COV, %
LFS-1N	P-152MR	CBR, %	4.9	0.2	4.1
		Moisture Content (M.C.), %	22.3	N/A	N/A
		In-Situ Dry Density, pcf	102.8	N/A	N/A
		Shear Strength, psi	24.9	1.9	7.7
		LWD Modulus, kips per square inch (ksi)	22.9	8.8	38.6
		Seismic Modulus, ksi	31.9	4.0	12.6
		GeoGauge Modulus, ksi	11.3	1.9	16.5
	P-209MR	Density (Nuclear), pcf	152.8	N/A	N/A
		M.C. (Nuclear), %	2.1	N/A	N/A
		LWD Modulus, ksi	26.7	2.2	8.2
		Seismic Modulus, ksi	74.0	10.0	13.5
		GeoGauge Modulus, ksi	13.2	1.6	12.2
	P-403MR	Mat Density, %	95.1	N/A	N/A
		Joint Density, %	88.7	N/A	N/A
		Lab Air Voids, %	5.1	N/A	N/A
	P-401MR	Mat Density, %	96.6	N/A	N/A
		Joint Density, %	93.6	N/A	N/A
		Lab Air Voids, %	4.1	N/A	N/A
		Seismic Modulus, ksi	3,204.9	159.7	5.0
		Elastic Modulus, ksi	1,460.0	148.8	10.2
LFS-1S	P-152MR	CBR, %	4.5	0.2	4.7
		M.C., %	24.4	N/A	N/A
		In-Situ Dry Density, pcf	100.0	N/A	N/A
		Shear Strength, psi	19.5	4.3	22.2
		LWD Modulus, ksi	8.0	2.9	37.0
		Seismic Modulus, ksi	19.4	2.7	13.9
		GeoGauge Modulus, ksi	8.9	2.1	23.3
	P-209MR	Density (Nuclear), pcf	155.8	N/A	N/A
		M.C. (Nuclear), %	1.8	N/A	N/A
		LWD Modulus, ksi	31.9	3.4	10.7
		Seismic Modulus, ksi	95.7	16.6	17.4
		GeoGauge Modulus, ksi	14.5	2.6	17.8
	P-403MR	Mat Density, %	94.2	N/A	N/A
		Joint Density, %	88.7	N/A	N/A

Test Item	Material[1]	Parameter	Average	Standard Deviation	COV, %
		Lab Air Voids, %	5.1	N/A	N/A
	P-401MR	Mat Density, %	95.1	N/A	N/A
		Joint Density, %	93.6	N/A	N/A
		Lab Air Voids, %	4.1	N/A	N/A
		Seismic Modulus, ksi	2,975.2	129.6	4.4
		Elastic Modulus, ksi	1,297.0	140.3	10.8
LFS-2N	P-152MR	CBR, %	5.1	0.4	7.1
		M.C., %	23.2	N/A	N/A
		In-Situ Dry Density, pcf	102.7	N/A	N/A
		Shear Strength, psi	23.6	3.1	13.3
		LWD Modulus, ksi	17.2	6.7	38.9
		Seismic Modulus, ksi	26.5	4.6	17.3
		GeoGauge Modulus, ksi	14.5	3.3	23.0
	P-209MR	Density (Nuclear), pcf	151.6	N/A	N/A
		M.C. (Nuclear), %	2.2	N/A	N/A
		LWD Modulus, ksi	26.3	1.5	5.5
		Seismic Modulus, ksi	67.6	12.7	18.7
		GeoGauge Modulus, ksi	14.7	2.7	18.4
	P-403MR	Mat Density, %	95.5	N/A	N/A
		Joint Density, %	89.1	N/A	N/A
		Lab Air Voids, %	5.1	N/A	N/A
	P-401MR	Mat Density, %	95.1	N/A	N/A
		Joint Density, %	94.1	N/A	N/A
		Lab Air Voids, %	5.9	N/A	N/A
		Seismic Modulus, ksi	3,135.3	157.7	5.0
		Elastic Modulus, ksi	1,158.3	111.7	9.6
LFS-2S	P-152MR	CBR, %	5.1	0.1	1.1
		M.C., %	25.3	N/A	N/A
		In-Situ Dry Density, pcf	98.2	N/A	N/A
		Shear Strength, psi	19.3	1.7	9.1
		LWD Modulus, ksi	8.0	3.8	47.9
		Seismic Modulus, ksi	18.1	1.4	7.6
		GeoGauge Modulus, ksi	13.9	2.4	17.4
	P-209MR	Density (Nuclear), pcf	152.8	N/A	N/A
		M.C. (Nuclear), %	2.1	N/A	N/A
		LWD Modulus, ksi	28.5	2.6	9.1
		Seismic Modulus, ksi	87.6	15.7	17.9
		GeoGauge Modulus, ksi	15.2	2.2	14.5

Test Item	Material[1]	Parameter	Average	Standard Deviation	COV, %
	P-403MR	Mat Density, %	94.5	N/A	N/A
		Joint Density, %	89.1	N/A	N/A
		Lab Air Voids, %	5.1	N/A	N/A
	P-401MR	Mat Density, %	94.0	N/A	N/A
		Joint Density, %	94.1	N/A	N/A
		Lab Air Voids, %	4.1	N/A	N/A
		Seismic Modulus, ksi	3,050.4	104.2	3.4
		Elastic Modulus, ksi	1,579.3	179.9	11.4

[1]Tests reported were those conducted on the final surface lift.

Table A-2. Material Acceptance and Characterization Results for the Geosynthetics Test Area

Test Item	Material[1]	Parameter	Average	Standard Deviation	COV, %
LFC-3N	P-152MR	CBR, %	4.8	0.6	12.6
		M.C., %	27.0	N/A	N/A
		In-Situ Dry Density, pcf	97.3	N/A	N/A
		Shear Strength, psi	14.7	1.8	12.2
		LWD Modulus, ksi	8.0	3.9	48.8
		Seismic Modulus, ksi	14.8	2.2	14.8
		GeoGauge Modulus, ksi	11.3	2.2	19.2
	P-154MR	Density (nuclear), pcf	138.9	N/A	N/A
		Moisture (nuclear), %	3.6	N/A	N/A
		LWD Modulus, ksi	14.4	0.8	5.9
		Seismic Modulus, ksi	68.8	10.1	14.7
		GeoGauge Modulus, ksi	18.0	2.8	15.5
	P-209MR	Density (Nuclear), pcf	151.4	N/A	N/A
		M.C. (Nuclear), %	2.6	N/A	N/A
		LWD Modulus, ksi	20.1	1.4	7.0
		Seismic Modulus, ksi	44.8	7.5	16.8
		GeoGauge Modulus, ksi	11.4	1.1	9.6
	P-401MR	Mat Density, %	97.9	N/A	N/A
		Joint Density, %	91.3	N/A	N/A
		Lab Air Voids, %	4.1	N/A	N/A
		Seismic Modulus, ksi	3,405.2	144.9	4.3
		Elastic Modulus, ksi	1,112.7	48.8	4.4
LFC-3S	P-152MR	CBR, %	4.8	0.5	9.5
		M.C., %	27.1	N/A	N/A
		In-Situ Dry Density, pcf	96.9	N/A	N/A
		Shear Strength, psi	18.4	3.9	21.2
		LWD Modulus, ksi	9.3	4.9	53.1
		Seismic Modulus, ksi	15.7	2.7	17.4
		GeoGauge Modulus, ksi	13.1	1.8	13.9
	P-154MR	Density (nuclear), pcf	141.1	N/A	N/A
		Moisture (nuclear), %	3.1	N/A	N/A
		LWD Modulus, ksi	15.3	1.6	10.7
		Seismic Modulus, ksi	70.8	14.5	20.4
		GeoGauge Modulus, ksi	18.6	3.3	17.7
	P-209MR	Density (Nuclear), pcf	151.3	N/A	N/A
		M.C. (Nuclear), %	2.3	N/A	N/A

Test Item	Material[1]	Parameter	Average	Standard Deviation	COV, %
		LWD Modulus, ksi	25.2	2.2	8.5
		Seismic Modulus, ksi	66.2	11.1	16.8
		GeoGauge Modulus, ksi	13.9	1.6	11.3
	P-401MR	Mat Density, %	94.4	N/A	N/A
		Joint Density, %	91.3	N/A	N/A
		Lab Air Voids, %	4.1	N/A	N/A
		Seismic Modulus, ksi	3,213.1	125.7	3.9
		Elastic Modulus, ksi	903.0	180.0	19.9

[1]Tests reported were those conducted on the final surface lift.

Table A-3. Material Acceptance and Characterization Results for the CTPB Test Area

Test Item	Material[1]	Parameter	Average	Standard Deviation	COV, %
LFS-4N	P-152MR	CBR, %	5.4	0.4	7.7
		M.C., %	24.0	N/A	N/A
		In-Situ Dry Density, pcf	99.4	N/A	N/A
		Shear Strength, psi	18.2	3.8	21.1
		LWD Modulus, ksi	6.8	4.9	71.9
		Seismic Modulus, ksi	22.4	4.5	19.9
		GeoGauge Modulus, ksi	14.0	3.0	21.2
	P-154MR	Density (nuclear), pcf	138.7	N/A	N/A
		Moisture (nuclear), %	3.4	N/A	N/A
		LWD Modulus, ksi	14.1	0.9	6.1
		Seismic Modulus, ksi	64.9	7.4	11.5
		GeoGauge Modulus, ksi	16.6	2.1	12.9
	P-307MR	7-day Compressive Strength[2], psi	1441	354	24.6
		Coefficient of Permeability, ft/day	3871	N/A	N/A
		7-day LWD Modulus, ksi	228.8	29.0	12.7
		7-day Compressive Strength[3], psi	1068.9	345.0	32.3
		7-day Flexural Strength, psi	318.9	57.5	18.0
		28-day LWD Modulus, ksi	248.2	31.5	12.7
		28-day Compressive Strength[3], psi	1118.3	318.2	28.5
		28-day Flexural Strength, psi	330.0	55.2	16.7
	P-401MR	Mat Density, %	98.1	N/A	N/A
		Joint Density, %	95.6	N/A	N/A
		Lab Air Voids, %	4.1	N/A	N/A

Test Item	Material[1]	Parameter	Average	Standard Deviation	COV, %
		Seismic Modulus, ksi	3,337.0	104.3	3.1
		Elastic Modulus, ksi	1,194.0	161.2	13.5
LFC-4S	P-152MR	CBR, %	5.3	0.5	10.0
		M.C., %	27.1	N/A	N/A
		In-Situ Dry Density, pcf	95.5	N/A	N/A
		Shear Strength, psi	14.6	3.4	23.1
		LWD Modulus, ksi	6.8	4.9	71.9
		Seismic Modulus, ksi	15.9	2.3	14.4
		GeoGauge Modulus, ksi	11.6	2.4	20.5
	P-154MR	Density (nuclear), pcf	138.9	N/A	N/A
		Moisture (nuclear), %	4.2	N/A	N/A
		LWD Modulus, ksi	14.4	0.6	4.3
		Seismic Modulus, ksi	74.8	8.3	11.1
		GeoGauge Modulus, ksi	17.3	1.3	7.7
	P-209MR	Density (Nuclear), pcf	152.4	N/A	N/A
		M.C. (Nuclear), %	2.0	N/A	N/A
		LWD Modulus, ksi	23.2	1.8	7.9
		Seismic Modulus, ksi	67.6	11.0	16.3
		GeoGauge Modulus, ksi	14.1	1.6	11.4
	P-401MR	Mat Density, %	95.6	N/A	N/A
		Joint Density, %	91.2	N/A	N/A
		Lab Air Voids, %	4.1	N/A	N/A
		Seismic Modulus, ksi	3,063.0	221.2	7.2
		Elastic Modulus, ksi	1,494.0	230.8	15.5

[1]Tests reported were those conducted on the final, surface lift.
[2]Cylinders were consolidated using the method described in ASTM C31.
[3]Cylinders were consolidated using the method described in ASTM C1688 and finishing with a strike off plate.

TableA-4. Material Acceptance and Characterization Results for the Overload Test Area

Test Item	Material[1]	Parameter	Average	Standard Deviation	COV, %
LFC-5N	P-152MR	CBR, %	5.5	0.2	3.8
		M.C., %	24.2	N/A	N/A
		In-Situ Dry Density, pcf	100.1	N/A	N/A
		Shear Strength, psi	14.8	1.6	10.6
		LWD Modulus, ksi	12.6	4.0	32.1
		Seismic Modulus, ksi	20.6	1.7	8.0
		GeoGauge Modulus, ksi	15.8	2.6	16.8
	P-154MR	Density (nuclear), pcf	141.5	N/A	N/A
		Moisture (nuclear), %	3.7	N/A	N/A
		LWD Modulus, ksi	13.2	1.5	11.6
		Seismic Modulus, ksi	66.6	13.6	20.4
		GeoGauge Modulus, ksi	15.1	1.8	11.9
	P-209MR	Density (Nuclear), pcf	154.2	N/A	N/A
		M.C. (Nuclear), %	2.5	N/A	N/A
		LWD Modulus, ksi	22.5	2.2	9.9
		Seismic Modulus, ksi	53.5	16.6	31.1
		GeoGauge Modulus, ksi	13.2	1.4	10.4
	P-401MR	Mat Density, %	93.7	N/A	N/A
		Joint Density, %	94.3	0.8	0.8
		Lab Air Voids, %	6.4	N/A	N/A
		Seismic Modulus, ksi	2,289.0	584.1	25.5
		Elastic Modulus, ksi	891.7	84.3	9.5
LFC-5S	P-152MR	CBR, %	5.2	0.3	5.8
		M.C., %	24.0	N/A	N/A
		In-Situ Dry Density, pcf	99.8	N/A	N/A
		Shear Strength, psi	12.3	1.0	8.0
		LWD Modulus, ksi	7.1	3.3	46.5
		Seismic Modulus, ksi	17.2	2.1	12.4
		GeoGauge Modulus, ksi	14.3	3.0	21.1
	P-154MR	Density (nuclear), pcf	138.8	N/A	N/A
		Moisture (nuclear), %	4.4	N/A	N/A
		LWD Modulus, ksi	13.8	2.0	14.4
		Seismic Modulus, ksi	62.5	9.0	14.4
		GeoGauge Modulus, ksi	16.0	1.2	7.6
	P-209MR	Density (Nuclear), pcf	151.8	N/A	N/A
		M.C. (Nuclear), %	2.2	N/A	N/A

Test Item	Material[1]	Parameter	Average	Standard Deviation	COV, %
		LWD Modulus, ksi	20.2	1.0	5.1
		Seismic Modulus, ksi	46.1	10.0	21.8
		GeoGauge Modulus, ksi	13.3	2.0	14.7
	P-401MR	Mat Density, %	95.2	N/A	N/A
		Joint Density, %	94.3	0.8	0.8
		Lab Air Voids, %	6.4	N/A	N/A
		Seismic Modulus, ksi	2,013.2	285.7	14.2
		Elastic Modulus, ksi	839.0	92.8	11.1

[1]Tests reported were those conducted on the final surface lift.

APPENDIX B—SENSOR LOCATIONS

Table B-1. Locations of Embedded Sensors in Test Item LFS-1N

Sensor ID	Station (ft)	Transverse Offset (ft)	Embedment Depth (in.)
CS-LFS1N-1	22.5	-12.75	12
CS-LFS1N-2	22.5	-12.75	15
CS-LFS1N-3	22.5	-12.75	37.92
CS-LFS1N-4	22.5	-12.75	40.92
CS-LFS1N-5	30	-15	12
CS-LFS1N-6	30	-15	15
CS-LFS1N-7	30	-15	18
CS-LFS1N-8	30	-15	21
CS-LFS1N-9	30	-15	24
CS-LFS1N-10	30	-15	27
CS-LFS1N-11	30	-15	30
CS-LFS1N-12	30	-15	33
CS-LFS1N-13	30	-15	36
LSG-LFS1N-1	5	-17.25	11
LSG-LFS1N-2	7	-17.25	11
LSG-LFS1N-3	5	-12.75	11
LSG-LFS1N-4	7	-12.75	11
MS-LFS1N-1	21.5	-14	43
MS-LFS1N-2	22.5	-14	46
MS-LFS1N-3	23.5	-14	49
PC-LFS1N-1	22.5	-15	11
PC-LFS1N-2	22.5	-15	37
T-LFS1N-1	22.5	-27	0
T-LFS1N-2	22.5	-27	1
T-LFS1N-3	22.5	-27	2
T-LFS1N-4	22.5	-27	3
T-LFS1N-5	22.5	-27	4
T-LFS1N-6	22.5	-27	7.5
T-LFS1N-7	22.5	-27	11
TSG-LFS1N-1	9	-17.25	11
TSG-LFS1N-2	11	-17.25	11
TSG-LFS1N-3	9	-12.75	11
TSG-LFS1N-4	11	-12.75	11

Table B-2. Locations of Embedded Sensors in Test Item LFS-1S

Sensor ID	Station (ft)	Transverse Offset (ft)	Embedment Depth (in.)
CS-LFS1S-1	22.5	12.75	10
CS-LFS1S-2	22.5	12.75	13
CS-LFS1S-3	22.5	12.75	36
CS-LFS1S-4	22.5	12.75	39
CS-LFS1S-5	30	15	10
CS-LFS1S-6	30	15	13
CS-LFS1S-7	30	15	16
CS-LFS1S-8	30	15	19
CS-LFS1S-9	30	15	22
CS-LFS1S-10	30	15	25
CS-LFS1S-11	30	15	28
CS-LFS1S-12	30	15	31
CS-LFS1S-13	30	15	34
LSG-LFS1S-1	5	12.75	9
LSG-LFS1S-2	7	12.75	9
LSG-LFS1S-3	5	17.25	9
LSG-LFS1S-4	7	17.25	9
MS-LFS1S-1	21.5	16	41
MS-LFS1S-2	22.5	16	44
PC-LFS1S-1	22.5	15	9
PC-LFS1S-2	22.5	15	35
T-LFS1S-1	22.5	27	0
T-LFS1S-2	22.5	27	1
T-LFS1S-3	22.5	27	2
T-LFS1S-4	22.5	27	3
T-LFS1S-5	22.5	27	4
T-LFS1S-6	22.5	27	6.5
T-LFS1S-7	22.5	27	9
TSG-LFS1S-1	9	12.75	9
TSG-LFS1S-2	11	12.75	9
TSG-LFS1S-3	9	17.25	9
TSG-LFS1S-4	11	17.25	9

Table B-3. Locations of Embedded Sensors in Test Item LFS-2N

Sensor ID	Station (ft)	Transverse Offset (ft)	Embedment Depth (in.)
CS-LFS2N-1	82.5	-12.75	12
CS-LFS2N-2	82.5	-12.75	15
CS-LFS2N-3	82.5	-12.75	42
CS-LFS2N-4	82.5	-12.75	45
LSG-LFS2N-1	65	-17.25	11
LSG-LFS2N-2	67	-17.25	11
LSG-LFS2N-3	65	-12.75	11
LSG-LFS2N-4	67	-12.75	11
MS-LFS2N-1	81.5	-14	47
MS-LFS2N-2	82.5	-14	50
PC-LFS2N-1	82.5	-15	11
PC-LFS2N-2	82.5	-15	41
TSG-LFS2N-1	69	-17.25	11
TSG-LFS2N-2	71	-17.25	11
TSG-LFS2N-3	69	-12.75	11
TSG-LFS2N-4	71	-12.75	11

Table B-4. Locations of Embedded Sensors in Test Item LFS-2S

Sensor ID	Station (ft)	Transverse Offset (ft)	Embedment Depth (in.)
CS-LFS2S-1	82.5	12.75	10
CS-LFS2S-2	82.5	12.75	13
CS-LFS2S-3	82.5	12.75	40
CS-LFS2S-4	82.5	12.75	43
LSG-LFS2S-1	65	12.75	9
LSG-LFS2S-2	67	12.75	9
LSG-LFS2S-3	65	17.25	9
LSG-LFS2S-4	67	17.25	9
MS-LFS2S-1	81.5	16	45
MS-LFS2S-2	82.5	16	48
PC-LFS2S-1	82.5	15	9
PC-LFS2S-2	82.5	15	39
TSG-LFS2S-1	69	12.75	9
TSG-LFS2S-2	71	12.75	9
TSG-LFS2S-3	69	17.25	9
TSG-LFS2S-4	71	17.25	9

Table B-5. Locations of Embedded Sensors in Test Item LFC-3N

Sensor ID	Station (ft)	Transverse Offset (ft)	Embedment Depth (in.)
CS-LFC3N-1	142.5	-12.75	14
CS-LFC3N-2	142.5	-12.75	17
CS-LFC3N-3	142.5	-12.75	43
CS-LFC3N-4	142.5	-12.75	46
LSG-LFC3N-1	125	-17.25	5
LSG-LFC3N-2	127	-17.25	5
LSG-LFC3N-3	125	-12.75	5
LSG-LFC3N-4	127	-12.75	5
MS-LFC3N-1	141.5	-15	48.96
PC-LFC3N-1	142.5	-15	5
PC-LFC3N-2	142.5	-15	15
PC-LFC3N-3	142.5	-15	21
PC-LFC3N-4	142.5	-15	44
T-LFC3N-1	142.5	-27	0
T-LFC3N-2	142.5	-27	1
T-LFC3N-3	142.5	-27	2
T-LFC3N-4	142.5	-27	3
T-LFC3N-5	142.5	-27	4
T-LFC3N-6	142.5	-27	5
TSG-LFC3N-1	129	-17.25	5
TSG-LFC3N-2	131	-17.25	5
TSG-LFC3N-3	129	-12.75	5
TSG-LFC3N-4	131	-12.75	5

Table B-6. Locations of Embedded Sensors in Test Item LFC-3S

Sensor ID	Station (ft)	Transverse Offset (ft)	Embedment Depth (in.)
CS-LFC3S-1	142.5	12.75	14
CS-LFC3S-2	142.5	12.75	17
CS-LFC3S-3	142.5	12.75	43
CS-LFC3S-4	142.5	12.75	46
CS-LFC3S-5	150	15	5.54
CS-LFC3S-6	150	15	8.54
CS-LFC3S-7	150	15	11.54
CS-LFC3S-8	150	15	14.54
LSG-LFC3S-1	125	12.75	5
LSG-LFC3S-2	127	12.75	5
LSG-LFC3S-3	125	17.25	5
LSG-LFC3S-4	127	17.25	5
MS-LFC3S-1	141.5	15	48
PC-LFC3S-1	142.5	15	5
PC-LFC3S-2	142.5	15	13
PC-LFC3S-3	142.5	15	19
PC-LFC3S-4	142.5	15	44
TSG-LFC3S-1	129	12.75	5
TSG-LFC3S-2	131	12.75	5
TSG-LFC3S-3	129	17.25	5
TSG-LFC3S-4	131	17.25	5

Table B-7. Locations of Embedded Sensors in Test Item LFC-4N

Sensor ID	Station (ft)	Transverse Offset (ft)	Embedment Depth (in.)
CS-LFC4N-1	202.5	-12.75	14
CS-LFC4N-2	202.5	-12.75	17
CS-LFC4N-3	202.5	-12.75	43
CS-LFC4N-4	202.5	-12.75	46
LSG-LFS4N-1	185	-17.25	5
LSG-LFS4N-2	187	-17.25	5
LSG-LFS4N-3	185	-12.75	5
LSG-LFS4N-4	187	-12.75	5
MS-LFS4N-1	202.5	-15	48
PC-LFS4N-1	202.5	-15	13
PC-LFS4N-2	202.5	-15	42
T-LFS4N-1	202.8	-28.71	0
T-LFS4N-2	202.8	-28.71	1
T-LFS4N-3	202.8	-28.71	2
T-LFS4N-4	202.8	-28.71	3
T-LFS4N-5	202.8	-28.71	4
T-LFS4N-6	202.8	-28.71	5
TSG-LFS4N-1	189	-17.25	5
TSG-LFS4N-2	191	-17.25	5
TSG-LFS4N-3	189	-12.75	5
TSG-LFS4N-4	191	-12.75	5

Table B-8. Locations of Embedded Sensors in Test Item LFS-4S

Sensor ID	Station (ft)	Transverse Offset (ft)	Embedment Depth (in.)
CS-LFC4S-1	202.5	12.75	14
CS-LFC4S-2	202.5	12.75	17
CS-LFC4S-3	202.5	12.75	43
CS-LFC4S-4	202.5	12.75	46
CS-LFC4S-5	210	15	5.54
CS-LFC4S-6	210	15	8.54
CS-LFC4S-7	210	15	11.54
CS-LFC4S-8	210	15	14.54
LSG-LFC4S-1	185	12.75	5
LSG-LFC4S-2	187	12.75	5
LSG-LFC4S-3	185	17.25	5
LSG-LFC4S-4	187	17.25	5
MS-LFC4S-1	202.5	15	48
PC-LFC4S-1	202.5	15	5
PC-LFC4S-2	202.5	15	13
PC-LFC4S-3	202.5	15	19
PC-LFC4S-4	202.5	15	42
TSG-LFC4S-1	189	12.75	5
TSG-LFC4S-2	191	12.75	5
TSG-LFC4S-3	189	17.25	5
TSG-LFC4S-4	191	17.25	5

Table B-9. Locations of Embedded Sensors in Test Item LFC-5N

Sensor ID	Station (ft)	Transverse Offset (ft)	Embedment Depth (in.)
CS-LFC5N-1	262.52	-17.27	30.58
CS-LFC5N-2	262.52	-17.27	33.58
CS-LFC5N-3	262.45	-12.79	30.48
CS-LFC5N-4	262.45	-12.79	33.48
LSG-LFC5N-1	245	-17.25	3
LSG-LFC5N-2	247	-17.25	3
LSG-LFC5N-3	245	-12.75	3
LSG-LFC5N-4	247	-12.75	3
LSG-LFC5N-5	276	-17.25	3
LSG-LFC5N-6	276	-12.75	3
MS-LFC5N-1	262.5	-15	35
MS-LFC5N-2	262.5	-15	42
PC-LFC5N-1	262.5	-15	9
PC-LFC5N-2	262.5	-15	29
T-LFC5N-1	262.5	-27	0
T-LFC5N-2	262.5	-27	1
T-LFC5N-3	262.5	-27	2
T-LFC5N-4	262.5	-27	3
TSG-LFC5N-1	249	-17.25	3
TSG-LFC5N-2	251	-17.25	3
TSG-LFC5N-3	249	-12.75	3
TSG-LFC5N-4	251	-12.75	3
TSG-LFC5N-5	278	-17.25	3
TSG-LFC5N-6	278	-12.75	3

Table B-10. Locations of Embedded Sensors in Test Item LFC-5S

Sensor ID	Station (ft)	Transverse Offset (ft)	Embedment Depth (in.)
CS-LFC5S-1	262.44	17.19	30.66
CS-LFC5S-2	262.44	17.19	33.66
CS-LFC5S-3	262.46	12.77	30.58
CS-LFC5S-4	262.46	12.77	33.58
LSG-LFC5S-1	245	12.75	3
LSG-LFC5S-2	247	12.75	3
LSG-LFC5S-3	245	17.25	3
LSG-LFC5S-4	247	17.25	3
LSG-LFC5S-5	276	12.75	3
LSG-LFC5S-6	276	17.25	3
MS-LFC5S-1	262.5	15	35
PC-LFC5S-1	262.5	15	9
PC-LFC5S-2	262.5	15	29
TSG-LFC5S-1	249	12.75	3
TSG-LFC5S-2	251	12.75	3
TSG-LFC5S-3	249	17.25	3
TSG-LFC5S-4	251	17.25	3
TSG-LFC5S-5	278	12.75	3
TSG-LFC5S-6	278	17.25	3

APPENDIX C—TRAFFIC LOG

CC9	Vehicle Pass Number	Pass # by Test Item											Insert #	Daily Notes
		1N	1S	2N	2S	3N	3S	4N	4S	5N	5S	Wander Number	Wanders (Daily)	
Vehicle Pass:	96,294	75,042	75,042	75,042	75,042	40,920	40,920	40,920	40,920	56,628	56,100			
4/5/2021	132	132	132	132	132	132	132	132	132			2	2	Start of Test - 1N/S, 2N/S, 3N/S, 4N/S only - 2 Wanders
4/6/2021	330	330	330	330	330	330	330	330	330			5	3	1N/S, 2N/S, 3N/S, 4N/S only - 3 Wanders
4/12/2021	462	462	462	462	462	462	462	462	462			7	2	1N/S, 2N/S, 3N/S, 4N/S only - 2 Wanders
4/13/2021	660	660	660	660	660	660	660	660	660			10	3	1N/S, 2N/S, 3N/S, 4N/S only - 3 Wanders
4/14/2021	858	858	858	858	858	858	858	858	858			13	3	1N/S, 2N/S, 3N/S, 4N/S only - 3 Wanders
4/19/2021	1,056	1,056	1,056	1,056	1,056	1,056	1,056	1,056	1,056			16	3	1N/S, 2N/S, 3N/S, 4N/S only - 3 Wanders
4/20/2021	1,254	1,254	1,254	1,254	1,254	1,254	1,254	1,254	1,254			19	3	1N/S, 2N/S, 3N/S, 4N/S only - 3 Wanders
4/21/2021	1,452	1,452	1,452	1,452	1,452	1,452	1,452	1,452	1,452			22	3	1N/S, 2N/S, 3N/S, 4N/S only - 3 Wanders
4/26/2021	1,650	1,650	1,650	1,650	1,650	1,650	1,650	1,650	1,650			25	3	1N/S, 2N/S, 3N/S, 4N/S only - 3 Wanders
4/27/2021	1,848	1,848	1,848	1,848	1,848	1,848	1,848	1,848	1,848			28	3	1N/S, 2N/S, 3N/S, 4N/S only - 3 Wanders
4/28/2021	2,046	2,046	2,046	2,046	2,046	2,046	2,046	2,046	2,046			31	3	1N/S, 2N/S, 3N/S, 4N/S only - 3 Wanders
5/3/2021	2,244	2,244	2,244	2,244	2,244	2,244	2,244	2,244	2,244			34	3	1N/S, 2N/S, 3N/S, 4N/S only - 3 Wanders
5/4/2021	2,442	2,442	2,442	2,442	2,442	2,442	2,442	2,442	2,442			37	3	1N/S, 2N/S, 3N/S, 4N/S only - 3 Wanders
5/5/2021	2,640	2,640	2,640	2,640	2,640	2,640	2,640	2,640	2,640			40	3	1N/S, 2N/S, 3N/S, 4N/S only - 3 Wanders
5/10/2021	2,838	2,838	2,838	2,838	2,838	2,838	2,838	2,838	2,838			43	3	1N/S, 2N/S, 3N/S, 4N/S only - 3 Wanders
5/11/2021	3,036	3,036	3,036	3,036	3,036	3,036	3,036	3,036	3,036			46	3	1N/S, 2N/S, 3N/S, 4N/S only - 3 Wanders
5/12/2021	3,234	3,234	3,234	3,234	3,234	3,234	3,234	3,234	3,234			49	3	1N/S, 2N/S, 3N/S, 4N/S only - 3 Wanders
5/28/2021	3,366	3,366	3,366	3,366	3,366	3,366	3,366	3,366	3,366			51	2	1N/S, 2N/S, 3N/S, 4N/S only - 2 Wanders
6/1/2021	3,564	3,564	3,564	3,564	3,564	3,564	3,564	3,564	3,564			54	3	1N/S, 2N/S, 3N/S, 4N/S only - 3 Wanders
6/2/2021	3,762	3,762	3,762	3,762	3,762	3,762	3,762	3,762	3,762			57	3	1N/S, 2N/S, 3N/S, 4N/S only - 3 Wanders
6/7/2021	3,960	3,960	3,960	3,960	3,960	3,960	3,960	3,960	3,960			60	3	1N/S, 2N/S, 3N/S, 4N/S only - 3 Wanders
6/8/2021	4,158	4,158	4,158	4,158	4,158	4,158	4,158	4,158	4,158			63	3	1N/S, 2N/S, 3N/S, 4N/S only - 3 Wanders
6/9/2021	4,356	4,356	4,356	4,356	4,356	4,356	4,356	4,356	4,356			66	3	1N/S, 2N/S, 3N/S, 4N/S only - 3 Wanders
6/14/2021	4,554	4,554	4,554	4,554	4,554	4,554	4,554	4,554	4,554			69	3	1N/S, 2N/S, 3N/S, 4N/S only - 3 Wanders
6/15/2021	4,752	4,752	4,752	4,752	4,752	4,752	4,752	4,752	4,752			72	3	1N/S, 2N/S, 3N/S, 4N/S only - 3 Wanders
6/16/2021	4,950	4,950	4,950	4,950	4,950	4,950	4,950	4,950	4,950			75	3	1N/S, 2N/S, 3N/S, 4N/S only - 3 Wanders
6/21/2021	5,148	5,148	5,148	5,148	5,148	5,148	5,148	5,148	5,148			78	3	1N/S, 2N/S, 3N/S, 4N/S only - 3 Wanders
6/22/2021	5,346	5,346	5,346	5,346	5,346	5,346	5,346	5,346	5,346			81	3	1N/S, 2N/S, 3N/S, 4N/S only - 3 Wanders
6/23/2021	5,544	5,544	5,544	5,544	5,544	5,544	5,544	5,544	5,544			84	3	1N/S, 2N/S, 3N/S, 4N/S only - 3 Wanders
7/6/2021	264									264	198	4	4	5N/S only - 4 Wanders. Wander No. 1: 5N received overload traffic, 5S no traffic. Pass Nos. start over at 1.
7/7/2021	726									726	660	11	7	5N/S only - 7 Wanders
7/8/2021	1,254									1,254	1,188	19	8	5N/S only - 8 Wanders
7/9/2021	1,518									1,518	1,452	23	4	5N/S only - 4 Wanders
7/12/2021	2,046									2,046	1,980	31	8	5N/S only - 8 Wanders
7/13/2021	2,640									2,640	2,574	40	9	5N/S only - 9 Wanders
7/14/2021	3,168									3,168	3,102	48	8	5N/S only - 8 Wanders
7/15/2021	3,696									3,696	3,630	56	8	5N/S only - 8 Wanders
7/16/2021	3,960									3,960	3,894	60	4	5N/S only - 4 Wanders
7/26/2021	4,422									4,422	4,356	67	7	5N/S only - 7 Wanders
7/27/2021	5,016									5,016	4,950	76	9	5N/S only - 9 Wanders
7/28/2021	5,544									5,544	5,478	84	8	5N/S only - 8 Wanders
8/2/2021	5,742	5,742	5,742	5,742	5,742	5,742	5,742	5,742	5,742	5,742	5,676	87	3	All CC9 - 3 Wanders.
8/3/2021	5,940	5,940	5,940	5,940	5,940	5,940	5,940	5,940	5,940	5,940	5,874	90	3	All CC9 - 3 Wanders.
8/4/2021	6,138	6,138	6,138	6,138	6,138	6,138	6,138	6,138	6,138	6,138	6,072	93	3	All CC9 - 3 Wanders.
8/9/2021	6,336	6,336	6,336	6,336	6,336	6,336	6,336	6,336	6,336	6,336	6,270	96	3	All CC9 - 3 Wanders.
8/10/2021	6,534	6,534	6,534	6,534	6,534	6,534	6,534	6,534	6,534	6,534	6,468	99	3	All CC9 - 3 Wanders.
8/11/2021	6,666	6,666	6,666	6,666	6,666	6,666	6,666	6,666	6,666	6,666	6,600	101	2	All CC9 - 2 Wanders.
8/17/2021	6,864	6,864	6,864	6,864	6,864	6,864	6,864	6,864	6,864	6,864	6,798	104	3	All CC9 - 3 Wanders.
8/18/2021	7,062	7,062	7,062	7,062	7,062	7,062	7,062	7,062	7,062	7,062	6,996	107	3	All CC9 - 3 Wanders.
8/24/2021	7,128	7,128	7,128	7,128	7,128	7,128	7,128	7,128	7,128	7,128	7,062	108	1	All CC9 - 1 Wander.
8/25/2021	7,326	7,326	7,326	7,326	7,326	7,326	7,326	7,326	7,326	7,326	7,260	111	3	All CC9 - 3 Wanders.
8/26/2021	7,524	7,524	7,524	7,524	7,524	7,524	7,524	7,524	7,524	7,524	7,458	114	3	All CC9 - 3 Wanders.
8/27/2021	7,722	7,722	7,722	7,722	7,722	7,722	7,722	7,722	7,722	7,722	7,656	117	3	All CC9 - 3 Wanders.

CC9	Vehicle Pass Number	Pass # by Test Item											Insert #	Daily Notes
		1N	1S	2N	2S	3N	3S	4N	4S	5N	5S	Wander Number	Wanders (Daily)	
Vehicle Pass:	96,294	75,042	75,042	75,042	75,042	40,920	40,920	40,920	40,920	56,628	56,100			
8/30/2021	7,920	7,920	7,920	7,920	7,920	7,920	7,920	7,920	7,920	7,920	7,854	120	3	All CC9 - 3 Wanders.
8/31/2021	8,118	8,118	8,118	8,118	8,118	8,118	8,118	8,118	8,118	8,118	8,052	123	3	All CC9 - 3 Wanders.
9/1/2021	8,316	8,316	8,316	8,316	8,316	8,316	8,316	8,316	8,316	8,316	8,250	126	3	All CC9 - 3 Wanders.
9/7/2021	8,514	8,514	8,514	8,514	8,514	8,514	8,514	8,514	8,514	8,514	8,448	129	3	All CC9 - 3 Wanders.
9/8/2021	8,712	8,712	8,712	8,712	8,712	8,712	8,712	8,712	8,712	8,712	8,646	132	3	All CC9 - 3 Wanders.
9/9/2021	8,910	8,910	8,910	8,910	8,910	8,910	8,910	8,910	8,910	8,910	8,844	135	3	All CC9 - 3 Wanders.
9/10/2021	9,108	9,108	9,108	9,108	9,108	9,108	9,108	9,108	9,108	9,108	9,042	138	3	All CC9 - 3 Wanders.
9/13/2021	9,306	9,306	9,306	9,306	9,306	9,306	9,306	9,306	9,306	9,306	9,240	141	3	All CC9 - 3 Wanders.
9/14/2021	9,504	9,504	9,504	9,504	9,504	9,504	9,504	9,504	9,504	9,504	9,438	144	3	All CC9 - 3 Wanders.
9/15/2021	9,702	9,702	9,702	9,702	9,702	9,702	9,702	9,702	9,702	9,702	9,636	147	3	All CC9 - 3 Wanders.
9/20/2021	9,900	9,900	9,900	9,900	9,900	9,900	9,900	9,900	9,900	9,900	9,834	150	3	All CC9 - 3 Wanders.
9/21/2021	10,098	10,098	10,098	10,098	10,098	10,098	10,098	10,098	10,098	10,098	10,032	153	3	All CC9 - 3 Wanders.
9/22/2021	10,296	10,296	10,296	10,296	10,296	10,296	10,296	10,296	10,296	10,296	10,230	156	3	All CC9 - 3 Wanders.
9/23/2021	10,494	10,494	10,494	10,494	10,494	10,494	10,494	10,494	10,494	10,494	10,428	159	3	All CC9 - 3 Wanders.
9/24/2021	10,692	10,692	10,692	10,692	10,692	10,692	10,692	10,692	10,692	10,692	10,626	162	3	All CC9 - 3 Wanders.
9/27/2021	10,890	10,890	10,890	10,890	10,890	10,890	10,890	10,890	10,890	10,890	10,824	165	3	All CC9 - 3 Wanders.
9/28/2021	11,088	11,088	11,088	11,088	11,088	11,088	11,088	11,088	11,088	11,088	11,022	168	3	All CC9 - 3 Wanders.
9/29/2021	11,286	11,286	11,286	11,286	11,286	11,286	11,286	11,286	11,286	11,286	11,220	171	3	All CC9 - 3 Wanders.
10/5/2021	11,484	11,484	11,484	11,484	11,484	11,484	11,484	11,484	11,484	11,484	11,418	174	3	All CC9 - 3 Wanders.
10/6/2021	11,682	11,682	11,682	11,682	11,682	11,682	11,682	11,682	11,682	11,682	11,616	177	3	All CC9 - 3 Wanders.
10/7/2021	11,880	11,880	11,880	11,880	11,880	11,880	11,880	11,880	11,880	11,880	11,814	180	3	All CC9 - 3 Wanders.
10/8/2021	12,078	12,078	12,078	12,078	12,078	12,078	12,078	12,078	12,078	12,078	12,012	183	3	All CC9 - 3 Wanders.
10/12/2021	12,210	12,210	12,210	12,210	12,210	12,210	12,210	12,210	12,210	12,210	12,144	185	2	All CC9 - 2 Wanders.
10/13/2021	12,408	12,408	12,408	12,408	12,408	12,408	12,408	12,408	12,408	12,408	12,342	188	3	All CC9 - 3 Wanders.
10/14/2021	12,606	12,606	12,606	12,606	12,606	12,606	12,606	12,606	12,606	12,606	12,540	191	3	All CC9 - 3 Wanders.
10/15/2021	12,610	12,610	12,610	12,610	12,610	12,610	12,610	12,610	12,610	12,610	12,544	191.0606	0.0606	All CC9. Stop traffic for vehicle maintenance. 4 passes completed in wander no. 191.
2/22/2022	12,804	12,804	12,804	12,804	12,804	12,804	12,804	12,804	12,804	12,804	12,738	194	2.9394	Restart traffic after vehicle maintenance. Start at vehicle pass 12611 (seq. 5). All CC9 - 3 Wanders.
2/23/2022	13,002	13,002	13,002	13,002	13,002	13,002	13,002	13,002	13,002	13,002	12,936	197	3	All CC9 - 3 Wanders.
2/24/2022	13,200	13,200	13,200	13,200	13,200	13,200	13,200	13,200	13,200	13,200	13,134	200	3	All CC9 - 3 Wanders. Pass numbers incorrect in Daily Notes.
2/25/2022	13,398	13,398	13,398	13,398	13,398	13,398	13,398	13,398	13,398	13,398	13,332	203	3	All CC9 - 3 Wanders.
2/28/2022	13,596	13,596	13,596	13,596	13,596	13,596	13,596	13,596	13,596	13,596	13,530	206	3	All CC9 - 3 Wanders.
3/1/2022	13,794	13,794	13,794	13,794	13,794	13,794	13,794	13,794	13,794	13,794	13,728	209	3	All CC9 - 3 Wanders.
3/2/2022	13,992	13,992	13,992	13,992	13,992	13,992	13,992	13,992	13,992	13,992	13,926	212	3	All CC9 - 3 Wanders.
3/7/2022	14,190	14,190	14,190	14,190	14,190	14,190	14,190	14,190	14,190	14,190	14,124	215	3	All CC9 - 3 Wanders.
3/8/2022	14,388	14,388	14,388	14,388	14,388	14,388	14,388	14,388	14,388	14,388	14,322	218	3	All CC9 - 3 Wanders.
3/9/2022	14,586	14,586	14,586	14,586	14,586	14,586	14,586	14,586	14,586	14,586	14,520	221	3	All CC9 - 3 Wanders.
3/10/2022	14,784	14,784	14,784	14,784	14,784	14,784	14,784	14,784	14,784	14,784	14,718	224	3	All CC9 - 3 Wanders.
3/11/2022	14,982	14,982	14,982	14,982	14,982	14,982	14,982	14,982	14,982	14,982	14,916	227	3	All CC9 - 3 Wanders.
3/14/2022	15,180	15,180	15,180	15,180	15,180	15,180	15,180	15,180	15,180	15,180	15,114	230	3	All CC9 - 3 Wanders.
3/16/2022	15,378	15,378	15,378	15,378	15,378	15,378	15,378	15,378	15,378	15,378	15,312	233	3	All CC9 - 3 Wanders.
3/21/2022	15,576	15,576	15,576	15,576	15,576	15,576	15,576	15,576	15,576	15,576	15,510	236	3	All CC9 - 3 Wanders.
3/22/2022	15,774	15,774	15,774	15,774	15,774	15,774	15,774	15,774	15,774	15,774	15,708	239	3	All CC9 - 3 Wanders.
3/23/2022	15,972	15,972	15,972	15,972	15,972	15,972	15,972	15,972	15,972	15,972	15,906	242	3	All CC9 - 3 Wanders. No SPU files generated for passes 15875-15876
3/24/2022	16,170	16,170	16,170	16,170	16,170	16,170	16,170	16,170	16,170	16,170	16,104	245	3	All CC9 - 3 Wanders.
3/25/2022	16,368	16,368	16,368	16,368	16,368	16,368	16,368	16,368	16,368	16,368	16,302	248	3	All CC9 - 3 Wanders.
3/28/2022	16,566	16,566	16,566	16,566	16,566	16,566	16,566	16,566	16,566	16,566	16,500	251	3	All CC9 - 3 Wanders.
3/29/2022	16,764	16,764	16,764	16,764	16,764	16,764	16,764	16,764	16,764	16,764	16,632	254	3	All CC9 - 3 Wanders. Wander No. 252: 5N received overload traffic, 5S no traffic.
3/30/2022	16,962	16,962	16,962	16,962	16,962	16,962	16,962	16,962	16,962	16,962	16,830	257	3	All CC9 - 3 Wanders.
4/4/2022	17,160	17,160	17,160	17,160	17,160	17,160	17,160	17,160	17,160	17,160	17,028	260	3	All CC9 - 3 Wanders.
4/5/2022	17,358	17,358	17,358	17,358	17,358	17,358	17,358	17,358	17,358	17,358	17,226	263	3	All CC9 - 3 Wanders.
4/6/2022	17,556	17,556	17,556	17,556	17,556	17,556	17,556	17,556	17,556	17,556	17,424	266	3	All CC9 - 3 Wanders.
4/7/2022	17,754	17,754	17,754	17,754	17,754	17,754	17,754	17,754	17,754	17,754	17,622	269	3	All CC9 - 3 Wanders.
4/8/2022	17,952	17,952	17,952	17,952	17,952	17,952	17,952	17,952	17,952	17,952	17,820	272	3	All CC9 - 3 Wanders.

CC9	Vehicle Pass Number	Pass # by Test Item											Insert #	Daily Notes
		1N	1S	2N	2S	3N	3S	4N	4S	5N	5S	Wander Number	Wanders (Daily)	
Vehicle Pass:	96,294	75,042	75,042	75,042	75,042	40,920	40,920	40,920	40,920	56,628	56,100			
4/11/2022	18,150	18,150	18,150	18,150	18,150	18,150	18,150	18,150	18,150	18,150	18,018	275	3	All CC9 - 3 Wanders.
4/12/2022	18,348	18,348	18,348	18,348	18,348	18,348	18,348	18,348	18,348	18,348	18,216	278	3	All CC9 - 3 Wanders.
4/13/2022	18,480	18,480	18,480	18,480	18,480	18,480	18,480	18,480	18,480	18,480	18,348	280	2	All CC9 - 2 Wanders.
4/18/2022	18,678	18,678	18,678	18,678	18,678	18,678	18,678	18,678	18,678	18,678	18,546	283	3	All CC9 - 3 Wanders.
4/19/2022	18,876	18,876	18,876	18,876	18,876	18,876	18,876	18,876	18,876	18,876	18,744	286	3	All CC9 - 3 Wanders.
4/20/2022	19,074	19,074	19,074	19,074	19,074	19,074	19,074	19,074	19,074	19,074	18,942	289	3	All CC9 - 3 Wanders.
4/21/2022	19,272	19,272	19,272	19,272	19,272	19,272	19,272	19,272	19,272	19,272	19,140	292	3	All CC9 - 3 Wanders.
4/22/2022	19,470	19,470	19,470	19,470	19,470	19,470	19,470	19,470	19,470	19,470	19,338	295	3	All CC9 - 3 Wanders.
4/25/2022	19,668	19,668	19,668	19,668	19,668	19,668	19,668	19,668	19,668	19,668	19,536	298	3	All CC9 - 3 Wanders.
4/26/2022	19,866	19,866	19,866	19,866	19,866	19,866	19,866	19,866	19,866	19,866	19,734	301	3	All CC9 - 3 Wanders.
4/27/2022	20,064	20,064	20,064	20,064	20,064	20,064	20,064	20,064	20,064	20,064	19,932	304	3	All CC9 - 3 Wanders.
5/2/2022	20,328	20,328	20,328	20,328	20,328	20,328	20,328	20,328	20,328	20,328	20,196	308	4	All CC9 - 4 Wanders. PLC reset - passes 20065-20068 did not collect traffic files.
5/3/2022	20,592	20,592	20,592	20,592	20,592	20,592	20,592	20,592	20,592	20,592	20,460	312	4	All CC9 - 4 Wanders. Daily notes incorrectly numbers wanders (311 should be 312, etc.)
5/4/2022	20,856	20,856	20,856	20,856	20,856	20,856	20,856	20,856	20,856	20,856	20,724	316	4	All CC9 - 4 Wanders
5/5/2022	21,120	21,120	21,120	21,120	21,120	21,120	21,120	21,120	21,120	21,120	20,988	320	4	All CC9 - 4 Wanders
5/6/2022	21,384	21,384	21,384	21,384	21,384	21,384	21,384	21,384	21,384	21,384	21,252	324	4	All CC9 - 4 Wanders
5/9/2022	21,516	21,516	21,516	21,516	21,516	21,516	21,516	21,516	21,516	21,516	21,384	326	2	All CC9 - 2 Wanders. Daily Notes incorrectly states 4 wanders completed.
5/10/2022	21,780	21,780	21,780	21,780	21,780	21,780	21,780	21,780	21,780	21,780	21,648	330	4	All CC9 - 4 Wanders
5/11/2022	22,044	22,044	22,044	22,044	22,044	22,044	22,044	22,044	22,044	22,044	21,912	334	4	All CC9 - 4 Wanders
5/16/2022	22,308	22,308	22,308	22,308	22,308	22,308	22,308	22,308	22,308	22,308	22,176	338	4	All CC9 - 4 Wanders
5/17/2022	22,572	22,572	22,572	22,572	22,572	22,572	22,572	22,572	22,572	22,572	22,440	342	4	All CC9 - 4 Wanders
5/18/2022	22,836	22,836	22,836	22,836	22,836	22,836	22,836	22,836	22,836	22,836	22,704	346	4	All CC9 - 4 Wanders
5/19/2022	23,100	23,100	23,100	23,100	23,100	23,100	23,100	23,100	23,100	23,100	22,968	350	4	All CC9 - 4 Wanders
5/23/2022	23,364	23,364	23,364	23,364	23,364	23,364	23,364	23,364	23,364	23,364	23,232	354	4	All CC9 - 4 Wanders
5/24/2022	23,628	23,628	23,628	23,628	23,628	23,628	23,628	23,628	23,628	23,628	23,496	358	4	All CC9 - 4 Wanders
5/25/2022	23,892	23,892	23,892	23,892	23,892	23,892	23,892	23,892	23,892	23,892	23,760	362	4	All CC9 - 4 Wanders
5/31/2022	24,156	24,156	24,156	24,156	24,156	24,156	24,156	24,156	24,156	24,156	24,024	366	4	All CC9 - 4 Wanders
6/1/2022	24,420	24,420	24,420	24,420	24,420	24,420	24,420	24,420	24,420	24,420	24,288	370	4	All CC9 - 4 Wanders
6/2/2022	24,684	24,684	24,684	24,684	24,684	24,684	24,684	24,684	24,684	24,684	24,552	374	4	All CC9 - 4 Wanders
6/3/2022	24,948	24,948	24,948	24,948	24,948	24,948	24,948	24,948	24,948	24,948	24,816	378	4	All CC9 - 4 Wanders
6/6/2022	25,212	25,212	25,212	25,212	25,212	25,212	25,212	25,212	25,212	25,212	25,080	382	4	All CC9 - 4 Wanders
6/7/2022	25,476	25,476	25,476	25,476	25,476	25,476	25,476	25,476	25,476	25,476	25,344	386	4	All CC9 - 4 Wanders
6/8/2022	25,740	25,740	25,740	25,740	25,740	25,740	25,740	25,740	25,740	25,740	25,608	390	4	All CC9 - 4 Wanders
6/13/2022	26,004	26,004	26,004	26,004	26,004	26,004	26,004	26,004	26,004	26,004	25,872	394	4	All CC9 - 4 Wanders
6/14/2022	26,268	26,268	26,268	26,268	26,268	26,268	26,268	26,268	26,268	26,268	26,136	398	4	All CC9 - 4 Wanders
6/15/2022	26,532	26,532	26,532	26,532	26,532	26,532	26,532	26,532	26,532	26,532	26,400	402	4	All CC9 - 4 Wanders
6/16/2022	26,796	26,796	26,796	26,796	26,796	26,796	26,796	26,796	26,796	26,796	26,664	406	4	All CC9 - 4 Wanders. Passes 26797-26769 uncollected for SPU1 due to server crash
6/21/2022	27,060	27,060	27,060	27,060	27,060	27,060	27,060	27,060	27,060	27,060	26,928	410	4	All CC9 - 4 Wanders
6/22/2022	27,324	27,324	27,324	27,324	27,324	27,324	27,324	27,324	27,324	27,324	27,192	414	4	All CC9 - 4 Wanders
6/27/2022	27,588	27,588	27,588	27,588	27,588	27,588	27,588	27,588	27,588	27,588	27,456	418	4	All CC9 - 4 Wanders
6/28/2022	27,852	27,852	27,852	27,852	27,852	27,852	27,852	27,852	27,852	27,852	27,720	422	4	All CC9 - 4 Wanders
6/29/2022	28,116	28,116	28,116	28,116	28,116	28,116	28,116	28,116	28,116	28,116	27,984	426	4	All CC9 - 4 Wanders
6/30/2022	28,314	28,314	28,314	28,314	28,314	28,314	28,314	28,314	28,314	28,314	28,182	429	3	All CC9 - 3 Wanders
7/5/2022	28,578	28,578	28,578	28,578	28,578	28,578	28,578	28,578	28,578	28,578	28,446	433	4	All CC9 - 4 Wanders
7/6/2022	28,842	28,842	28,842	28,842	28,842	28,842	28,842	28,842	28,842	28,842	28,710	437	4	All CC9 - 4 Wanders
7/7/2022	29,106	29,106	29,106	29,106	29,106	29,106	29,106	29,106	29,106	29,106	28,974	441	4	All CC9 - 4 Wanders
7/8/2022	29,370	29,370	29,370	29,370	29,370	29,370	29,370	29,370	29,370	29,370	29,238	445	4	All CC9 - 4 Wanders
7/11/2022	29,634	29,634	29,634	29,634	29,634	29,634	29,634	29,634	29,634	29,634	29,502	449	4	All CC9 - 4 Wanders
7/12/2022	29,898	29,898	29,898	29,898	29,898	29,898	29,898	29,898	29,898	29,898	29,766	453	4	All CC9 - 4 Wanders
7/13/2022	30,162	30,162	30,162	30,162	30,162	30,162	30,162	30,162	30,162	30,162	30,030	457	4	All CC9 - 4 Wanders
7/18/2022	30,426	30,426	30,426	30,426	30,426	30,426	30,426	30,426	30,426	30,426	30,294	461	4	All CC9 - 4 Wanders
7/19/2022	30,690	30,690	30,690	30,690	30,690	30,690	30,690	30,690	30,690	30,690	30,558	465	4	All CC9 - 4 Wanders
7/20/2022	30,954	30,954	30,954	30,954	30,954	30,954	30,954	30,954	30,954	30,954	30,822	469	4	All CC9 - 4 Wanders

CC9	Vehicle Pass Number	Pass # by Test Item											Insert #	Daily Notes
		1N	1S	2N	2S	3N	3S	4N	4S	5N	5S	Wander Number	Wanders (Daily)	
Vehicle Pass:	96,294	75,042	75,042	75,042	75,042	40,920	40,920	40,920	40,920	56,628	56,100			
7/21/2022	31,218	31,218	31,218	31,218	31,218	31,218	31,218	31,218	31,218	31,218	31,086	473	4	All CC9 - 4 Wanders
7/26/2022	31,416	31,416	31,416	31,416	31,416	31,416	31,416	31,416	31,416	31,416	31,284	476	3	All CC9 - 3 Wanders
7/27/2022	31,680	31,680	31,680	31,680	31,680	31,680	31,680	31,680	31,680	31,680	31,548	480	4	All CC9 - 4 Wanders
7/28/2022	31,944	31,944	31,944	31,944	31,944	31,944	31,944	31,944	31,944	31,944	31,812	484	4	All CC9 - 4 Wanders
8/1/2022	32,208	32,208	32,208	32,208	32,208	32,208	32,208	32,208	32,208	32,208	32,076	488	4	All CC9 - 4 Wanders
8/2/2022	32,472	32,472	32,472	32,472	32,472	32,472	32,472	32,472	32,472	32,472	32,340	492	4	All CC9 - 4 Wanders
8/3/2022	32,736	32,736	32,736	32,736	32,736	32,736	32,736	32,736	32,736	32,736	32,604	496	4	All CC9 - 4 Wanders
8/4/2022	33,000	33,000	33,000	33,000	33,000	33,000	33,000	33,000	33,000	33,000	32,868	500	4	All CC9 - 4 Wanders
8/5/2022	33,264	33,264	33,264	33,264	33,264	33,264	33,264	33,264	33,264	33,264	33,132	504	4	All CC9 - 4 Wanders
8/8/2022	33,528	33,528	33,528	33,528	33,528	33,528	33,528	33,528	33,528	33,528	33,396	508	4	All CC9 - 4 Wanders
8/9/2022	33,660	33,660	33,660	33,660	33,660	33,660	33,660	33,660	33,660	33,660	33,528	510	2	All CC9 - 2 Wanders
8/10/2022	33,924	33,924	33,924	33,924	33,924	33,924	33,924	33,924	33,924	33,924	33,792	514	4	All CC9 - 4 Wanders
8/15/2022	34,188	34,188	34,188	34,188	34,188	34,188	34,188	34,188	34,188	34,188	34,056	518	4	All CC9 - 4 Wanders
8/16/2022	34,452	34,452	34,452	34,452	34,452	34,452	34,452	34,452	34,452	34,452	34,320	522	4	All CC9 - 4 Wanders
8/17/2022	34,716	34,716	34,716	34,716	34,716	34,716	34,716	34,716	34,716	34,716	34,584	526	4	All CC9 - 4 Wanders
8/18/2022	34,914	34,914	34,914	34,914	34,914	34,914	34,914	34,914	34,914	34,914	34,782	529	3	All CC9 - 3 Wanders
8/19/2022	35,178	35,178	35,178	35,178	35,178	35,178	35,178	35,178	35,178	35,178	35,046	533	4	All CC9 - 4 Wanders
8/22/2022	35,376	35,376	35,376	35,376	35,376	35,376	35,376	35,376	35,376	35,376	35,244	536	3	All CC9 - 3 Wanders
8/23/2022	35,640	35,640	35,640	35,640	35,640	35,640	35,640	35,640	35,640	35,640	35,508	540	4	All CC9 - 4 Wanders
8/24/2022	35,904	35,904	35,904	35,904	35,904	35,904	35,904	35,904	35,904	35,904	35,772	544	4	All CC9 - 4 Wanders
8/29/2022	36,102	36,102	36,102	36,102	36,102	36,102	36,102	36,102	36,102	36,102	35,970	547	3	All CC9 - 3 Wanders
8/30/2022	36,366	36,366	36,366	36,366	36,366	36,366	36,366	36,366	36,366	36,366	36,234	551	4	All CC9 - 4 Wanders
8/31/2022	36,630	36,630	36,630	36,630	36,630	36,630	36,630	36,630	36,630	36,630	36,498	555	4	All CC9 - 4 Wanders
9/1/2022	36,894	36,894	36,894	36,894	36,894	36,894	36,894	36,894	36,894	36,894	36,762	559	4	All CC9 - 4 Wanders
9/2/2022	37,026	37,026	37,026	37,026	37,026	37,026	37,026	37,026	37,026	37,026	36,894	561	2	All CC9 - 2 Wanders
9/6/2022	37,290	37,290	37,290	37,290	37,290	37,290	37,290	37,290	37,290	37,290	37,158	565	4	All CC9 - 4 Wanders
9/7/2022	37,554	37,554	37,554	37,554	37,554	37,554	37,554	37,554	37,554	37,554	37,422	569	4	All CC9 - 4 Wanders
9/12/2022	37,604	37,604	37,604	37,604	37,604	37,604	37,604	37,604	37,604	37,604	37,472	569.7576	0.7576	All CC9 - 0 Wanders completed. Stopped at seq. 50 of 570th wander due to vehicle faulting.
9/13/2022	37,610	37,610	37,610	37,610	37,610	37,610	37,610	37,610	37,610	37,610	37,478	569.8485	0.0909	All CC9 - 0 Wanders. 6 passes in 570th wander.
9/14/2022	37,614	37,614	37,614	37,614	37,614	37,614	37,614	37,614	37,614	37,614	37,482	569.9091	0.0606	All CC9 - 0 Wanders. 4 passes in 570th wander.
9/15/2022	37,818	37,818	37,818	37,818	37,818	37,818	37,818	37,818	37,818	37,818	37,686	573	3.0909	All CC9 - 4 Wanders completed. Started seq. 61 of 570th wander (vehicle pass 37615).
9/16/2022	38,082	38,082	38,082	38,082	38,082	38,082	38,082	38,082	38,082	38,082	37,950	577	4	All CC9 - 4 Wanders
9/19/2022	38,346	38,346	38,346	38,346	38,346	38,346	38,346	38,346	38,346	38,346	38,214	581	4	All CC9 - 4 Wanders
9/20/2022	38,610	38,610	38,610	38,610	38,610	38,610	38,610	38,610	38,610	38,610	38,478	585	4	All CC9 - 4 Wanders
9/21/2022	38,874	38,874	38,874	38,874	38,874	38,874	38,874	38,874	38,874	38,874	38,742	589	4	All CC9 - 4 Wanders
9/26/2022	39,138	39,138	39,138	39,138	39,138	39,138	39,138	39,138	39,138	39,138	39,006	593	4	All CC9 - 4 Wanders
9/27/2022	39,402	39,402	39,402	39,402	39,402	39,402	39,402	39,402	39,402	39,402	39,270	597	4	All CC9 - 4 Wanders
9/28/2022	39,666	39,666	39,666	39,666	39,666	39,666	39,666	39,666	39,666	39,666	39,534	601	4	All CC9 - 4 Wanders
9/29/2022	39,864	39,864	39,864	39,864	39,864	39,864	39,864	39,864	39,864	39,864	39,732	604	3	All CC9 - 3 Wanders
9/30/2022	40,128	40,128	40,128	40,128	40,128	40,128	40,128	40,128	40,128	40,128	39,996	608	4	All CC9 - 4 Wanders
10/3/2022	40,392	40,392	40,392	40,392	40,392	40,392	40,392	40,392	40,392	40,392	40,260	612	4	All CC9 - 4 Wanders
10/4/2022	40,656	40,656	40,656	40,656	40,656	40,656	40,656	40,656	40,656	40,656	40,524	616	4	All CC9 - 4 Wanders
10/5/2022	40,920	40,920	40,920	40,920	40,920	40,920	40,920	40,920	40,920	40,920	40,788	620	4	All CC9 - 4 Wanders
10/12/2022	41,316									41,316		626	6	Overload 5N only - 6 Wanders
10/13/2022	41,844									41,844	41,316	634	8	5N/S only - 8 Wanders
10/14/2022	42,372									42,372	41,844	642	8	5N/S only - 8 Wanders
10/17/2022	42,900									42,900	42,372	650	8	5N/S only - 8 Wanders
10/19/2022	43,428									43,428	42,900	658	8	5N/S only - 8 Wanders
10/21/2022	43,956									43,956	43,428	666	8	5N/S only - 8 Wanders
10/24/2022	44,484									44,484	43,956	674	8	5N/S only - 8 Wanders
10/25/2022	44,550									44,550	44,022	675	1	5N/S only - 1 Wander
10/25/2022	44,616	40,920	40,920	40,920	40,920	40,932	40,932	40,932	40,932	44,616	44,088	676	1	Test Loading Items 1-5, stopped after 12 passes (54 uncompleted Passes). Nominal Load on Items 1-2
10/26/2022	45,012									45,012	44,484	682	6	5N/S only - 6 Wanders

CC9	Vehicle Pass Number	Pass # by Test Item											Insert #	Daily Notes
		1N	1S	2N	2S	3N	3S	4N	4S	5N	5S	Wander Number	Wanders (Daily)	
Vehicle Pass:	96,294	75,042	75,042	75,042	75,042	40,920	40,920	40,920	40,920	56,628	56,100			
10/27/2022	45,540									45,540	45,012	690	8	5N/S only - 8 Wanders
10/28/2022	46,068									46,068	45,540	698	8	5N/S only - 8 Wanders
10/31/2022	46,596									46,596	46,068	706	8	5N/S only - 8 Wanders
11/1/2022	47,124									47,124	46,596	714	8	5N/S only - 8 Wanders
11/2/2022	47,652									47,652	47,124	722	8	5N/S only - 8 Wanders
11/7/2022	48,180									48,180	47,652	730	8	5N/S only - 8 Wanders
11/8/2022	48,708									48,708	48,180	738	8	5N/S only - 8 Wanders
11/9/2022	49,236									49,236	48,708	746	8	5N/S only - 8 Wanders
11/10/2022	49,764									49,764	49,236	754	8	5N/S only - 8 Wanders
11/14/2022	50,292									50,292	49,764	762	8	5N/S only - 8 Wanders
11/15/2022	50,754									50,754	50,226	769	7	5N/S only - 7 Wanders
11/16/2022	51,084									51,084	50,556	774	5	5N/S only - 5 Wanders
11/21/2022	51,612									51,612	51,084	782	8	5N/S only - 8 Wanders
11/22/2022	52,140									52,140	51,612	790	8	5N/S only - 8 Wanders
11/23/2022	52,470									52,470	51,942	795	5	5N/S only - 5 Wanders
11/28/2022	52,998									52,998	52,470	803	8	5N/S only - 8 Wanders
11/29/2022	53,526									53,526	52,998	811	8	5N/S only - 8 Wanders
11/30/2022	54,054									54,054	53,526	819	8	5N/S only - 8 Wanders
12/5/2022	54,582									54,582	54,054	827	8	5N/S only - 8 Wanders
12/7/2022	54,596									54,596	54,068	827.2121	0.2121	5N/S only - Only 14 Passes completed - NAPTV repair needed
12/13/2022	55,110									55,110	54,582	835	7.7879	NAPTV Fixed - 5N/S only - Finished previous wander, completed 7 after
12/14/2022	55,572									55,572	55,044	842	7	5N/S only - 7 Wanders
12/16/2022	55,704									55,704	55,176	844	2	5N/S only - 2 Wanders
12/20/2022	56,232									56,232	55,704	852	8	5N/S only - 8 Wanders
12/21/2022	56,628									56,628	56,100	858	6	NAPTV C2M2 Broken Valve stem - 5N/S only - 6 Wanders (Done item 5)
1/3/2023	56,892	41,184	41,184	41,184	41,184							862	4	Started Trafficking CC9 Fatigue Model/Base Thickness items 1 and 2 Only - 4 Wanders
1/4/2023	57,288	41,580	41,580	41,580	41,580							868	6	1N/S and 2N/S only - 6 Wanders
1/9/2023	57,684	41,976	41,976	41,976	41,976							874	6	1N/S and 2N/S only - 6 Wanders
1/10/2023	58,080	42,372	42,372	42,372	42,372							880	6	1N/S and 2N/S only - 6 Wanders
1/11/2023	58,476	42,768	42,768	42,768	42,768							886	6	1N/S and 2N/S only - 6 Wanders
1/17/2023	58,478	42,770	42,770	42,770	42,770							886.0303	0.0303	1N/S and 2N/S only - Only 2 Passes completed - NAPTV repair needed
2/2/2023	58,872	43,164	43,164	43,164	43,164							892	5.9697	1N/S and 2N/S only - NAPTV repairs completed - Finished last unfinished wander (887) - 6 Wanders
2/6/2023	59,268	43,560	43,560	43,560	43,560							898	6	1N/S and 2N/S only - 6 Wanders
2/7/2023	59,664	43,956	43,956	43,956	43,956							904	6	1N/S and 2N/S only - 6 Wanders
2/9/2023	60,060	44,352	44,352	44,352	44,352							910	6	1N/S and 2N/S only - 6 Wanders
2/14/2023	60,390	44,682	44,682	44,682	44,682							915	5	1N/S and 2N/S only - 5 Wanders
2/15/2023	60,786	45,078	45,078	45,078	45,078							921	6	1N/S and 2N/S only - 6 Wanders
2/21/2023	61,182	45,474	45,474	45,474	45,474							927	6	1N/S and 2N/S only - 6 Wanders
2/22/2023	61,578	45,870	45,870	45,870	45,870							933	6	1N/S and 2N/S only - 6 Wanders
2/23/2023	61,908	46,200	46,200	46,200	46,200							938	5	1N/S and 2N/S only - 5 Wanders
2/24/2023	62,304	46,596	46,596	46,596	46,596							944	6	1N/S and 2N/S only - 6 Wanders
2/27/2023	62,700	46,992	46,992	46,992	46,992							950	6	1N/S and 2N/S only - 6 Wanders
2/28/2023	63,096	47,388	47,388	47,388	47,388							956	6	1N/S and 2N/S only - 6 Wanders
3/1/2023	63,558	47,850	47,850	47,850	47,850							963	7	1N/S and 2N/S only - 7 Wanders
3/6/2023	64,020	48,312	48,312	48,312	48,312							970	7	1N/S and 2N/S only - 7 Wanders - Last Day using 58-kip for 3D gear configuration
3/7/2023	64,482	48,774	48,774	48,774	48,774							977	7	1N/S and 2N/S only - 7 Wanders - First Day using 65-kip for 3D gear configuration
3/8/2023	64,746	49,038	49,038	49,038	49,038							981	4	1N/S and 2N/S only - 4 Wanders - Multiple Vehicle Faults, Test Parameters changed to 0-10 to 1+05
3/9/2023	65,208	49,500	49,500	49,500	49,500							988	7	1N/S and 2N/S only - 7 Wanders
3/10/2023	65,670	49,962	49,962	49,962	49,962							995	7	1N/S and 2N/S only - 7 Wanders
3/13/2023	66,132	50,424	50,424	50,424	50,424							1002	7	1N/S and 2N/S only - 7 Wanders
3/14/2023	66,594	50,886	50,886	50,886	50,886							1009	7	1N/S and 2N/S only - 7 Wanders
3/15/2023	66,924	51,216	51,216	51,216	51,216							1014	5	1N/S and 2N/S only - 5 Wanders
3/20/2023	67,320	51,612	51,612	51,612	51,612							1020	6	1N/S and 2N/S only - 6 Wanders

CC9	Vehicle Pass Number	Pass # by Test Item											Insert #	Daily Notes
		1N	1S	2N	2S	3N	3S	4N	4S	5N	5S	Wander Number	Wanders (Daily)	
Vehicle Pass:	96,294	75,042	75,042	75,042	75,042	40,920	40,920	40,920	40,920	56,628	56,100			
3/21/2023	67,716	52,008	52,008	52,008	52,008							1026	6	1N/S and 2N/S only - 6 Wanders
3/22/2023	68,178	52,470	52,470	52,470	52,470							1033	7	1N/S and 2N/S only - 7 Wanders
3/23/2023	68,640	52,932	52,932	52,932	52,932							1040	7	1N/S and 2N/S only - 7 Wanders
3/24/2023	69,036	53,328	53,328	53,328	53,328							1046	6	1N/S and 2N/S only - 6 Wanders
3/27/2023	69,498	53,790	53,790	53,790	53,790							1053	7	1N/S and 2N/S only - 7 Wanders
3/28/2023	69,960	54,252	54,252	54,252	54,252							1060	7	1N/S and 2N/S only - 7 Wanders
3/29/2023	70,290	54,582	54,582	54,582	54,582							1065	5	1N/S and 2N/S only - 5 Wanders
1/23/2024	70,290	54,582	54,582	54,582	54,582							1065	0	1N/S and 2N/S only - Shakedown Lower loading CC9 2024
1/25/2024	70,752	55,044	55,044	55,044	55,044							1072	7	1N/S and 2N/S only - 7 Wanders - First Day of Trafficking CC9 2024
1/26/2024	71,346	55,638	55,638	55,638	55,638							1081	9	1N/S and 2N/S only - 9 Wanders
1/29/2024	71,940	56,232	56,232	56,232	56,232							1090	9	1N/S and 2N/S only - 9 Wanders
1/30/2024	72,534	56,826	56,826	56,826	56,826							1099	9	1N/S and 2N/S only - 9 Wanders
1/31/2024	72,732	57,024	57,024	57,024	57,024							1102	3	1N/S and 2N/S only - 3 Wanders
2/1/2024	73,326	57,618	57,618	57,618	57,618							1111	9	1N/S and 2N/S only - 9 Wanders
2/2/2024	73,590	57,882	57,882	57,882	57,882							1115	4	1N/S and 2N/S only - 4 Wanders - Weekly NDT (HWD & Leica Scan)
2/5/2024	74,184	58,476	58,476	58,476	58,476							1124	9	1N/S and 2N/S only - 9 Wanders - Crack observed LFS-2S
2/6/2024	74,778	59,070	59,070	59,070	59,070							1133	9	1N/S and 2N/S only - 9 Wanders - Cracking observed LFS-2S/T-2S
2/7/2024	75,240	59,532	59,532	59,532	59,532							1140	7	1N/S and 2N/S only - 7 Wanders - Cracking observed LFS-1S
2/8/2024	75,702	59,994	59,994	59,994	59,994							1147	7	1N/S and 2N/S only - 7 Wanders - Cracking observed LFS-1S
2/9/2024	75,966	60,258	60,258	60,258	60,258							1151	4	1N/S and 2N/S only - 4 Wanders - Weekly NDT (HWD & Leica Scan)
2/12/2024	76,560	60,852	60,852	60,852	60,852							1160	9	1N/S and 2N/S only - 9 Wanders - Cracking observed LFS-1S
2/13/2024	77,088	61,380	61,380	61,380	61,380							1168	8	1N/S and 2N/S only - 8 Wanders
2/14/2024	77,550	61,842	61,842	61,842	61,842							1175	7	1N/S and 2N/S only - 7 Wanders - Cracking observed LFS-1S
2/15/2024	78,144	62,436	62,436	62,436	62,436							1184	9	1N/S and 2N/S only - 9 Wanders -
2/16/2024	78,408	62,700	62,700	62,700	62,700							1188	4	1N/S and 2N/S only - 4 Wanders - Weekly NDT (HWD & Leica Scan)
2/20/2024	78,870	63,162	63,162	63,162	63,162							1195	7	1N/S and 2N/S only - 7 Wanders -
2/21/2024	79,464	63,756	63,756	63,756	63,756							1204	9	1N/S and 2N/S only - 7 Wanders - Cracking observed LFS-2S/T-2S
2/22/2024	80,058	64,350	64,350	64,350	64,350							1213	9	1N/S and 2N/S only - 9 Wanders - Cracking observed LFS-2S/T-2S
2/23/2024	80,322	64,614	64,614	64,614	64,614							1217	4	1N/S and 2N/S only - 4 Wanders - Weekly NDT (HWD & Leica Scan)
2/26/2024	80,916	65,208	65,208	65,208	65,208							1226	9	1N/S and 2N/S only - 9 Wanders - Cracking observed LFS-1S
2/27/2024	81,510	65,802	65,802	65,802	65,802							1235	9	1N/S and 2N/S only - 9 Wanders - Cracking observed LFS-1S
2/28/2024	81,686	65,978	65,978	65,978	65,978							1237.67	2.67	1N/S and 2N/S only - <3 Wanders - Tire Blowout on C1M3S, Trafficking halted
3/4/2024	82,236	66,528	66,528	66,528	66,528							1246	8.33	1N/S and 2N/S only - 8.3 Wanders - Cracking observed LFS-1S
3/5/2024	82,698	66,990	66,990	66,990	66,990							1253	7	1N/S and 2N/S only - 7 Wanders - Cracking observed LFS-1S
3/6/2024	83,292	67,584	67,584	67,584	67,584							1262	9	1N/S and 2N/S only - 9 Wanders - Cracking observed LFS-1S
3/7/2024	83,688	67,980	67,980	67,980	67,980							1268	6	1N/S and 2N/S only - 6 Wanders - Cracking observed LFS-1S, LFS-2S
3/8/2024	83,952	68,244	68,244	68,244	68,244							1272	4	1N/S and 2N/S only - 4 Wanders - Weekly NDT (HWD & Leica Scan)
3/11/2024	84,282	68,574	68,574	68,574	68,574							1277	5	1N/S and 2N/S only - 5 Wanders - Cracking observed LFS-1S, LFS-2S
3/12/2024	84,612	68,904	68,904	68,904	68,904							1282	5	1N/S and 2N/S only - 5 Wanders - Cracking observed LFS-1S, LFS-2S
3/13/2024	85,206	69,498	69,498	69,498	69,498							1291	9	1N/S and 2N/S only - 9 Wanders - Cracking observed LFS-1S
3/14/2024	85,734	70,026	70,026	70,026	70,026							1299	8	1N/S and 2N/S only - 8 Wanders - Cracking observed LFS-1S, LFS-2S
3/15/2024	85,998	70,290	70,290	70,290	70,290							1303	4	1N/S and 2N/S only - 4 Wanders - Weekly NDT (HWD & Leica Scan)
3/18/2024	86,526	70,818	70,818	70,818	70,818							1311	8	1N/S and 2N/S only - 8 Wanders - Cracking observed LFS-1S, LFS-2S
3/19/2024	86,988	71,280	71,280	71,280	71,280							1318	7	1N/S and 2N/S only - 7 Wanders - Cracking observed LFS-1S
3/20/2024	87,516	71,808	71,808	71,808	71,808							1326	8	1N/S and 2N/S only - 8 Wanders - Cracking observed LFS-1S, LFS-2S
3/21/2024	87,912	72,204	72,204	72,204	72,204							1332	6	1N/S and 2N/S only - 6 Wanders - Cracking observed LFS-1S, LFS-2S
3/22/2024	88,176	72,468	72,468	72,468	72,468							1336	4	1N/S and 2N/S only - 4 Wanders - Last Weekly NDT (HWD & Leica Scan) TO21
3/25/2024	88,704	72,996	72,996	72,996	72,996							1344	8	1N/S and 2N/S only - 8 Wanders
3/26/2024	89,122	73,414	73,414	73,414	73,414							1350.33	6.33	1N/S and 2N/S only - 6.33 Wanders Trafficking stopped due to electrical issues
3/28/2024	89,430	73,722	73,722	73,722	73,722							1355	4.67	1N/S and 2N/S only - 4.67 Wanders -
3/29/2024	89,958	74,250	74,250	74,250	74,250							1363	8	
4/1/2024	90,222	74,514	74,514	74,514	74,514							1367	4	
4/2/2024	90,750	75,042	75,042	75,042	75,042							1375	8	End of Test

APPENDIX D—THREE-DIMENSIONAL LASER SCANS OF PAVEMENT SURFACE

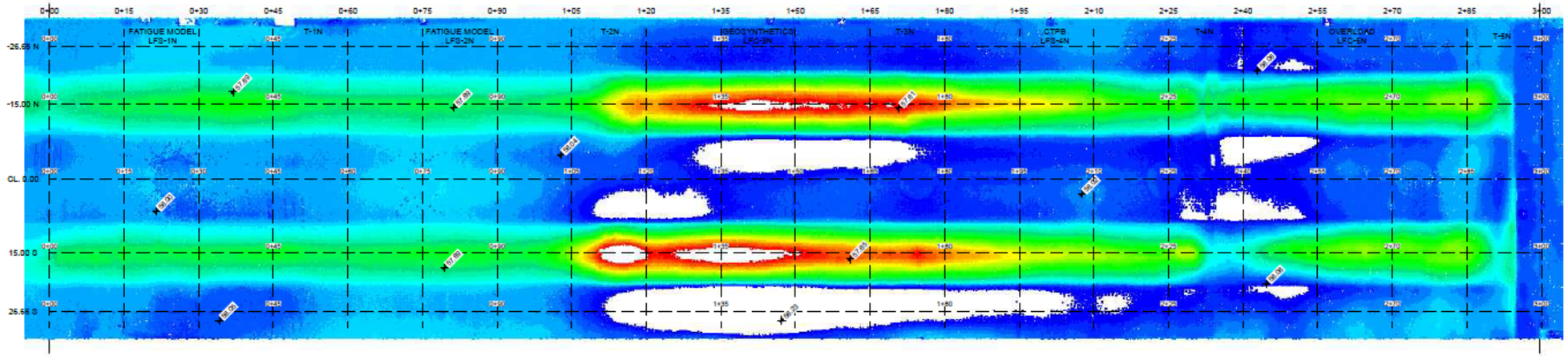

NOTES:

1. THE COLOR MAP ABOVE DEPICTS DATA OBTAINED ON 01/13/2023 THROUGH THE USE OF A HIGH DEFINITION LASER SCAN.
2. THE PROFILES AND SECTIONS SHOWN IN SHEETS 2 THROUGH 6 COMPARE TWO SET OF HIGH DEFINITION LASER SCANS:
   A) GREY = 04/02/2021
   B) BLACK = 01/13/2023
3. HORIZONTAL AND VERTICAL INFORMATION IS BASED UPON INFORMATION PROVIDED IN DIGITAL CAD FILE NAMED CC09-DEMO-ABLT.dwg.

Color Range= 100 colors — Color Increment= .05'

57.80 — 57.85 — 58.10

10 0 10 20 30

GRAPHIC SCALE

HORIZONTAL 1"=10'

NO.	REVISIONS	DATE	BY	CHK	APR

LOCATION KEY MAP

NAPTF BUILDING

NORTH WALL

Data Collection Area

SOUTH WALL

ARA FOR

NATIONAL AIRPORT PAVEMENT TEST FACILITY
ATLANTIC CITY AIRPORT
NEW JERSEY 08234

	NAME	DATE
DRAWN	G HOLLEY	01/18/2023
CHECKED	C MAZZOTTA	01/20/2023
FAA APPROVAL DATE:		

PROJECT NO: CC9

PLAN VIEW

20220113_TRAFFIC SCAN 00

SIZE: ANSI D | SCALE: AS NOTED | SHEET 1 OF 6

CAD FILE: 20230113_FAA-ATRD-WS00.DWG

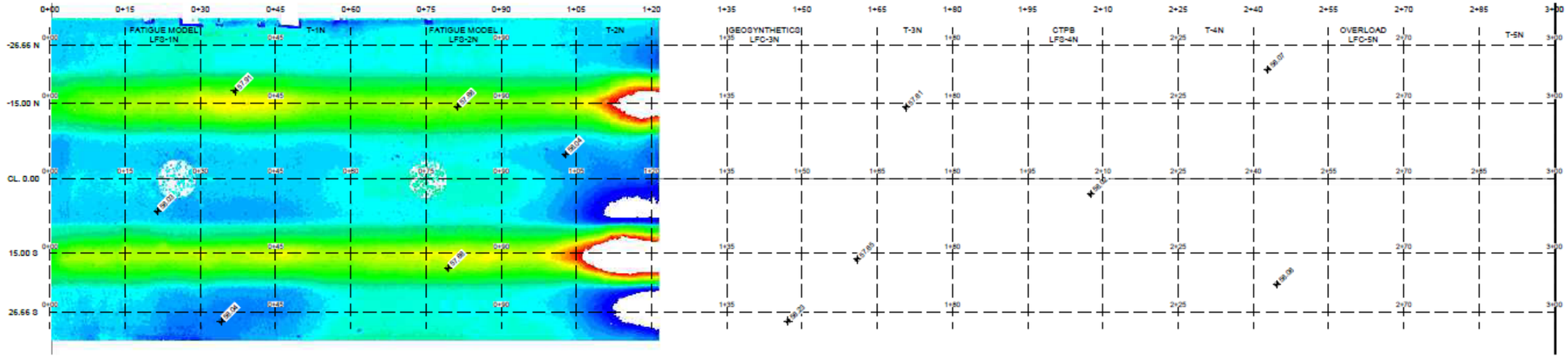

NOTES:

1. THE COLOR MAP ABOVE DEPICTS DATA OBTAINED ON 04/04/2024 THROUGH THE USE OF A HIGH DEFINITION LASER SCAN.
2. THE PROFILES AND SECTIONS SHOWN IN SHEETS 2 THROUGH 6 COMPARE TWO SET OF HIGH DEFINITION LASER SCANS:
   A) GREY = 04/02/2021
   B) BLACK = 04/04/2024
3. HORIZONTAL AND VERTICAL INFORMATION IS BASED UPON INFORMATION PROVIDED IN DIGITAL CAD FILE NAMED CC09-DEMO-ABLT.dwg.

Color Range= 100 colors — Color Increment= .05'

57.80 — 57.85 — 58.10

GRAPHIC SCALE

NO.	REVISIONS	DATE	BY	CHK	APR

LOCATION KEY MAP

NAPTF BUILDING

NORTH WALL

Data Collection Area

SOUTH WALL

ARA FOR NATIONAL AIRPORT PAVEMENT TEST FACILITY ATLANTIC CITY AIRPORT NEW JERSEY 08234

	NAME	DATE
DRAWN	D EVANS	06/14/2024
CHECKED	C MAZZOTTA	06/14/2024
FAA APPROVAL DATE:		

PROJECT NO: CC9

PLAN VIEW

20240404_TRAFFIC SCAN 00

SIZE: ANSI D | SCALE: AS NOTED | SHEET 1 OF 6

CAD FILE: CC9 20240404 TEST6_FAA-ATRD-WS00.DWG